

ABSTRACT

The vasculoid is a single, complex, multisegmented nanotechnological medical robotic system capable of duplicating all essential thermal and biochemical transport functions of the blood, including circulation of respiratory gases, glucose, hormones, cytokines, waste products, and cellular components. This nanorobotic system, a very aggressive and physiologically intrusive macroscale nanomedical device comprised of ~500 trillion stored or active individual nanorobots, weighs ~2 kg and consumes from 30–200 watts of power in the basic human model, depending on activity level. The vasculoid system conforms to the shape of existing blood vessels and serves as a complete replacement for natural blood. This paper presents a preliminary theoretical scaling analysis including transport capacity, thermal conduction, control and biocompatibility considerations, along with a hypothetical installation scenario and a description of some useful optional equipment. A discussion of repair procedures and various applications of the personal vasculoid appliance is deferred to subsequent papers.

DR.RUPNATHJY (DR.RUPAK NATH)

OUTLINE OF THE PAPER

1. Introduction

1.1 The Vasculoid Concept

1.2 Some Benefits of Vasculoid Installation

2. Physiological Materials Transport

2.1 Molecular Transport

2.1.1 Respiratory Gases

2.1.2 Water

2.1.3 Glucose

2.1.4 Nonprotein Nitrogenous Molecules

2.1.5 Plasma Proteins

2.1.6 Lipids

2.1.7 Other Molecules

2.1.8 Summary of Molecular Transport

2.2 Cellular Transport

2.2.1 Leukocytes and Stem Cells

2.2.2 Platelets

2.2.3 Erythrocytes

2.2.4 Summary of Cellular Transport

2.3 Ciliary Distribution Subsystem

2.3.1 Description of the Cilium

DR. RUPNATHJI (DR. RUPAK NATH)

2.3.2 Ciliary Subsystem Requirements

2.4 Docking Bays and Cellulocks

2.4.1 Docking Bays for Tankers

2.4.2 Cellulocks for Boxcars

2.4.3 Container Routing and Identification

2.4.4 Potential Transport Bottlenecks

2.4.4.1 Water Absorption and Elimination

2.4.4.2 Glucose Absorption and Elimination

2.4.4.3 Boxcar Clearance in Narrow Capillaries

2.4.4.4 Tanker Monolayer Transport

2.5 Mobile Vasculocytes

2.6 Appliance Power Requirement

3. Preliminary Thermal Conductivity Analysis

4. Biocompatibility of Vasculoid Systems

4.1 Mechanical Interaction with Vascular Endothelium

4.1.1 Modulation of Endothelial Phenotype and Function

4.1.2 Vascular Response to Stenting

4.1.3 Nanorobotic Destructive Vasculopathies

4.1.3.1 Nanorobotic Ulcerative Vasculopathy

4.1.3.2 Nanorobotic Lacerative Vasculopathy

4.1.3.3 Nanorobotic Concussive Vasculopathy

4.1.4 Mechanical Interactions with Glycocalyx

4.2 Interruption of Plasmatic Water and Lymphatic Flows

4.3 Immune System Interactions

4.4 Inflammation

DR. RUPNATHJIK (DR. RUPAK NATH)

- 4.5 Thrombogenesis
- 4.6 Regulation of Angiogenesis and Vasculogenesis
- 4.7 Vascular Patency and Relaxation

- 5. Control Systems and Computational Requirements

- 6. Overall System Reliability

- 7. Hypothetical Vasculoid Installation Scenarios
 - 7.1 Cellular Ischemispecific Limits
 - 7.2 Patient Preparation
 - 7.3 Vascular Washout
 - 7.4 Vascular Plating
 - 7.5 Defluidization
 - 7.6 Initialization and Cold Start
 - 7.7 Vasculoid Removal
 - 7.8 Aggressive Installation Scenario

- 8. Vasculoid Optional Equipment
 - 8.1 External Ports
 - 8.2 Thermal Comfort Subsystem
 - 8.3 Internal Caching
 - 8.4 Breathing in Low–Oxygen Environments
 - 8.5 Lymphovasculoid and Pathogen Disposal
 - 8.6 Extravasculoid Devices
 - 8.7 Active Thermal Damage Suppression
 - 8.8 Active Resistance To Mechanical Damage

DR. RUPNATHJI (DR. RUPAK NATH)

1. Introduction

This paper reports the very preliminary technical examination of an idea originally referred to as “roboblood” that was first proposed by one of the authors (C. Phoenix) in June 1996 [1]. The concept stimulated informal interest in a particularly aggressive nanomedical design and elicited considerable online popular discussion on sci.nanotech and elsewhere. The need for a detailed technical analysis soon became apparent, which led to an intermittent but constructive collaboration between R. Freitas [4] and C. Phoenix during 1996–2002, culminating in the present work.

This paper is not intended to represent an actual engineering design for a future nanomedical product. Rather, the purpose here is merely to examine a set of appropriate design constraints, scaling issues, and reference designs to investigate whether or not the basic idea of a blood replacement appliance might be feasible, and to determine key limitations of such designs. The reader also is warned that, in order to maintain tight focus, this paper necessarily ignores many possible future nanomedical practices and augmentations to human cellular, tissue, and organ systems that would clearly be accessible to a molecular manufacturing nanotechnology capable of building the vasculoid appliance, and which might significantly influence vasculoid architecture, utility or the advisability of its use.

1.1 The Vasculoid Concept

The idea of the vasculoid originated in the asking of a simple question: Once a mature molecular nanotechnology becomes available, could we replace blood with a single, complex robot? This robot would duplicate all essential thermal and biochemical transport functions of the blood, including circulation of respiratory gases, glucose, hormones, cytokines, waste products, and all necessary cellular components. The device would conform to the shape of existing blood vessels. Ideally, it would replace natural blood so thoroughly that the rest of the body would remain, at least physiochemically, essentially unaffected, but sustained in a cardioplegic state. It is, in effect, a mechanically engineered redesign of the human circulatory system that attempts to integrate itself as an intimate personal appliance with minimal adaptation on the part of the host human body.

A robotic device that replaces and extends the human vascular system is properly called a “vasculoid,” a vascular-like machine. But the vasculoid is more than just an artificial vascular system. Rather, it is a member of a class of space- or volume-filling nanomedical augmentation devices whose function applies to the human vascular tree. The device is extremely complex, having ~500 trillion independent cooperating nanorobots. In simplest terms, the vasculoid is a watertight coating of nanomachinery distributed across the luminal surface of the entire human vascular tree. This nanomachinery uses a ciliary array to transport important nutrients and biological cells to the tissues, containerized either in “tankers” (for molecules) or “boxcars” (for cells). The basic device weighs ~2 kg and releases ~30 watts of waste heat at a basal activity level and a maximum of ~200 watts of power at peak (e.g., Olympic sprint) activity level (Section 2.6). The power dissipation of the human body ranges from ~100 watts (basal) to ~1600 watts (peak) ([4], Section 6.5.2), so the device presents no adverse thermogenic consequences to the user. The appliance is powered by glucose and oxygen, as may be common in medical nanorobotic systems [2–11].

The most important basic structural component of the exemplar vasculoid robot (Table 1) is a ~300 m² two-dimensional vascular-surface-conforming array of ~150 trillion “sapphiroid” (i.e., using sapphire-like building materials) basic plates. (Thermal conductivity favors sapphire over diamond; Section 3.) These square plates are nanorobots that cover the entire luminal surface of all blood vessels in the body, to one-plate thickness. Each basic plate is an individual self-contained nanorobot ~1 micron thick and ~2 micron² in surface area, a size small enough to allow adequate clearance even in the narrowest human capillaries. Molecule-conveying “docking bays” (Section 2.4.1) comprise ~24 trillion, or 16%, of all vasculoid basic plates. Tankers containing molecules for distribution can dock at these bays and load or unload their cargo. Cell-conveying “cellulocks” (Section 2.4.2) are built on “cellulock plates” which span the area of 30 basic plates, or 60 micron² each. Boxcars containing biological cells for distribution can dock at these cellulocks and load or unload their cargo. With only 32.6 billion cellulock plates in the entire vasculoid design, cellulocks occupy the area of 0.978 trillion basic plates or only 0.65% of the entire vasculoid surface. The remaining ~125 trillion basic plates are reserved for special equipment (Section 8) and other as-yet undefined applications. All nanomachinery within each plate is of modular design, permitting easy replacement and repair by mobile repair nanorobots called vasculocytes (Section 2.5).

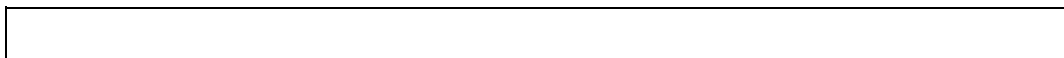


Table 1. Number, Mass and Volume of Exemplar Vasculoid System Components

System Component	Number of Nanorobots	Subsystem Mass	Subsystem Volume
Surface Plates		1.05 kg	
Docking bays	24×10^{12}	-----	48.0 cm^3
Cellulocks	0.0326×10^{12}	-----	1.956 cm^3
Applications plates	125×10^{12}	-----	250.0 cm^3
Container Fleet			
Tankers			
Active	166.2×10^{12}	0.133 kg	166.2 cm^3
Backups in storage	166.2×10^{12}	(0.133 kg)	(166.2 cm^3)
Boxcars			
Active	0.032×10^{12}	0.0768 kg	91.7 cm^3
Backups in storage	0.032×10^{12}	(0.0768 kg)	(91.7 cm^3)
Vasculocytes			
Active	0.200×10^{12}	0.002 kg	0.6 cm^3
Backups in storage	2.000×10^{12}	(0.02 kg)	(6.0 cm^3)
Storage Vesicles	0.5×10^6	0.460 kg	500.0 cm^3
Other structure, unspecified	16.3×10^{12}	0.2782 kg	141.544 cm^3
TOTALS	500.0×10^{12}	2.000 kg	1200.0 cm^3

(items in parens are already included in storage vesicles)

Adjacent plates abut through flexible but watertight mechanical interfaces on metamorphic bumpers along the entire perimeter of each plate (some details are in [4], Section 5.4). Each bumper has controllable variable volume, permitting the vasculoid surface: (1) to slightly expand or contract in area, or (2) to flex, either in response to macroscale body movements (Sections 7.4, 7.6, and 8.2) or in response to vascular surface corrugations or other irregularities to the same degree or better than the natural endothelium. Thus, plated surfaces readily accommodate the natural cyclical volume changes of various organs such as lung, bladder, or spleen. Rigidity of the plate array is also subject to engineering control and to localized real-time control as well, via the bumpers; diamondoid or sapphire plating may be made substantially stiffer than natural endothelium, if desired. The rupture strength of individual plates is $\sim 40,000 \text{ atm}$ ([4], Eqn. 10.13, taking plate wall thickness $t_{\text{wall}} \sim 0.1 \text{ mm}$, effective radius $R \sim 0.5 \text{ mm}$, and working stress $s_w \sim 10^{10} \text{ N/m}^2$ ([4], Table 9.3)). Bumper actuation power is of order $\sim 0.1 \text{ pW}$ ([4], Section 5.3.3), comparable to the power draw of a single plate cilium (Section 2.3.1).

1.2 Some Benefits of Vasculoid Installation

The advantages of installing a vasculoid are potentially numerous. Many of these benefits theoretically could be provided on a temporary or more limited basis using terabit-quantity doses of considerably less aggressive bloodborne nanomedical devices. However, the vasculoid appliance simultaneously provides all benefits on an essentially permanent and whole-body basis. Additionally, some benefits appear unique to the vasculoid and can be achieved in no other way. Whether the entire package is sufficiently attractive to warrant installation will probably be a matter of personal taste rather than of medical necessity, since a molecular nanotechnology capable of building and deploying a complex vasculoid is likely to offer complete non-vasculoid cures for most circulatory and blood-related disorders that plague humanity today, and biological enhancements may also be available. The choice between an augmentation technology that works alongside a natural system (e.g., respirocytes [6]) and an augmentation technology that entirely replaces a natural system (e.g., vasculoid) may involve significant safety, psychological, and even ethical considerations.

The most important benefits of vasculoid installation may include:

(1) Exclusion of parasites, bacteria, viruses, and metastasizing cancer cells from the bloodflow, thus limiting the spread of bloodborne disease. Such microorganisms and cells are easily eliminated from the blood using $\sim\text{cm}^3$ doses of appropriately programmed nanobiotics [2–4], but such individual nanorobotic devices might not normally be deployed on a permanent basis. Intracellular pathogens that can infect motile phagocytic cells (e.g., the tuberculosis *Mycobacterium* or the bacterium *Listeria*, both of which can reside inside macrophages [12]) cannot be directly excluded from the tissues when infected cells are transported by the vasculoid. However, cell surface markers will often reveal such infection, so vasculoid systems can check for the presence of such markers and thus deny these cells re-entry to human tissues. For example, the membrane surface of macrophages infected by *Mycobacterium microti* is antigenically different from that of uninfected macrophages [13]; *Listeria*-derived peptides are found acting as integral membrane proteins in the plasma membrane of infected macrophages [14], and other *Listeria*-infected antigen-presenting cells display hsp60 on their plasma membranes only when infected [15]. Note that the natural bacterial inhabitants of the human gastrointestinal tract should be relatively unaffected by the installation of a vasculoid appliance, since gut microbes normally do not enter the bloodstream; similar considerations apply to the natural microbial flora of the skin, mouth, nasal passages, and so forth. The vasculoid could also significantly reduce the prospect of death by cancer by refusing either to transport angiogenesis factors (in certain cases; Section 4.6) or to transport nonvalidated native stem cells* (thus preventing metastasis), or by refusing to install itself in any capillaries arising in locations where angiogenesis is disallowed in an adult body.

(2) Faster and more reliable trafficking of lymphocytes throughout the secondary lymphoid organs [16], allowing them to survey for targeted antigens in minutes or hours, rather than days (because both white cells and antigenic sources can be efficiently concentrated), thus greatly speeding the natural immune system response to foreign antigen. This lymphocyte function might also be augmented or replaced using individual histomobile medical nanorobots [4] or biorobots. If biorobots are developed first, many vasculoid installations might take place in patients possessing largely artificial immune systems, thus obviating the need for much of the cellular component trafficking described in Section 2.2.

(3) Eradication of most serious circulatory–related pathological conditions including all vascular disease (e.g., aortic dissection, vessel blockages, spasms, aneurysms, phlebitis, varicose veins), heart disease, syncope (including orthostatic hypotension) and shock, strokes, and bleeding, due to the elimination of unconstrained metabolite and fluid circulation. Certain other conditions due to localized prevention of blood flow such as bedsores** and subclinical paresthesias*** (e.g., “pins–and–needles” sensation) can also be ameliorated, since stiffened blood vessels will not be nearly so easy to close via external compression. Again, many of these conditions may already have adequate nanomedical treatments by the time the vasculoid can be built, but other conditions might not yet be readily or as conveniently treatable, such as the dangers of large–scale bleeding (both internal and external). Mechanical biocompatibility issues are discussed at length in Section 4.1.

(4) Reduced susceptibility to chemical, biochemical, and parasitic poisons of all kinds, including allergenic substances in food, air and water, although bloodborne nanotankers or phamacytes [3, 4] may be able to partially duplicate this function as well. Note that toxins, novel metabolites or other unknown foreign substances may arrive in the tissues via solvents penetrating the dermis (e.g., DMSO) or by other nonvascular routes, and would be removed from the natural blood in due course by the kidney which extracts all small molecules by default, then actively reabsorbs only useful molecules such as glucose, electrolytes, vitamins, and water. By contrast, in the present design the vasculoid transports only recognized substances. Novel undesired substances must therefore be removed by employing a small number of previously unallocated application plates: (a) as miniature analytical laboratories which can detect foreign analytes and alter a programmable binding site ([4], Section 3.5.7.4) to bind them, allowing transport to the kidney for disposal; (b) as miniature chemical processing systems, possibly involving well–designed sets of artificial digestive enzymes [2], which can break down the foreign substance into well–recognized simpler substances; or (c) as analytical laboratories or chemical processing systems previously described which can receive appropriate new instructions directly from the patient, the physician, or other external sources of information. The lymphatic system is unmodified in the basic appliance design and may also serve to remove nonvascular toxins. Processing of such toxins may be deferred to the points where the lymph is reabsorbed into the vasculoid system, using either dedicated application plates or specialized processing stations (Section 8.5).

(5) Faster metabolite transport and distribution, significantly improving physical endurance and stamina, including the ability to breathe at low O₂ partial pressures (Sections 8.3 and 8.4) and the ability to flush out unwanted specific biochemicals from the body (a feature which might be duplicated using bloodborne respirocyte–class devices [3–6]). The architecture would also permit convenient long–term storage of protein (Section 2.1.5), or amino acid recovery and recycling (Section 8.1), which could prove nutritionally useful. As another example, an installed vasculoid could mitigate the effects of weightlessness or acceleration on nutrient transport and somatic fluid distribution by decoupling transport from gravity. The appliance can differentially control the release of water and electrolytes in various regions of the body. In addition, by making the transport function independent of gravity, vasculoid avoids the hydrostatic effects of extreme, varying, or absent gravity vectors. This would eliminate the facial puffiness seen in astronauts and the dependence of fighter pilots on external prostheses to force blood out of the legs during high–G maneuvers.

(6) Direct, rapid user control of many hormonal– and neurochemical–mediated, and all blood–mediated, physiological responses. It would be difficult (though not impossible) to provide equivalent comprehensive whole–body physiological control using individual micron–scale bloodborne nanorobots alone. Additionally, the appliance can continuously monitor the basic physiochemical status of vascularized tissues to near–micron resolution if necessary, since each micron–size plate is initialized with its physical position relative to the vascular tree (Section 7.6), and medically relevant information is communicated back to a

central user (or physician) interface. This can permit extremely rapid and specific detection of health problems [17] as will generally be the case in nanomedicine ([4], Section 1.3.3(8)), although the vasculoid may provide an easier and more thorough method for accomplishing this.

(7) Voluntary control of capillary conductance and rigidity permitting conscious regulation of thermal energy exchange with the environment (Sections 8.2 and 8.7) and at least limited control of whole-body morphological structure, rigidity (e.g., stiffness, bending modulus, etc.), and volume with ~millisecond response times (Section 8.8).

(8) At least partial protection from various accidents and other physical harm (e.g., insect stings, animal bites, collisions, bullet or shrapnel penetrations, falling from heights) which may be described in a future paper (Sections 8.3–8.8). This is perhaps the only specific benefit of the vasculoid appliance that could not be achieved by any less radical means: extreme trauma resistance, especially resistance to exsanguination and cushioning against mechanical shock.

Medically oriented readers might properly wonder why anyone would want to discuss replacing a perfectly functional natural fluid transport system with an untested, complex, artificial, dry system with which humans have no experience today. There are several answers to this very good question. First of all, medical skeptics should bear in mind that the vasculoid appliance is clearly a highly sophisticated medical nanosystem. It cannot be built without using a manufacturing system based on a mature molecular nanotechnology. Its use would come only after many decades of previous engineering experience in building, testing, and operating such highly complex systems inside the human body. In the future nanomedicine-rich milieu in which it would be deployed, the vasculoid as a medical intervention may be closer to the typical than to the extreme (as it might appear today). It is as if we were looking forward from the limited vantage point of the 1950s – a technological era in which vacuum tubes still reigned supreme – to the year 2002, and estimating the future feasibility of a 1 GHz Pentium III laptop computer (a feat of prognostication actually achieved by ST Arthur C. Clarke [18]).

In the nanomedical era, it will be a matter of personal preference and choice for each patient, in consultation with their physician, whether the aforementioned benefits of the vasculoid appliance are worth the risks. This paper is only a preliminary scaling study intended solely to investigate whether the machinery involved will fit in the allotted space, perform all required functions fast enough to be useful, operate within an acceptable energy budget even at peak loads, promise a strong likelihood of being safe, reliable, and biocompatible, and so forth. We turn now to a more detailed discussion of the vasculoid design which includes a consideration of molecular and cellular transport (Section 2), thermal conductivity (Section 3), biocompatibility issues (Section 4), control and computational requirements (Section 5), system reliability (Section 6), a possible vasculoid installation procedure (Section 7), and a few of the more obvious alternatives for optional equipment (Section 8).

* R. Bradbury notes that the genetic dysregulation which occurs as cancer cells develop makes it highly unlikely that they could masquerade as legitimate stem cells or the other cells that require vasculoid transport. As a stopgap, the vasculoid could refuse to transport more than a specified number of suspicious cells per unit time, thus at least limiting the rate of growth of such misprogrammed cells.

** Bedsores can also occur in response to increased extravascular pressure, and these cases might still occur, though perhaps less easily, even with vasculoid.

*** Most clinically significant paresthesias are due to neuropathy or cerebral dysfunction, and thus would not be prevented by vasculoid.

2. Physiological Materials Transport

As outlined below, at peak average male human metabolic rates, $\sim 5400 \text{ cm}^3$ of circulating blood transports up to $\sim 125 \text{ cm}^3$ of essential molecules and up to $\sim 90 \text{ cm}^3$ of essential cellular elements (excluding erythrocytes; see Section 2.2.3). Consequently $\sim 96\%$ of blood volume (mostly water) may be rendered superfluous if its solvation* and suspension functions can be replaced with a more efficient and highly reliable nanomechanical transport mechanism.

Many alternative transport mechanisms were reviewed and rejected by the authors.** The resulting baseline vasculoid device conveys physiologically useful molecules and cells throughout its interior, and thence to the biological tissues, by containerizing all materials and then using a ciliary transport system to distribute the containers to appropriate destinations. This architecture thus utilizes the fractal branching vascular network that is characteristic of efficient fluid transport systems [19], although many architectures are possible in this design space.*** Section 2.1 describes molecular transport requirements; Section 2.2 describes cellular transport requirements. Descriptions of specific subsystems follow, including the ciliary distribution system (Section 2.3), docking bays and cellulocks (Section 2.4), and mobile vasculocytes (Section 2.5).

* Some solvent water is still required for limited purposes, as, for example, to facilitate the mobility of soluble substances such as glucose (Section 2.1.3) and to avoid irreversible denaturation of certain proteins and other substances if solvation shells are stripped before transport.

** For example, molecule transport via simple open conveyor belts (the original “roboblood” proposal) was rejected for energetic and volumetric inefficiency, unreasonable glucose replenishment times after strenuous activities, circuit complexity, and susceptibility to breakage, contamination, leakage, tangling, and difficulty

of repair following exposure to anticipated emergency physical stresses. Palletized conveyors have many similar problems. Containerized transport along fixed tracks is more energy efficient per molecule transported but has comparable safety risks and failure modes, and has greater difficulty accommodating the aortic bottleneck. Pressurized transport via diamondoid or sapphire micropipes (of radius R at pressure P) is energetically efficient. However, volumetric flow rate scales as PR^4 , so reducing flow rate by 90% (allowing for some solvent) only reduces R by 45%, seemingly not much improvement over natural plumbing (increasing P is similarly ineffective) and still possessing many of the deficiencies of the natural system (e.g. interior flooding upon micropipe rupture, difficulty of repair, carrier fluids or larger bore pipes required for lipids and blood cell components) which it was desired to avoid. (An *in vivo* $P > 1000$ atm gas/fluid transport system would introduce many unacceptable risks.) Linked or tethered containerized transport through micropipes, diffusion-based mechanisms, vacuum-ballistic and electrostatic transport systems also were considered and rejected.

*** M. Krummenacker suggests a “vasculoid-lite” approach in which the device interior is filled with saline solution instead of gas or vacuum, and the key function of the appliance is to control pathogens and to route gas containers and repair nanorobots to wherever needed using a network or grid of tough fibers placed along the vascular walls (in the manner of a railroad) for such navigation, and perhaps replacing bulky blood components such as erythrocytes and leukocytes with more efficient nanorobotic versions such as respirocetes [6] and microbivores [2].

2.1 Molecular Transport

In natural human physiology, the circulating blood moves $\sim 2 \times 10^{26}$ molecules/sec. However, most of these molecules are solvent water not strictly necessary in human metabolism. In the vasculoid, all non-cell materials transport takes place via ciliary transport of tanker vessels at a very conservative mean transport velocity of 1 cm/sec. (For comparison, blood velocity in the natural vasculature ranges from 0.02–0.15 cm/sec in the capillaries up to 17.5 cm/sec pulses in the femoral artery ([4], Table 8.1).) Tanker vessels are (1-micron)³ mostly-sapphire (possibly chamfered) cubes with 0.75 micron³ useful interior storage volume and $\sim 8 \times 10^{-16}$ kg dry mass. Gases are stored in tankers at 1000 atm pressure [5, 6]; this is highly conservative, as a sapphire pressure vessel should easily withstand $\sim 10^5$ atm without bursting [4]. Liquids and solids are packed at normal macroscopic densities. All tanker mechanical subsystems (other than passive hull) have at least tenfold redundancy, hence are extremely reliable (Section 6). Tanker docking bays are described in Section 2.4.1.

The following is an approximate inventory and assessment of the minimum human physiological molecular transport requirement.

2.1.1 Respiratory Gases

The human body consumes $1\text{--}20 \times 10^{20}$ molecules/sec of O_2 , depending on activity level [6]. Similar numbers of CO_2 molecules are generated as waste products. The human red blood cell mass (~ 2.4 liters of RBCs) has a total storage capacity of 3.2×10^{22} O_2 molecules, but since hemoglobin operates between 70%–95% saturation in normal physiological conditions, the active capacity of human blood is only 8.1×10^{21} O_2 molecules. Blood CO_2 capacity is roughly the same, and O_2/CO_2 are loaded/unloaded reciprocally at lungs and tissues. Packing density of CO_2 molecules (1.11×10^{28} molecules/ m^3) is slightly lower than for O_2 molecules (1.26×10^{28} molecules/ m^3) at 1000 atm, so CO_2 packing density controls respiratory tanker population.

Assuming a mean circulatory circuit of ~ 1.4 meter and a 1 cm/sec transport speed, continuous transport at the maximum 20×10^{20} CO_2 molecules/sec rate requires a circulating fleet of 33.6 trillion respiratory gas tankers. At normal basal metabolic rates, only 1.68 trillion active tankers are required; the remainder are held in reserve to support periods of more intense physical activity. Each tanker can hold 9.48×10^9 oxygen molecules or 8.36×10^9 molecules of carbon dioxide at 1000 atm pressure. Highly efficient reciprocal regenerative energy recovery is assumed during gas loading and unloading operations (Section 2.4.1), and unrecoverable gas compression energy losses should be minimal. Isothermal compression of $\sim 10^{10}$ O_2 or CO_2 molecules requires $-P_i V_i \ln(V_f/V_i) \sim (10^5 \text{ N/m}^2) (0.75 \times 10^{-15} \text{ m}^3/\text{tanker}) \ln(1/1000) = 0.5 \text{ pJ/tanker}$. Assuming a need for 2×10^{20} molecules/sec for O_2 and CO_2 at basal demand implies $\sim 2 \times 10^{10}$ tanker fills/sec or ~ 0.01 watt for both sets of gases, or up to ~ 0.2 watts at peak demand, for compression of gases.

Conservatively taking the CO_2 concentration in the vasculoid–endothelium interface fluid as equal to the normal CO_2 venous plasma concentration of $C = 0.45\text{--}1.14 \times 10^{24}$ molecules/ m^3 ([4], Appendix B), then the diffusion limit for loading CO_2 from the tissues to one side of a square plate area of $L^2 = 2$ micron², with the diffusion coefficient $D = 1.9 \times 10^{-9}$ m^2/sec for CO_2 at 310 K ([4], Table 3.3), is $J = (4/p^{1/2}) \text{ LDC} = 2.7\text{--}6.9 \times 10^9$ molecules/sec ([4], Section 3.2.2); a 10-second fill time (Section 2.4.1) allows system operation at about one order of magnitude below the diffusion limit. Similarly, normal alveolar partial pressure of O_2 is >100 mmHg [6], or $C \sim 3.1 \times 10^{24}$ molecules/ m^3 ; taking $D = 2.0 \times 10^{-9}$ m^2/sec for O_2 at 310 K ([4], Table 3.3), the diffusion limit for loading oxygen at the lungs is $J \sim 2 \times 10^{10}$ molecules/sec, which again allows system operation at about one order of magnitude below the diffusion limit assuming a 10-sec tanker fill time.

Tankers are used to transport O_2 and CO_2 , rather than the vasculoid interior in part because the theoretical rupture pressure ([4], Eqn. 10.14) of the natural cylindrical aorta is $p_{\text{max}} \sim 1$ atm (taking aortic wall thickness $t_{\text{wall}} = 1.5$ mm ([4], Table 8.1), aortic radius $R = 12.5$ mm ([4], Table 8.1), and working stress $s_w \sim 10^6$ N/m^2 ([4], Table 9.3)) and the rupture pressure of the vasculoid plate coating is $p_{\text{max}} \sim 8$ atm (taking vasculoid plate tube thickness $t_{\text{wall}} = 1$ micron, tube radius $R = 12.5$ mm ([4], Table 8.1), and working stress $s_w \sim 10^{10}$ N/m^2 ([4], Table 9.3)). At peak exertion levels, respiratory gases stored in the tanker fleet at 1000 atm would fill the 4.2 liters of free vasculoid internal volume to 3.2 atm of pressure, too high for reliable safe operation under all foreseeable circumstances. By comparison, the rupture strength of individual tankers exceeds $\sim 40,000$ atm (the rupture strength of individual plates; Section 1.1).

2.1.2 Water

The human body excretes $6\text{--}12 \times 10^{20}$ molecules/sec of urinary water under normal circumstances [3, 4]. The kidney continuously filters ~ 18 gallons/hour of blood ($\sim 7 \times 10^{23}$ H₂O molecules/sec) so much higher rates of urine generation are possible in theory, but it seems unnecessary to accommodate the vasculoid design to such extreme cases because the removal of waste molecules can be accomplished by direct molecular sorting rotor extraction rather than by bulk filtration and solvent repumping – that is, the principle blood–cleansing function of the kidneys is to pump nonaqueous molecules, not bulk water solvent molecules [20, 21]. With the vasculoid in place, only specific waste molecules and minimal quantities of carrier water need be discharged into the glomeruli of the $\sim 10^6$ nephrons of the kidney, with the result that gross water flows through the kidney and energy consumption in this biological organ can be significantly reduced [22] – but not reduced so far as to induce urinary stone disease [23] (urinary lithiasis [24] or urolithiasis [25]) or renal cytotoxicity from excessive pH [26], salinity (e.g., hyperosmotic stress) [27, 28], or toxin concentrations [29]. The precise volume and concentration of urine generated by the biological organ is regulated by hormones that control kidney function [21, 30–34], and these hormones may in turn be regulated by the vasculoid appliance.

Additionally, $2\text{--}186 \times 10^{20}$ molecules/sec of water are perspired through the skin, depending upon air temperature, humidity, activity level and mental state [3, 4]. Assuming the same transport parameters as before, the maximum requirement of 2.0×10^{22} H₂O molecules/sec (~ 0.6 cm³/sec) requires 110.5 trillion water tankers to be available, of which only 4.5 trillion will normally be active with the rest held in reserve for periods of peak exertion. Each tanker can hold 2.51×10^{20} water molecules in the liquid state.

2.1.3 Glucose

Typically 1.6×10^{22} molecules of glucose are present in the human bloodstream [4]. A human on a standard 2000 kcal/day diet metabolizes 3.08×10^{19} glucose molecules/sec throughout the body. However, during strenuous exercise this requirement can briefly rise to as much as 33,000 kcal/day, a 4.93×10^{20} molecule/sec rate. Assuming the usual ciliary transport parameters, we require 17.6 trillion glucose tankers, providing storage of 6.91×10^{22} glucose molecules in the system, four times the number present in normal blood. (Slightly smaller capacity might be realized if the glucose must be stored as a 70% aqueous solution concentrate to facilitate molecular mobility for sorting rotors (e.g., [4], Section 6.3.4.4(B)).) Only 1.1 trillion glucose tankers are needed to service basal metabolic needs; the remainder are held in reserve for periods of extreme physical activity.

The average human cell is a ~ 30 picowatt (basal) device, so each glucose tanker, with its full complement of 3.93×10^9 glucose molecules, yields ~ 400 basal cell–seconds of energy (assuming 65% efficiency for the natural cellular metabolic pathways using glycolysis and tricarboxylic acid cycles [35]). Note that at higher power levels, the delivery rate increases correspondingly (Section 2.4.1), so that even with random delivery at peak demand all cells should receive a sufficient fuel supply. Additionally, the average tissue cell normally contains an internal inventory of $\sim 3 \times 10^{10}$ glucose molecules (Section 7.1), an in cyto buffer supply equivalent to ~ 8 full tanker loads.

2.1.4 Nonprotein Nitrogenous Molecules

Normal bloodstream concentrations [4] of urea, uric acid, creatinine, creatine, ammonium salts, cerebroside, amino acids, etc. imply 1.73–2.49 gm present in the circulation and a maximum of 2.3 trillion tankers for full encapsulation and transport.

2.1.5 Plasma Proteins

All plasma proteins including most notably albumen, globulins (including antibodies), complement, fibrinogen and prothrombin constitute ~7% of adult blood plasma, or 210 gm, which would require 215 trillion tankers to encapsulate. Fortunately, on a transactional basis this figure is a gross overestimate. The RDA (Recommended Daily Allowance) active requirement for protein is ~70 gm/day for a 70-kg male human, an 8.1×10^{-7} kg/sec transport demand requiring only 0.12 trillion protein tankers for continuous ciliary transport, reducing mandatory instantaneous system storage capacity to ~0.12 gm of plasma proteins. However, almost the entire RDA protein intake is hydrolyzed to amino acids and dipeptides, so the actual protein transport needs should be far less. With no need to maintain osmotic pressure, there would be almost no reason to transport albumin within the system, although the dosage of protein-bound medication and hormones might need to be corrected. Finally, there is sufficient tanker capacity to increase protein transport capacity at least 100-fold above the RDA requirement if necessary, so the design is not particularly sensitive to this transport requirement.

Note also that the five antibody classes can be efficiently transported using just five types of sorting rotors having binding pockets complementary only to the constant Fc regions without regard to the numerous variable domains these antibodies may encode on their antigen-binding Fab regions, thus vastly reducing the required vasculoid rotor specificities needed to accomplish this task. Complement (immune system) components may be transported with similar efficiency.

The limited free enzyme activities that occur in natural blood can still take place in the fluids at the vasculoid-endothelial interface, with due care taken to avoid inducing localized hyperenzymemia [36] (which is often benign, as in hypertransaminasemia [37, 38]), although higher concentrations may be expected because of the lower total volume of the vasculoid-endothelial interface compared to the natural blood volume.

2.1.6 Lipids

The mass of lipids including fatty acids, cholesterol, triacylglycerides (transported in the plasma lipoproteins as triacylglycerols), and phospholipids present in the human bloodstream totals roughly 35–42 gm [4], which would require 55–66 trillion tankers to encapsulate. However, the RDA for fat is 23% of caloric intake. (Many people consume several times this amount, but others survive on fat-free diets, so the figure represents a reasonable compromise estimate of the typical human active requirement.) This implies a demand of 6.9×10^{-7} kg/sec for a 2000 kcal/day diet, requiring only 0.15 trillion lipid tankers for continuous ciliary transport and reducing the required vascular storage capacity to ~0.1 gm. As with plasma proteins, there is sufficient tanker capacity to increase lipid transport capacity to at least 100 times the RDA requirement, so once again the design is not particularly sensitive to this transport requirement.

2.1.7 Other Molecules

Human blood plasma contains ~40 gm of salts (e.g., electrolytes) including sodium, potassium, calcium, magnesium, chloride, phosphate, and sulfate; ~1.2 gm lactic acid and other non-nitrogenous waste products; ~0.23 gm of RNA and DNA; ~0.21 gm of enzymes (protein); ~0.15 gm testosterone in the male, ~0.03 gm progesterone in the female, ~0.02 gm of corticosteroids, and a total of ~0.002 gm of more than fifty other major biologically active hormones; ~0.04 gm of vitamins including A, B2, niacin, pantothenic acid, biotin, pteroylglutamic acid, choline, inositol, C, D, and E; ~0.03 gm of essential trace elements including iron, zinc, copper, manganese, iodine, and cobalt; and smaller masses of various cell-signaling (e.g., cytokines, autocrines, neuropeptides) and numerous other specialty proteins [4]. Other nonprotein regulatory molecules affecting numerous signaling pathways must also be locally regulated with precision by the vasculoid appliance. For example, in the present context the simple molecule NO is of particular importance as a neurotransmitter and vasoconstrictor [39, 40], though it is normally present only in exceedingly small quantities. Other molecules that mediate certain regulatory pathways may become unnecessary to transport after the vasculoid is installed, as for example the renin-angiotensin pathway (since there is no blood pressure to regulate).

The capacity demand totals ~43 gm, which would require ~43 trillion tankers for full encapsulation. However, the RDA for all minerals, electrolytes, vitamins and trace elements is just 6.8–16.1 gm/day for healthy adults, a maximum of 1.87×10^{-7} kg/sec, requiring only 0.03 trillion tankers assuming ciliary transport parameters as described above. (Sodium and potassium ion transport in individual neurons is $\sim 10^6$ ions/discharge; assuming $\sim 10^{10}$ active neurons firing at near-maximum ~ 100 Hz, whole-brain ion transport rate is $\sim 10^{18}$ ions/sec or $\sim 7 \times 10^{-8}$ kg/sec, well within the aforementioned mass flow budget for mineral and electrolyte transport. However, Na^+ and K^+ are very quickly recycled after each discharge, so the true transport requirement is more accurately measured by the small amounts of these electrolytes that are lost in the gut, sweat, and lymph.) Transport of lactic acid, RNA/DNA, enzymes (e.g., those present as a result of normal tissue breakdown such as CPK and transaminases), hormones, cytokines and so forth (~1.8 gm) requires 1.9 trillion additional tankers. In some cases these “other” molecules may be shipped mixed in a single container (Sections 2.4.1 and 2.4.3).

2.1.8 Summary of Molecular Transport

A total of 166.2 trillion tankers are required to transport all-important physiological molecules at maximum human metabolic rates. At basal metabolic rates, only 11.78 trillion tankers will typically be active. If, contrary to our assumption, RDA levels are found to be an inadequate substitute for natural blood storage of plasma proteins, lipids, minerals and vitamins, or if production and demand occur at different times and the blood volume performs a significant storage function, then vasculoid design may need to include up to ~300 cm³ of auxiliary bulk storage or caching (Section 8.3) to extend the “just in time” inventorying of these vital substances.

2.2 Cellular Transport

In addition to conveying molecules, the vasculoid must also transport physiologically important cellular species throughout the body. Cells to be transported (comprised mainly of white cells, platelets, and the few remaining red cells) generally range in size from 2–20 microns [41]. These are shipped in cylindrical mostly-sapphire “boxcars” 100 microns long and 6 microns in diameter. These containers, of which 75% (2120 micron³) is usable storage volume (~2.4 x 10⁻¹² kg dry mass per boxcar), will just fit through average-sized capillaries (~8 microns diameter, ~1000 microns in length) and all larger vessels, after accounting for plate thickness, and thus the boxcars have access to the vast majority of human tissues. The largest transportable cells (20-micron monocytes) must be temporarily dehydrated 50% by volume prior to loading*; such desiccated cells quickly rehydrate by natural osmosis upon release into the aqueous intercellular environment. Spherical cells 17.5 microns in diameter or smaller need not be dehydrated during loading, as they can fit into the available volume via change of shape. Typical transit time from point of entry to point of debarkation is ~70 sec (i.e., half the mean circuit length of 1.4 m, at 1 cm/sec; Section 2.3.2), well within cellular ischemic survival times (Section 7.1) except possibly for oxygen, which may need slight supplementation during transit.

Onboard computers and sensors embedded in interior boxcar walls allow the detection and interpretation of surface antigens on passenger cells to ensure that all transported cells are non-hostile, and if not, to refuse transport, convey them to a disposal site (Section 8.5), or destroy them after entry. Boxcar docking mechanisms (cellulocks) are described in Section 2.4.2, and small-capillary avoidance is discussed in Section 2.4.4.3.

The following is an assessment of the minimum human cell transport requirement for the vasculoid appliance.

* Most mammalian cells can survive the loss of 50% of their water [41]. Fibroblasts (e.g., mouse L-929 cells) have survived from 45% [42] to 65% [43] decrease in total cell volume (the latter representing 85% water loss by volume [44]) via dehydration, and erythrocytes have survived 73% volume reduction by dehydration [45]. Alternatively, desiccation for transport may be avoided by doubling boxcar length, but at the cost of decreased vehicle mobility, larger turning radius, and so forth – design tradeoffs that deserve further investigation.

2.2.1 Leukocytes and Stem Cells

Under normal physiological conditions, 27–54 billion leukocytes circulate in the human blood volume [4], although in cases of chronic myelogenous leukemia the total count may increase to 0.13–2.7 trillion white cells [46]. These 54 billion leukocytes consist approximately of 35–41 billion neutrophils (10–12 microns in diameter), 11–14 billion lymphocytes (8 microns), 1.6–4.3 billion monocytes (12–20 microns, average 15 microns), 1.1–2.7 billion eosinophils (12 microns), and 0.3 billion basophils (10 microns). Based on maximum container packing densities for each type of cell, 12–28 billion boxcars are required to encapsulate and transport all normal populations of bloodstream leukocytes. This will frequently include more than one cell per boxcar – multiple cells should be sedated for transport (using reversibly rotoed molecular agents) to avoid unwanted interactions such as clonal expansion or induction of apoptosis. Principal origination sites are the bone marrow, the spleen, and the lymph nodes, but leukocytes may be distributed to almost any location in the body. Giant macrophages (e.g. >30 microns) and fibroblasts already present in the tissues (that normally do not enter the bloodstream) cannot be relocated by the appliance, although fresh stem cell precursors of fibroblasts with appropriate activating cytokines can be relocated from their natural source site, as required.

A comparatively small population of circulating stem cells must also be transported by the vasculoid. For example, vasculogenesis is assisted by hematopoietic stem cells (surface marker CD34+) that originate in the bone marrow and enter the peripheral blood in response to colony stimulating factors, with 1–3% expressing the common leukocyte surface antigen CD45. Upon reaching the vascular surface and in the presence of the cytokine IL-3, these cells may differentiate either into leukocyte precursor (CD34+/CD45+) or into endothelial precursor (CD34+/CD45-). With the cytokine VEGF present, the latter cells further differentiate into new endothelial cells [47, 48]. The vasculoid must provide transport for stem cells of these and other types, along with the required cytokines, to ensure vascular repair of damaged endothelium and for other purposes. Fortunately there are only a limited number of such cell types, and the total population of stem cells requiring transport is many orders of magnitude smaller than the population of leukocytes. As a result, stem cell transport should be a comparatively minor – if physiologically essential – task for the previously-specified boxcar fleet.

2.2.2 Platelets

Although substitution of vasculoid transport for liquid blood eliminates much of the conventional health risk due to bleeding, blood vessel breaches that penetrate the endothelium but do not penetrate the vasculoid will still exude large amounts of extracellular serous fluid and other critical substances if the leakage is not promptly staunched.* Furthermore, platelets are storehouses for a variety of molecules that affect vascular tone, fibrinolysis (subsequent clot dissolution), and wound healing. These substances are released during the clotting process. Platelets also communicate via chemical messengers with other blood cells (e.g.

macrophages and fibroblasts) and with the endothelial cells that coat the interior of all blood vessels. Hence, platelets still have an important role in human physiology even after the vasculoid has been installed.

Approximately 2 trillion platelets (~2 microns in diameter) circulate in human blood [4]. Each boxcar can hold about 500 platelets, giving a requirement of 4 billion additional containers for platelet transport. As with white cells, multiple cells could easily activate and aggregate, hence their function should be heavily suppressed during transport (again, using reversibly rotoed molecular agents).

* A more effective response to such a breach might be the release of activated clotting factors, which are likely more stable during transport, rather than whole platelets.

2.2.3 Erythrocytes

In the vasculoid, all respiratory gases are transported in bulk and at high pressure. Boxcars could in principle be used to transport red cells, but RBCs have an effective storage pressure $\ll 1$ atm which is far less efficient than the 1000 atm storage pressure of the respiratory gas tankers. Consequently, the ~30 trillion red cells normally present in the human bloodstream [4] are superfluous and may be permanently removed from circulation. Beyond their respiratory function, red cells also are mechanically involved in the clotting process. However, the vascular plug typically contains mostly platelets, plasma fibronectin and factor XIII–crosslinked fibrin, plus small amounts of tenascin, thrombospondin, and SPARK (secreted protein acidic and rich in cysteine) [49] with a relatively minor RBC contribution, so RBCs probably are not essential to the clotting process or are necessary only in very small numbers.

A sufficient oxygen concentration maintained in kidney peritubular cells should reduce erythropoiesis to at most 1% of the normal rate of red cell production [6], requiring only ~34,700 red cells/sec to be conveyed from the erythroid marrow directly to the liver or spleen for disposal. Alternatively, erythropoiesis can be reduced by directly regulating the amount of erythropoietin that is allowed to reach the bone marrow. With few erythrocytes remaining to be destroyed in the liver, hepatic heme catabolism drops significantly, greatly reducing the production of bilirubin, a yellow bile waste pigment that plays no role in fat digestion in the gut but imparts the brown color to feces; as with hepatitis patients, the stool of the envasculoided user may become chalky white. Ciliary transport of boxcars containing the few remaining red cells over a ~1.4 meter circuit at a conservative mean velocity of 0.1 cm/sec (allowing plenty of time for docking and cell unloading) requires a circulating subfleet of just 34.7 million boxcars (only ~0.1% of the entire boxcar fleet).

2.2.4 Summary of Cellular Transport

A maximum of 32 billion boxcars are required to convey all essential bloodborne cells during normal physiological conditions, although at times as few as 16 billion boxcars may be actively involved in cellular transport. Since a principal benefit of vasculoid installation is a significant decline in susceptibility to microbial invasion, the above figures can probably be further reduced in actual clinical practice.

2.3 Ciliary Distribution Subsystem

The interior volume of the vasculoid is lined with a sapphire surface (comprised of watertight adjacent installed plates) from which protrude trillions of mechanical cilia ([4], Section 9.3.1.2) arranged in patterns designed to maximize transport speed and reliability. A secondary role is to assist the vasculocytes (small mobile nanorobots; Section 2.5) in cleaning up after accidental internal spills, component malfunctions, or other pathological events. Even by 1997 [50], prototype MEMS ciliary arrays ([4], Section 9.3.4) of up to 1024 cilia had already demonstrated transport speeds up to 200 microns/sec with ~3 micron positional accuracy.

2.3.1 Description of the Cilium

While a highly efficient specialized ciliary mechanism can undoubtedly be designed, for the present study each vasculoid cilium is conservatively assumed to be similar in size, shape, and performance characteristics to the vacuum-sealed robotic manipulator arm described by Drexler [7]. In brief, each cilium is a cylindrical assembly 100 nm long and 30 nm in diameter, having a transverse travel of 100 nm and a lateral speed of 1 cm/sec, consuming 0.1 picowatt during continuous operation at low load. Note that even if the vasculoid interior contained gas at 1 atm, viscous drag would contribute an additional power loss of only ~0.001 pW per cilium ([4], Eqn. 9.75, taking viscosity $\eta_{\text{air}} = 1.83 \times 10^{-5}$ kg/m-sec at 293 K).

Mean cilium/cargo contact time is ~10 microseconds. This implies an acoustic frequency >100 KHz, well above the conventional human threshold of hearing; however, ultrasonic hearing up to 108 KHz via otolithic conduction has been reported in humans [51], so further study is required to ensure restriction of transport motions to sufficiently high frequencies to preclude any perceptible hum directly due to ciliary operations, and possibly involving a variety of noise cancellation [52], anti-resonance (e.g., out-of-phase operation) and acoustic dampening techniques. Additionally, physical discomfort [53], intra-articular pain [54], and a lowering of electrical pain sensation threshold [55] due to ultrasound exposure have also been reported in humans. The possibility of indirect audible or infrasonic vibrations due to beat frequencies, spatial acoustic interference patterns, or various resonances should be investigated further, along with the possibility of undesired vibrational energy losses into the tissues.

Each cilium can apply ~1 nanonewton at the tip. This is sufficient force to accelerate a 1 micron³ block of water (weight ~0.01 piconewton) at 10⁵ G, or a 100–micron long, 6–micron wide water–filled sapphire–shell cylindrical boxcar at ~30 G. The human body is normally subject to accelerations far less than 30 G; with tenfold grasping redundancy (Section 2.3.2), the probability that a container will be shaken loose from the cilia and tumble uncontrolled into the vascular lumen, due to normal macroscale accelerations of the patient's body, is extremely remote. In the rare instance where such detachment occurs, the container will eventually be caught and returned to the flow; kinetic impact energy in such cases is relatively small. Whether such cross–luminal impacts can trigger a detachment avalanche should be investigated using computer simulations.

Changeable cilium tool tips may permit rapid, reversible, “blind” container grappling using van der Waals adhesive forces, which forces may be controlled by varying adhesive pad surface corrugations at the nanometer scale, or by other means. The cilia might also have a reversing function (e.g., for loosening container jams). Molecular dynamics simulations of these processes would be useful.

2.3.2 Ciliary Subsystem Requirements

The principal task of the ciliary distribution subsystem is to reliably transport a maximum of 166.2 trillion 1–micron cubical tankers and a maximum of 32 billion cylindrical 6 mm x 100 mm boxcars through a physical circuit ~1.4 meters in length. Because of their smaller size and greater number, ciliary subsystem design is driven almost entirely by tanker, not boxcar, requirements.

Although a single cilium can apply sufficient force to grapple and manipulate containers of either size, tenfold grappling is employed in the baseline design to achieve firm contact, to avoid physical escape of containers from the cargo traffic stream, to ensure massive redundancy hence high subsystem reliability, and to allow extremely precise steering. If a tanker occasionally encounters a patch of 9–contact cilia, or the even rarer 8–contact patch, steering or grappling capability should not be significantly reduced. Fail–safe grappling modes must be designed for cilium end–effectors.

Each tanker is normally in continuous contact with 10 cilia at all times during transport, so maximum ciliary spacing is 0.32 micron. A minimum of 3000 trillion cilia are needed to achieve 100% service over the entire ~300 m² vascular (mostly capillary) surface. A set of 3000 trillion cilia physically occupies ~2.1 m² (~7%) of the vascular surface. Assuming natural background radiation damage causes 1.5 x 10⁷ fatal hits/kg/sec [7] for nonredundant structures, the mean time to failure of a ~10⁻¹⁹ kg cilium is ~10¹² sec, which implies a mean failure rate of only ~2000 cilia/sec (~20 nanograms/day) throughout the entire vasculoid. Using redundant structures, mean failure rate may be considerably reduced.

Under resting metabolic conditions, 11.78 trillion tankers are transported by 117.8 trillion cilia generating waste heat of ~11.8 watts, an increment of only ~12% over the basal human metabolic rate. During periods of maximum exertion and thermoregulatory stress, 166.2 trillion tankers are transported by 1662 trillion cilia generating excess heat of ~166 watts, well below the maximum human metabolic rate of 1600 watts and just

slightly exceeding the ~100 watt effective load error [56] that could trigger a response from the human thermoregulatory control system ([4], Section 6.5.2).

2.4 Docking Bays and Cellulocks

Once molecules or cells have been transported to the appropriate site, the container in which they reside must dock with the vasculoid surface on the interior side, and pass the delivered materials through this surface to the interstitial side of the vasculoid wall, whereupon the cargo can diffuse or migrate into the tissues as required. Tankers offload their molecular cargo in docking bays (Section 2.4.1) whereas boxcars unload their cellular passengers at cellulocks (Section 2.4.2).

Possible undesired long-term chemical interactions of transported nutrients discharged into the fluids of the vasculoid-endothelial interface at above-physiological concentrations must be carefully analyzed. For example, high concentrations of glucose akin to chronic hyperglycemia [57] could enhance protein glycosylation of long-lived proteins (e.g., vascular and myocardial collagen) which undergo continual cross-linking during aging because of the formation of advanced glycosylation end-products (AGEs) [58], most significantly (for this paper) in endothelial cells [60] which may be partly responsible for arterial stiffening and higher blood pressure with age (and which drugs like ALT-711 [58, 59], benfotiamine [60], nitric oxide [61] and other substances may reverse). AGEs can also induce apoptosis and vascular endothelial growth factor overproduction in capillary pericytes [62].

2.4.1 Docking Bays for Tankers

Physiologically relevant molecules are delivered to specific locations by docking at 2 micron² (~1.4-micron square) tanker docking bays embedded at appropriate spatial intervals across the vasculoid surface. After securely connecting to the docking bay structure, and after the tanker's cargo manifest is scanned by the docking bay computer and said cargo is approved for receipt (Section 5), the tanker can be pumped dry by molecular sorting rotors in ~10 seconds, then sealed, remanifested, undocked, and released empty back into the traffic. Empty tankers may be reloaded with molecular cargo by a similar process in a similar time. Note that tankers carrying liquid or gas may discharge their contents into the narrow end of a funnel-shaped manifold leading to the active rotor banks at the wider end, to minimize the required tanker connection aperture. In different operating modes, tankers might be only partially emptied at each stop, or might be partially emptied more rapidly via bulk-flow exhausting rather than molecular rotoring. Docking bays include buffer tanks so that offloaded materials can be metered out to the underlying tissues over time periods longer than 10 seconds.

If the average endothelial cell (of which blood vessel walls are comprised) has a flat luminal area of 300–1200 micron² [63], then the ~300 m² vascular surface may be comprised of up to ~1 trillion endothelial

cells.* This vascular surface could theoretically accommodate a maximum of 300 trillion tankers positioned side by side. At basal metabolic rates, only 11.78 trillion tankers are actively on the move (Section 2.1.8). Even during peak exertion, a maximum of 166.2 trillion tankers are being transported, requiring just 55% of the available vasculoid luminal surface for their passage assuming all tankers are traveling in monolayer (Section 2.4.4.4). Other functionally equivalent modes might include operating all tankers at reduced capacity or reduced duty cycle during periods of basal demand, or reducing the transport velocity. A detailed computer simulation study of optimal traffic patterns near peak capacity would be valuable to perform.

A maximum of 166.2 trillion tankers circulating through an average ~1.4 meter circuit at ~1 cm/sec implies a docking bay cargo unloading requirement of ~1.2 trillion tankers/sec. Docks operate on a 50% duty cycle to allow plenty of time for maintenance and repair, although in a less conservative design the duty cycle could possibly be boosted as high as 99% (Section 2.5). Tankers are emptied in 10 sec, so ~24 trillion docking bays are needed for reliable operation at peak loads. Docking bays occupy ~16% of the vasculoid surface and have a mean center-to-center separation of ~3.5 microns. Each endothelial cell is serviced by up to ~24 docking bays.

Normally only a small fraction of the body's tissue cells are directly bathed in blood. Hence, delivery of molecules to each endothelial cell surface must be sufficient to supply the needs of the up to ~30 tissue cells that lie, on average, within ~3 cell widths of the nearest capillary. The maximum whole-body transport requirement of 2.25×10^{22} molecules/sec, consisting principally of respiratory gases, water, and glucose, gives an endothelial surface mass transport rate of 2.25×10^{10} molecules/sec/endothelial cell. This transport rate may be satisfied using a minimum of 45,000 molecular sorting rotors (for description, see [4–7]) per endothelial cell operating on a 50% duty cycle.

With 24 docking bays per endothelial cell, the requirement is ~0.94 billion molecules/sec per docking bay. Allowing tenfold multiplicity of sorting rotors to ensure high reliability (Section 6) requires 18,750 sorting rotors per docking bay, of which only 57 will be active at the basal rate and up to 9375 will be active during maximum physical exertion; 18,750 sorting rotors measuring 98 nm^2 on the ventral surface (facing the endothelium) [6] cover 1.84 micron^2 , essentially coating the entire undercarriage of the 2 micron^2 docking bay facility. This provides a $\sim 7.5 \times 10^8$ molecule/sec supply per tissue cell.

At peak metabolic load, maximum molecule offloading rates as constrained by possible effervescence and crystallence effects ([4], Section 9.2.6) appear acceptable in this application for all low-volume molecules and for glucose and CO_2 , but unfortunately exceed the effervescence limit for O_2 by a factor of ten, due to the relatively poor aqueous solubility of oxygen. Hence at peak load this gas must be offloaded either ~10 times more slowly than indicated above for a single release site, or at the indicated flow rate from ten discrete release sites all spatially separated by more than the largest possible O_2 effervescence bubble radius.

To simplify rotor system design, there are four classes of docking bays approximately matching the anticipated four principal tanker populations. Of the ~24 docking bays overlying each endothelial cell, ~5 stations are designated to handle tankers carrying respiratory gases, and possess rotors (on the tissue side) designed to reversibly bind only oxygen or carbon dioxide molecules. Another ~14 docking bays receive only water-bearing tankers, and employ rotors specializing in water molecule transport. Another ~3 stations accept only glucose cargoes, and use only glucose sorting rotors. The remaining ~2 docking bays are

general-purpose stations equipped with rotors of up to tens of thousands of different types capable of reversibly binding all remaining biologically useful molecules (or classes of molecules) that must be transported through the vasculoid surface.**

In addition to gas, water, glucose, and specialty tankers, there is a fifth class called power tankers that support the docking bay oxyglucose metabolism. Power tankers transport stoichiometric parcels of oxygen and glucose, and also remove carbon dioxide byproduct for disposal at the lungs. (Vasculoid power may be generated by glucose engines, glucose fuel cells, or other energy conversion devices that consume oxygen and native glucose ([4], Section 6.3.4); water produced by glucose engines may be vented into the biological tissues.) All docking bays can accept power tankers, which supply the docking bay's own internal energy needs. Tankers reload their own oxyglucose engines and fuel tanks as they make their rounds of the various docking bays. Tanker duties are not energy intensive, so tankers refuel at most once a day, at the docking bays.

Rotors conveying molecules from tankers (at high concentration) through the vasculoid integument to the endothelial surface (at low concentration) generate positive mechanical energy, which may be used to largely offset the work of concentration that must be expended to transfer molecules in the reverse direction when loading tankers from the tissue space. Concentration work losses can be reduced almost to zero in an efficient system, with systemwide entropic losses in the compression-expansion cycle as low as 0.01–0.2 watts (Section 2.1.1). Hence the primary energy loss is the drag power per rotor, $\sim 10^{-16}$ watts or ~ 0.1 zJ/molecule assuming a transfer rate of $\sim 10^6$ molecules/rotor-sec ([7], Section 13.2.1.e). Taking the whole-body transport requirement range as $10\text{--}225 \times 10^{20}$ molecules/sec, the net molecular transport power dissipated per docking bay is thus 0.004–0.09 picowatt depending on physical exertion level, or 0.1–2.25 watts for the entire vasculoid docking bay subsystem. (Rotor systems that do not include efficient energy recovery and must dissipate the work of concentration, perhaps up to ~ 20 zJ/molecule ([4], Section 3.4.2), may require a different appliance architecture.)

To hold docking bay subsystem total power requirement for computational tasks to a 10-watt budget, nanocomputers using an appropriate mix of local and distributed computing costing $\sim 6 \times 10^{-17}$ watts/(ops/sec) [4, 7] can provide ~ 200 billion MIPS systemwide or $\sim 10,000$ ops/sec per docking bay (Section 5), costing ~ 0.6 pW per docking bay. These rates have been enhanced by employing reversible logic [4, 7, 64]. Hence the total power per docking bay for both mechanical and computational tasks ranges from ~ 0.604 pW (basal) to ~ 0.69 pW (peak), or 14.5–16.6 watts for the entire system of 24 trillion docking bays. If power is supplied by a glucose engine achieving mechanochemical power conversion at $\sim 10^9$ watts/m³ [4–7], a 16.6 watt peak energy budget for all docking bays requires one glucose engine only ~ 0.0007 micron³ in volume ($\sim 0.03\%$ of bay volume), per dock, and a similar volume of fuel tankage.

* Cardiac endothelium or endocardium [65–67] has a somewhat different cell shape and cytoskeletal organization than vascular endothelium, and differences in permeability compared to the coronary vascular endothelium.

** This is almost certainly a significant overestimate of the needed capabilities. For instance, to reduce the required number of specific recognition devices (and thus decrease system complexity), R. Smigrodzki suggests using devices packaging all molecules of a particular size class, plus a few specific transporters for

small ligands. R. Bradbury notes that heavily multipurpose rotor banks may be needed only at the capillaries of the intestine and liver. It will soon be known exactly which hormones are supposed to be delivered at what levels to specific organs (e.g., insulin going mostly to the muscles and liver, erythropoietin to the bone marrow, etc.), requiring the transport of much lower quantities of most of these molecules because they can be targeted more precisely to the tissues that use them as signals.

2.4.2 Cellulocks for Boxcars

Biological cells are delivered to specific locations by docking at cellulock stations embedded at appropriate intervals across the vasculoid surface, often preferentially located near specialized post-capillary blood vessels less than 30 microns in diameter found in lymphoid tissues, commonly known as high endothelial venules (HEVs) [68–73]. Cellulock density requirements also vary on a tissue-by-tissue basis – for instance, intestines, lungs, throat and nasal cavity probably have much higher requirements than heart or brain. After securely docking with their loading face pressed firmly against the vasculoid surface, boxcar doors dilate open to make a 30 micron² (~6.2-micron diameter circle) aperture. Cellulock doors (constructed of self-cleaning sliding spiral graphene segments in snug facial contact) then dilate to the same diameter, exposing passenger cells to the interstitial fluid. Passenger cells are gently pistoned out through the opening, taking care to minimize extracellular fluid entry. The cycle ends as all doors reseal and the boxcar undocks, resuming its travels.

Biochemical signals of cellular distress (e.g. cytokines such as interleukin–1 or tumor necrosis factor) are received by sensors on the interstitial side of the vasculoid. Upon receipt of this chemical signal, the cilia at that site are programmed to call for leukocyte activity there. Cellulock and boxcar interiors may employ a small set of presentation semaphores [4] which expose to the interstitial fluid minute quantities of various chemoattractants [74, 75] and chemorepellents [75–78] keyed to each major type of cell to be transported. These chemicals are permanently bound to the rotors and are not released from the vasculoid; like semaphores, each rotor position may present differing concentrations of one chemical species, or a selection of different chemical species. White cells of the type desired to be transported can be encouraged to enter or exit, as required, by positioning presentation rotor settings so as to create “chemotactic funnels” – programmable patterns of varying concentration gradient to steer motile cells toward, or away from, the cellulock aperture (e.g., haptotaxis [79–81]). Contact sensors around the aperture detect the presence of a motile cell “requesting entry” to the transport system. Motile cells presenting themselves for entry at the interstitial side of the cellulock are, at minimum, subjected to a rudimentary cell protein coat identification test before they are allowed admittance. Affirmatively recognized harmful foreign pathogens such as bacteria or viruses and infected native motile cells may be transported to a specific disposal site or destroyed (Section 8.5), rather than being admitted freely for transport elsewhere in the tissues.

The cellulock mechanism covers 60 micron² (~7.7-micron square) of vasculoid surface. If spiral door segments slide past each other at 0.004 m/sec over an average of one-half rotation or ~15.4 microns, dilation (or resealing) of the cellulock door takes 3.85 milliseconds. Sliding friction for 16 nm² contact surfaces traveling 20 nm at 0.004 m/sec dissipates ~10⁻²⁴ joules, or ~3.13 joules/m²-meter [7]. Thus ~30 micron² cellulock sliding door surfaces moving ~15.4 microns to open, then again to close, require ~3 x 10⁻¹⁵ joules to

complete one dilation cycle. Assuming a maximum rate of 32 billion boxcars per (normal blood circulation time of) ~60 sec to emulate typical physiological delivery rates, the population of vasculoid cellulocks must process a total of 533 million boxcars/sec. If there are therefore also 533 million cellulock dilation cycles/sec, frictional waste heat generated by moving door segments in the entire vasculoid cellulock subsystem is a negligible ~1.5 microwatts. Taking cellulock power as equal to the basal rate for 30 docking bays gives a requirement of ~18 pW/cellulock, or ~0.59 watts for the entire cellulock subsystem. Serum glucose and oxygen to provide cellulock power (a minor volumetric requirement) may be rotated in directly from the interstitial fluid on the external side of the vasculoid surface.

Since the active tanker/boxcar ratio varies from 736 (basal) to 5194 (max) depending on metabolic load, there should be no less than one cellulock per 736 tanker docking bays, or a total of 32.6 billion cellulocks in the vasculoid surface, again allowing a 50% duty cycle for maintenance and repair. Thus there is approximately one cellulock for every boxcar in circulation. Cellulocks occupy ~0.65% of the vasculoid surface and have a mean center-to-center separation of ~96 microns. Each cellulock services an average of ~31 endothelial cells, though the actual spatial distribution of cellulocks is expected to be highly nonuniform (e.g., clustering near HEVs). The average capillary is ~1 mm long and is made up of ~60 endothelial cells, and there are ~19 billion capillaries in the human body ([4], Table 8.1), so on average ~1 cellulock resides at either end of every capillary vessel in the body.

The maximum white cell transit rate through injured or diseased tissue is ~1 cell/sec/mm³ [82]. With 32.6 billion cellulocks there are ~163 cellulocks/mm³ of tissue. Each cellulock has ~163 sec to pass each white cell, even at maximum traffic flows. This should be sufficient, given that cellulock doors open and close in milliseconds, and natural white cell transendothelial diapedesis may occur in as little as ~3 minutes [4]. The creation of unnecessary interior voids where unwanted opportunistic pathogens might flourish should be avoided. It is probably unnecessary to maintain voids between vasculoid and endothelium near cellulocks because: (1) the time allocated to cycle the cellulocks appears adequate to permit WBC diapedesis, and (2) diapedesis can probably be expedited using chemical factors emitted by the vasculoid.

2.4.3 Container Routing and Identification

The ideal method for container routing will be completely automatic, consuming no incremental power or compute cycles. To this end, the outer surfaces of each of the five types of tankers (Gas, Water, Glucose, Power, and Other) and the four types of boxcars (Red Cell, White Cell, Platelet, and Other) bear a specific repeating interlock pattern ([4], Section 5.3.2.5), crudely analogous to Braille. These patterns remain in place on the container surface unless the container is affirmatively “reset” to carry a different cargo, in response to varying physiological needs and local container availability.*

Cilia surrounding each docking bay or cellulock are outfitted with gripper pads (Section 2.3.1) that adhere adequately to all container surfaces, but strongly only to the surface pattern of the container type sought by the docking bay or cellulock with which the cilia are associated. These pad “recognition” types normally remain constant over time, but, like the container surfaces, may be modified as required in special circumstances. Efficient methods for handling Other-type tankers that can avoid the need for time-consuming docking and

downloading of manifests should be investigated further.

Cilia that have “recognized” a desired container transmit a trigger signal to nearby cilia, activating a collective stereotypical docking sequence. Thus, although containers follow statistically random paths across the vasculoid surface, each docking bay and cellulock automatically receives the cargo it requires from the passing container stream. Docking acquisition is demand–regulated locally.

* R. Smigrodzki suggests that a more sophisticated system might employ rewritable tags for (a) the trafficking of waste, (b) the transport of nutrients in the hepatic portal system, and (c) the transport of hormones in the hypothalamic–pituitary portal system. Gas carriers could also be routed between lungs and peripheral tissues, while the bulk of the other carriers would never visit lungs, instead circulating between the gut, kidney, and the peripheral tissue.

2.4.4 Potential Transport Bottlenecks

The exemplar vasculoid has been scaled to transport essential molecules and cells at maximum physiological transfer rates. However, all engineering systems involve design tradeoffs and limitations, and the present design invokes a number of potential transport bottlenecks including intestinal water absorption and renal water elimination (Section 2.4.4.1), glucose absorption and elimination at peak loading (Section 2.4.4.2), boxcar geometrical clearance in narrow capillaries (Section 2.4.4.3), and geometrical limitations of tanker monolayer transport (Section 2.4.4.4).

2.4.4.1 Water Absorption and Elimination

The ~6 meter–long intestinal tract has a simple cylindrical surface area of ~0.65 m², but the ~5 x 10⁶ villi of the small intestines (which is most of the length) increase the effective absorbing surface to ~10 m² [4]. The ileum, the lower portion of the small intestine, absorbs water into the bloodstream at the maximum rate of ~0.07 cm³/sec. The cylindrical villi, typically measuring ~200 microns wide and ~1000 microns long, are heavily capillarized; assuming ~1000 capillaries/mm³, each villus has ~30 capillaries presenting a total ~8 x 10⁵ micron² of absorbing surface – for the entire ileum, that's ~4 x 10¹² micron², a water transport rate of ~6 x 10⁸ molecules/sec–micron². If maintenance activities are temporarily suspended during peak demand, water tankers loaded with 2.51 x 10¹⁰ water molecules at 2 micron² docking bays can provide the same transport rate of 6 x 10⁸ molecules/sec–micron² if 49% of the vasculoid surface in the ileum is given over to water transport – potentially crowding out some “applications plates” at this surface. (The requirement for alimentary water can also be greatly lessened by reducing the need for water solvent in urine (Section 2.1.2), by reducing the need for water cooling in sweat (Section 8.2), and possibly by reducing water losses in the

alveoli (which could be covered with an improved waterproofing surfactant.)

Excretion of $\sim 0.023 \text{ cm}^3/\text{sec}$ aqueous waste at the kidneys occurs primarily through the renal glomeruli which have a total surface area of $\sim 1.4 \text{ m}^2$, giving a maximum water export rate of $\sim 5 \times 10^8$ molecules/sec–micron². If maintenance activities are temporarily suspended during peak demand, water tankers loaded with 2.51×10^{10} water molecules at 2 micron² docking bays can provide the required transport rate if 40% of the vasculoid surface in the glomeruli is given over to water transport. The $\sim 0.001 \text{ gm}/\text{sec}$ ($\sim 4 \times 10^6$ molecules/sec–micron²) solute waste stream is conveyed on mixed–cargo tankers carrying $\sim 10^9$ solute molecules per tanker, which may be unloaded at mixed–cargo docking bays covering only 8% of the vasculoid surface in the glomeruli. Other aspects of water transport in relation to kidney requirements are discussed in Section 2.1.2.

2.4.4.2 Glucose Absorption and Elimination

Glucose is absorbed in the small intestine, mostly in the duodenum and the jejunum, at a maximum rate of $\sim 10^{20}$ glucose molecules/sec [4], somewhat less than our maximum glucose requirement of 5×10^{20} molecule/sec (Section 2.1.3). Given a capillary absorptive area of $\sim 3 \times 10^{12}$ micron² in the upper small intestine, the natural glucose transport rate is $\sim 3 \times 10^7$ molecules/sec–micron². As before, if maintenance activities are temporarily suspended during peak demand, glucose tankers loaded with 3.93×10^9 glucose molecules at 2 micron² docking bays can provide the same transport rate if 17% of the vasculoid surface in the duodenum and jejunum is given over to glucose transport.

A related issue is the vasculoid's response to severe gastrointestinal overloading, as for example the rapid ingestion of a large quantity of pure sugar by the user. Sugar has a tremendous irritating effect on the stomach, with 15–30 gm (60–120 kcal) producing great outpourings of stomach mucous; as little as 0.25 liter of 20% sugar solution (78 gm, 300 kcal) is sufficient to cause vomiting in some patients with chronic gastritis, according to century-old laboratory experiments [83]. A rapid 2000 kcal (1.75×10^{24} glucose molecules) ingestion would represent a bulging stomach–full (<1.5 liters [4]) of >22% sugar solution (~ 526 gm of sugar) which would be severely irritating to tissues and toxic to cells, almost certainly exceeds the natural absorption abilities of the small intestine, and would likely prove emetic. Urination at the physiological maximum $\sim 10^{20}$ glucose molecule/sec elimination rate unloads a 2000 kcal sugar binge in ~ 5 hours, a renal export rate of 7.14×10^7 molecules/sec–micron² that can be handled at glucose docking bays covering 36% of the vasculoid surface in the renal glomeruli. Alternatively, some excess sugar can be routed to the liver or other organs for conversion to glycogen or starch.

2.4.4.3 Boxcar Clearance in Narrow Capillaries

Cell-carrying boxcars 6 microns in diameter cannot squeeze through the narrowest of capillaries, most notably those found in the human retina which may be as small as 4 microns wide ([4], Section 8.2.1.2). This has two operational implications.

First, boxcars carrying cellular cargo destined for tissues having capillaries <8 microns must onload and offload at cellulocks located outside such tissues, relying on natural transtissue mobility to achieve the desired placement of the transported cells. In this the vasculoid mimics the natural transport process.

Second, boxcars must be capable of being rerouted around narrow capillary bottlenecks to their flow, else the carriers may lodge in the narrow passage and become an obstacle to the free flow of materials as sometimes occurs with leukocyte plugging in certain pathological conditions such as diabetes [84, 85]. Cilia with boxcar-coded gripper pads located at the entrances of difficult passages may be programmed to refuse boxcars, and may also utilize reverse ciliary flows to assist this process. Alternatively, boxcars may be designed with flexible metamorphic surfaces [4] (and thus a limited ability to change shape) to allow tight passage when traveling empty. With metamorphic boxcars, cilia can allow boxcars to pass that will empty their contents before reaching a capillary. Another alternative is that the vasculoid could be used directly to induce changes in capillary size.

2.4.4.4 Tanker Monolayer Transport

If container traffic is strictly limited to a single monolayer at the artery or vein wall, then ciliary transport produces a tanker bottleneck in medium- and large-diameter vessels of the arteriovenous (noncapillary) vasculature. This is most clearly illustrated in the aorta. The circulation time of ~140 sec (1.4 m circuit at $v_{\text{tanker}} = 1$ cm/sec transport speed) implies a system flux of 8.4×10^{10} tankers/sec at basal load and 1.2×10^{12} tankers/sec at peak load. However, the luminal surface of an aorta of diameter $2R_{\text{aorta}} = 2.5$ cm has room to accommodate only a flux of $2\pi R_{\text{aorta}} v_{\text{tanker}} / S_{\text{tanker}} = 7.9 \times 10^8$ tankers/sec per monolayer of coverage, assuming $S_{\text{tanker}} = 1 \text{ mm}^2$ tankers traveling at $v_{\text{tanker}} = 1$ cm/sec.

The operational implication is that most tankers must be allowed to transit the aorta as a multilayer averaging 0.11 mm deep (~110 tanker layers) or <1% of available luminal diameter at basal load, and up to 1.5 mm deep (~1,500 tanker layers) or ~12% of available luminal diameter at peak load. This bottleneck extends to a lesser degree throughout the arteriovenous vasculature, with the number of required tanker transport layers decreasing rapidly with decreasing vessel diameter. Purely monolayer tanker transport becomes tenable in blood vessels with diameters <200 microns (e.g., arterioles and large venules) at basal load or <20 microns (e.g., metarterioles) at peak load. Tankers can employ one or more simple grapples or temporary coupling mechanisms to join up into progressively lengthening chains (of linked tankers) as they pass blood vessel bifurcations moving upstream, and then to gradually detach and shorten the chains as they move downstream. Even a single cilium can exert sufficient force to pull a fully-loaded 1000-tanker chain at ~100 G (Section 2.3.1), although the tanker at the base of each chain will normally be grasped by up to 10 independent cilia (Section 2.3.2). Nevertheless, chain linkage reliability and the effects of such extended chains on flow viscosity should be studied more thoroughly. Other approaches, including facultative lateral links between chains to improve transport stability, tanker bloc motions, independently ciliated tankers

(allowing high flow rates in large vessels with low inter-laminar slip rates [86]), mechanically valved free flow, extensive water and respiratory gas caching to reduce tanker count, and increasing transport speeds up to 1 m/sec in large blood vessels, are potentially useful strategies but will not be explored further here.

2.5 Mobile Vasculocytes

An additional small population of mobile legged nanorobots, or “vasculocytes,” continuously patrols the vasculoid interior. Vasculocytes are independent nanodevices several microns in size, replete with ambulatory appendages, manipulator arms, repair and assembly tools/materials, onboard computers with mass memories, communications and sensory equipment, and independent power supplies and fuel tankage. A description of a similar system is in [8]; a fuller discussion of these capabilities is in [3, 4] and is beyond the scope of this paper. Like other vasculoid subsystems, to ensure high reliability vasculocytes are designed with the usual tenfold redundancy in most major components.

Vasculocytes in the vasculoid appliance have many important functions, including: (1) general maintenance and repair activities; (2) plugging internal leaks and breaches, cleaning spills, leak scavenging, and maintaining an orderly particle-free internal environment; (3) repairing or replacing malfunctioning ciliary leg mechanisms (designed for modular changeout); (4) clearing of jammed docking bays or cellulocks; (5) reconstruction of the vasculoid sapphire surface plate array after a breach or other catastrophic failure; (6) physical reconfiguration and remodeling of the vasculoid microstructure, as for example to extend additional segments into new capillaries following angiogenesis, to remove vasculoid tendrils from dead capillaries, or to expand or contract existing segments (details deferred to another paper); and (7) installation and removal of vasculoid systems from the human body (Section 7). Specialization of vasculocyte subspecies which would each most efficiently serve just one or more of the above functions should be investigated but is beyond the scope of this paper.

With a vasculocyte mass of ~ 10 picograms, volume $\sim 3 \text{ micron}^3$, and peak power consumption ~ 50 picowatts [8] to allow bursts of more intensive computation (at up to nearly ~ 1 megaflop/sec [2]) or other activity, a 10-watt vasculocyte subsystem energy budget permits the deployment of 200 billion continuously active devices, a total 2-gm mass of nanorobots. Deployment of this number of devices would allow, for example, at least one vasculocyte to visit all 24 trillion docking bays once a day, spending 720 sec per visit, enough time to perform $\sim 10^9$ manipulatory operations using a 10^6 Hz robotic arm [7]. Alternatively, this would allow 7200 visits/day per docking bay, each visit lasting ~ 100 msec ($\sim 10^5$ operations; travel time between adjacent bays at 1 cm/sec is only 0.35 msec) which is long enough to run a simple diagnostic set and to detect plate malfunction within just ~ 12 seconds (on average) of its initial occurrence. It would also allow one visit per day to each of 3000 trillion cilia, spending ~ 6 sec/visit ($\sim 10^7$ operations). This seems sufficient.*

Assuming ~ 0.1 pW per vasculocyte leg (similar to cilium; Section 2.3.1) and 4 legs in motion, simple walking consumes only ~ 0.4 pW of mechanical power; a 10,000 ops/sec computation budget to control simple walking, costing $\sim 6 \times 10^{-17}$ watts/(ops/sec) (Section 2.4.1), adds another ~ 0.6 pW, giving a total power requirement of just ~ 1 pW for continuous simple walking. An onboard 1 micron³ fuel tank with energy storage density of $\sim 2 \times 10^{10}$ J/m³ for externally-supplied O₂ ([4], Table 6.1), gives each 1–50 pW vasculocyte

a range of 400–20,000 sec between refueling stops, or ~100–5,000 sec if the O₂ is stored internally. The power draw of the entire 200 billion vasculocyte fleet is 0.2–10 watts.

During vasculoid installation, the patient is injected with a population of vasculocytes adequate to construct the initial configuration in a reasonable period of time (Section 7). After installation, a sufficient number of spare vasculocytes are stored internally in dormant condition in the vesicles (Section 7.6) until needed for repair, maintenance, or injury response functions. Active vasculocytes have highly redundant subsystems, hence fail infrequently. Upon such infrequent failure, they are replaced with reactivated dormant devices. (Self-repairing vasculocytes are possible in principle – e.g., modular repair-by-replacement – but would add significantly to overall system complexity, hence are not included in this scaling study.) Nanorobot detritus and internal waste is containerized and ciliated to an appropriate internal holding area located in the vesicles. New vasculocytes, replacement modules, and other necessary spare parts and repair materials may be exchanged into the user as consumables, when required.

Vasculocytes performing general repair and maintenance on tanker docking bays have been allocated up to 10 sec per docking cycle for this task (Section 2.4.1), a very conservative 50% duty cycle for docking bays. Vasculocyte system subtasks which must be subsumed within this time budget may include: (1) Detection and analysis of system fault; (2) determination of appropriate response; (3) dispatch of appropriate repair mechanism to problem site, including travel time and docking; (4) on-site verification that the problem is as reported, and that the repair plan is correct; (5) deployment of tools and materials; (6) performance of repair work possibly including plate changeout, rotor replacements, sensor recalibration, etc.; (7) verification of correct completion of repairs and that the faulty subsystem is now performing properly; (8) retracting/repacking all tools with final verification of job completion; and (9) undocking and return to transport stream for storage or to receive instructions for the next assignment. The vasculoid configuration, including numbers of components, their locations, their accessibility for repair and their ease of disconnection/reconnection will influence the rapidity of these steps.

Of course, most of the time there will be no fault at a particular docking bay, and running a diagnostic is much quicker than correcting a fault. Since there are only enough vasculocytes to allow up to 720 seconds/day of repair and maintenance activity at each docking bay (see above), and since a 50% duty cycle implies that each docking bay is allocated ~42,200 sec/day for this activity, then it might be possible to significantly increase the docking bay duty cycle up to $(86,400 - 720)/(86,400) \sim 99\%$ in a less conservative design.

* If diagnostics on “Other” docking bays prove too complex, these bays might be replaced with simpler organ-specific docking bays that handle far fewer molecule types.

2.6 Appliance Power Requirement

Power is supplied to the vasculoid appliance via the chemical combination of oxygen and glucose ([4], Section 6.3.4), both of which are plentiful in the human body. Total body power dissipation is ~100 watts at the basal rate and ~1600 watts at peak ([4], Section 6.5.2, Table 6.8). As a further point of comparison, the basal human heart power output is $p_{\text{heart}} \sim P_{\text{systolic}} V_{\text{blood}} / t_{\text{circ}} = 1.4$ watts (taking pumping pressure $P_{\text{systolic}} = 120$ mmHg (1.59×10^4 N/m²), pumped blood volume $V_{\text{blood}} = 5.4$ liters, and circulation time $t_{\text{circ}} = 60$ sec [4]), rising to ~8.0 watts when cardiac output reaches ~30 liters/minute at peak exertion, assuming no rise in pressure. Experiments confirm that the basal power output of a 350 gm resting heart is ~3.5 milliwatts/gm or ~1.2 watts [87], and patients with chronic congestive heart failure can achieve measured peak cardiac outputs no higher than ~2 watts [88]; efficient total artificial hearts (TAH) may draw ~5 watts of power [89].

The four most significant subsystems requiring a regular energy supply include ciliary transport (11.8–166.2 watts; Section 2.3.2), docking bays (14.5–16.6 watts; Section 2.4.1), vasculocytes (0.2–10 watts; Section 2.5), and cellulocks (~0.6 watts; Section 2.4.2), giving a requirements range of 27.1 watts (basal) to 193.4 watts (peak). There are also 125 trillion applications plates which are unused in the basic vasculoid model described in this paper. If each applications plate is allotted a 0.6 pW energy budget comparable to the docking bays, and if all possible applications plates are simultaneously activated, then the applications subsystem could require an additional 75 watts, boosting the total power draw of the vasculoid appliance to 102.1–268.4 watts, which is still only at the borderline of thermogenic significance ([4], Section 6.5.2).

3. Preliminary Thermal Conductivity Analysis

Besides providing systemic materials transport throughout the human body, the water component of blood also serves an important thermoregulatory function. Removing most of the circulating water from the vasculature eliminates one of the means by which the body regulates its gross thermal conductivity. In addition, the extremely high thermal conductivity of diamond imposes the requirement for a vasculoid design using mostly sapphire, rather than diamond, construction materials, even though diamondoid materials have been more extensively discussed in connection with molecular nanotechnology [7] and medical nanorobots [3–6] and may still be employed in lesser quantities (e.g., as thin coatings) throughout the vasculoid structure.

Aside from blackbody radiation, sweating, and behavioral thermoregulation (including respiratory cooling), the body regulates its temperature and offloads excess heat principally via two mechanisms:

First, there is passive conduction. Heat travels by pure conduction through fat and muscle from the body core out to the periphery. The thermal conductivity of human tissue is $K_t \sim 0.5$ watts/m-K, so for a typical $L = 10$ cm path length (~half-torso thickness), heat flow $H_f \sim K_t / L = 5$ watts/m²-K, or ~10 watts/K for a 2 m² human body. In a cold room, the mean temperature differential between core and periphery $DT \sim 11$ K [4], so $H_f \sim 100$ watts, which is approximately the basal metabolic rate. Experiments confirm that 5–9 watts/m²-K is the minimum heat flow in very cold conditions (the actual value depending largely upon the

thickness of subcutaneous fat layers) [90]. In this case, the peripheral capillary blood flow has slowed to a trickle, producing the minimum thermal conductivity of the human body in cold conditions. On the other hand, in a warm room or during heavy exercise, $DT \sim 1$ K, so $H_f \sim 10$ watts. Thus, paradoxically, at warmer temperatures when the human body is generating considerable surplus heat, the body's passive heat flow is actually very low because of the smaller temperature differential between core and periphery.

Second, heat is transported via the active blood flow. In warm rooms, not only are the peripheral capillary sphincters fully dilated, allowing more blood to flow through the peripheral capillaries relative to the core capillaries, but also the total volume of blood flow may increase. (During heavy exercise, total blood flow volume may rise by a factor of 4 or 5.) Diathermy experiments suggest that the active blood flow mechanism alone may carry off 100–200 watts of heat before core temperature starts to rise [4]. In cold rooms and in the absence of heavy exercise, peripheral capillary sphincters are maximally contracted, thus minimizing blood flow (and hence heat transport) to the periphery.

To summarize: The passive conduction mechanism can throw off ~ 100 watts of waste heat when the human body is in a cold room but only ~ 10 watts when the body is in a warm room, while the active conduction mechanism can throw off negligible heat in a cold room but up to 100–200 watts in a warm room. Thus as the external environment warms up, the human body shifts from passive conduction to active conduction (via increased blood flow and capillary sphincter widening); if the environment becomes hotter still, or the person begins exercising, then sweating eventually comes to dominate both processes.

If we now remove the active blood flow regulatory mechanism, inhibit capillary sphincter expansion, and emplace artificial tubes inside all the blood vessels and capillaries of the body (i.e., install the vasculoid), the sweating process and surface thermal radiation remain unaltered. Thus the principal changes to the human thermoregulatory system are in the passive and active conduction systems.

First, consider the active conduction system. In a working vasculoid operating at the maximum tanker flow rate, we have ~ 0.133 kg (dry mass) of tankers moving around the body in ~ 100 sec per circuit. We assume all tankers are filled with water, for a total water mass of 0.125 kg. Diamond has a heat capacity of 519 joules/kg–K; sapphire is 728 joule/kg–K and water is 4218 joule/kg–K at 310 K. Hence the circulating tanker fleet can transport at most ~ 6 watts/K of heat from the core to the periphery. Given that DT might be as small as 1 K, the “active conduction system” is essentially disabled by installation of a vasculoid that is constructed either of diamond or sapphire.

Second, consider the passive conduction system. For a natural biological–tissue body, heat flow is $H_f = K_t / L = 5$ watts/m²–K. For a human body shape comprised entirely of pure diamond ($K_t \sim 2000$ watts/m–K at 310 K [91]) and again taking $L = 10$ cm, then $H_f = 20,000$ watts/m²–K. For a diamond–envasculoided human body, taking a mass of ~ 1.7 kg of diamond thoroughly interwoven with 68.3 kg of mostly aqueous biological tissue mass (for a standard 70 kg male body), as a crude estimate the effective heat flow becomes $H_f \sim 500$ watts/m²–K, or ~ 100 times more thermally conductive than before. For comparison, a pure metal human form would have $H_f \sim 170$ watts/m²–K for stainless steel, ~ 350 watts/m²–K for lead, ~ 780 watts/m²–K for iron, or ~ 3800 watts/m²–K for copper. Hence a diamond–envasculoided human body would have passive conduction properties similar to those of solid metal.

This has implications for the maximum DT that can be maintained between core and periphery. Consider a human-shaped tissue-mass with half-thickness $L \sim 10$ cm and surface area $A \sim 2$ m², sufficiently heated from the inside to cause $P \sim 100$ watts (human basal rate) to flow via passive conduction from core to periphery, establishing a temperature differential $DT \sim P L / A K_t \sim 10$ K for natural human tissue with $K_t = 0.5$ watts/m-K. Upon switching to diamondoid envasculoided tissue, mean tissue thermal conductivity would rise to $K_t \sim 50$ watts/m-K and so DT would fall to ~ 0.1 K. In effect, the entire human body would become isothermal to within 100 millikelvins; even at the peak power output of 1600 watts for the human body, DT rises to just ~ 1.6 K. Thus a diamond-ensvasculoided human body would tend to become isothermal with its surroundings very quickly (although partially offset by subcutaneous fat), a clear hazard to normal human health especially in very hot or very cold environments. The thermal equilibration time is approximately $t_{EQ} \sim L / v_{thermal} \sim 0.1$ millisecond, where $v_{thermal} \sim K_t / h_{plate} C_V = 1000$ m/sec for neighboring vasculoid plates in good thermal contact with each other and having thickness $h_{plate} \sim 1$ micron, with $K_t = 2000$ watts/m-K and $C_V = 1.8 \times 10^6$ joules/m³-K for diamond at 310 K, and taking $L = 10$ cm as before. This is far shorter than the typical 1-10 sec thermal response time of the purely-biological human vasculature.

Substitution of sapphire for diamond significantly improves thermal performance. The thermal conductivity of synthetic sapphire may be as low as $K_t \sim 2.3$ watts/m-K for sapphire at 310 K [92], roughly a thousandfold lower than for diamond, when measured in the direction normal to the symmetry or optic axis (c-axis); heat capacity ($C_V = 2.9 \times 10^6$ J/m³-K) and density (3970 kg/m³) of sapphire are slightly higher than for diamond. Thus for a sapphire-ensvasculoided human body, taking a mass of ~ 1.9 kg of sapphire (at 25 watts/m²-K for $L = 10$ cm) thoroughly interwoven with 68.1 kg of mostly aqueous biological tissue mass (at 5 watts/m²-K), the total heat flow is just 5.5 watts/m²-K, which differs insignificantly from natural biological tissue [94]. At $P = 100$ watts, DT falls to 2 K compared to 10 K for natural tissue and 0.1 K for diamond-ensvasculoided tissue; $t_{EQ} \sim 1$ sec for sapphire vs. 10^{-4} sec for diamond.

Two complications regarding sapphire require additional research. First, the thermal conductivity of sapphire may vary significantly with both composition and crystallographic orientation, a fact which might impose additional and unknown constraints on the present design. For instance, one source reports heat flow values interpolated to 310 K of 21 watts/m-K normal to the c-axis and 23 watts/m-K parallel to the c-axis [91]; minor extrapolations of other sources to 310 K (i.e. slightly outside the exact temperature ranges measured experimentally) imply values of 2.0 [93] and 2.3 [92] watts/m-K for heat flows normal to the c-axis. However, all reported values for sapphire are at least two orders of magnitude more insulating than diamond.

Second, much like diamond, the thermal conductivity of sapphire varies with temperature. For example, at ~ 200 K (near dry ice temperature) sapphire's thermal conductivity rises to 5 watts/m-K. At liquid nitrogen temperature (77 K), K_t soars to ~ 1000 watts/m-K; the peak is ~ 6000 watts/m-K at 35 K [91-93]. (Diamond's conductivity also rises as it cools [91-93].) At the other temperature extreme, sapphire's thermal conductivity rises to 3.9 watts/m-K by 523 K. Diamond thermal conductivity also varies significantly with isotopic composition (e.g., ¹²C vs. ¹³C [95, 96]); it is unknown whether similar opportunities may exist for the engineering of desired levels or patterns of thermal conductivity in isotopically-controlled sapphire.

Finally, we note that much burn damage occurs due to a failure to dissipate heat. Selectively increasing the thermal conductivity of certain parts of the body at certain chosen times is a useful feature that could mitigate

the effects of transient local heating (Section 8.2). Note that blood is an excellent electrical conductor, and its replacement by an inorganic construct may reduce the susceptibility of the body to electrical burns under ordinary conditions. Pure single-crystal alumina (sapphire), roughly analogous to the core material of the vasculoid plates, is one of the best electrical insulators known [97]. Pure bulk diamond is also an excellent insulator, but hydrogen-terminated diamond surface shows a high p-type surface conductivity [98], and slight impurities (e.g., p-type (boron) or n-type (phosphorus) [99]) or dislocations may also permit conduction, so a diamond-coated sapphire vasculoid plate should be somewhat more electrically conductive than bulk sapphire. The vasculoid is envisioned as a primarily mechanical system and so its electrical characteristics have not yet been investigated. The susceptibility of the appliance to electrostatic charge transfer, electromagnetic interference or electromagnetic pulses (EMP) is unknown.

4. Biocompatibility of Vasculoid Systems

A detailed study of biocompatibility issues will also be necessary to firmly establish the feasibility of the present proposal. Such issues, which may include the trimming of cellular glycocalyx by spinning molecular sorting rotors, surface electrical thrombogenicity, inflammation and phagocyte activation by diamondoid or sapphire materials, and the impact of a cessation of mechanical pulsing on tissue health and lymph flow, have been briefly examined in [6] but need further study [3]. A comprehensive treatment is beyond the scope of this paper, but a few of the relevant issues may be at least cursorily addressed here. Most of the discussion in this Section is drawn from Chapter 15 of Nanomedicine, Volume II [3], where the biocompatibility of diamond and sapphire materials is more extensively reviewed in the context of medical nanorobotics.

4.1 Mechanical Interaction with Vascular Endothelium

Perhaps the single most important biocompatibility factor involving the vasculoid has been termed “vascular mechanocompatibility” by Freitas [3]. Vasculoid nanorobots in all their forms must be as mechanically biocompatible with the vascular walls (Section 4.1.1) as are stents (Section 4.1.2) and must not produce destructive mechanical vasculopathies (Section 4.1.3) or disrupt the endothelial glycocalyx (Section 4.1.4).

4.1.1 Modulation of Endothelial Phenotype and Function

The luminal surfaces of all blood and lymph vessels consist of a thin monolayer (the intima) comprised of flat, polygonal squamous endothelial cells (EC) covering a much thicker layer (the media) comprised of vascular smooth muscle cells (SMC). Under normal physiological conditions, both layers are subject (and respond) to tangential fluid shear stresses across the endothelial cell surface due to the bulk flow of blood [103–108], normal hydrostatic pressure stress acting radially on the vessel wall due to the propagation of the pressure wave, and cyclic stretch or strain due to blood vessel circumferential expansion in vivo [108–110], and thus might also be sensitive to similar mechanical stresses that may be applied by stationary or cytoambulatory intravascular nanorobots such as the vasculoid basic plates.

Endothelial cells (EC) are randomly oriented in areas of low shear stress but elongated and aligned in the direction of fluid flow in regions of high shear stress [111–113]. In vitro endothelial cells previously acclimatized to physiological fluid shear stresses respond to artificial changes in local fluid shear stress only very slowly, and in three stages [113]. In the first stage, EC initially respond to the imposition of stress within 3 hours by enhancing their attachments to the substrate and to neighboring cells; the cells elongate and have more stress fibers, thicker intercellular junctions, and more apical microfilaments. In the second stage, after 6 hours the EC show constrained motility as they realign, losing their dense peripheral bands and relocating more of their microtubule organizing centers and nuclei to the upstream region of the cell. In the third stage, after 12 hours the EC become elongated cells oriented in the new apparent direction of fluid flow; stress fibers are thicker and longer, the height and thickness of intercellular junctions are higher, and the number and height of apical microfilaments are increased. This produces a new cytoskeletal organization that alters how the forces produced by fluid flow act on the cell and how the forces are transmitted to the cell interior and substrate [113].

Physiological fluid mechanical stimuli (e.g., fluid shear stresses*) are important modulators of regional endothelial phenotype and function [114–118]. For example, endothelium exposed to fluid shear stress undergoes cell shape change, alignment, and microfilament network remodeling in the direction of flow (though this may be blocked via microtubule disruption using nocodazole) [119]. Interestingly, the application of a steady laminar shear stress (a physiological stimulus) upregulates the human prostaglandin transporter (hPGT) gene at the level of transcriptional activation, whereas a comparable level of turbulent shear stress (a nonphysiological stimulus) or low stress (such as would be produced by a vascular surface coated with sessile nanorobots) does not [118]. A few of the many quantitative experimental observations include:

- (1) shear stresses from 0.02–1.70 N/m² produce flow-induced membrane K⁺ currents [114];
- (2) physiological shear stresses of 0.35–11.7 N/m² stimulates mitogen-activated protein kinase in a 5-min peak response time [120];
- (3) 0.04–6 N/m² shear stress increases inositol trisphosphate levels in human endothelial cells, with a 10–30 sec peak response time [121, 122];
- (4) shear stresses from 0.5–1.8 N/m² regulate (in frequency and amplitude) oscillating K⁺ currents known as spontaneous transient outward currents or STOC which are observed both in isolated bovine aortic endothelial cells and in intact endothelium; activation of STOC depends on the existence of a Ca⁺⁺ influx and is blocked by 50 microM of Gd⁺⁺⁺ or is significantly reduced by 20 microM of ryanodine [123];
- (5) shear stress of 1.2 N/m² induces transcription factor activation over response times ranging from 0.3–2 hours [100];

(6) arterial shear stresses of 1.5–2.5 N/m² (but not a venous shear stress of 0.4 N/m²) induce endothelial fibrinolytic protein secretion [116];

(7) shear stress of 2 N/m² induces TGF- β 1 transcription and production in a ~60 sec initial response time, with a sustaining increase in expression after 2 hours [124];

(8) a shear stress of 2 N/m² suppresses ET-1 mRNA on confluent bovine aortic endothelial cell monolayers [125]; these effects of shear may be completely blocked (thus allowing ET-1 to be expressed) using 875 nM of herbimycin to inhibit tyrosine kinases or 10 microM of quin 2-AM to chelate intracellular Ca⁺⁺, partially inhibited using 3mM of tetraethylammonium (TEA), or attenuated by elevated extracellular K⁺ at 70 mM or completely inhibited by K⁺ at 135 mM [125];

(9) shear stress of 3 N/m² induces Ca⁺⁺ membrane currents in a 30 sec peak response time [126];

(10) shear stress of 6 N/m² applied for 12 hours causes endothelial cells to align with their longitudinal axes parallel to flow [111];

(11) membrane hyperpolarization occurs as a function of local shear stress up to 12.0 N/m², with an exponential approach to steady state in ~1 minute; the process is fully reversed once the artificial fluid flow stress is removed [115];

(12) critical shear stress of 42 N/m² is the disruptive threshold for endothelial cells, inducing cell mobility [127]; and

(13) shearing stresses of 5–100 N/m² occur at the contact interface when a leukocyte is adhering to or rolling on the endothelium of a venule [128].

Endothelial cells thus respond to sustained physiological fluid shear stresses from 0.02–100 N/m², spanning the range of normal arterial wall fluid shear stresses of 1.0–2.6 N/m² from the aorta through the capillaries [19, 129] and 0.14–0.63 N/m² for the venous circulation [19, 130]. By contrast, legged vasculomobile medical nanorobots may apply shear stresses during luminal anchorage or cytoambulation at velocities up to 1 cm/sec of at least 40–200 N/m² or higher ([4], Section 9.4.3.5). (Self-expanding aortic stents forcibly pulled from the vessel require an extraction force of ~400 N/m² assuming a 10-cm length, rising to ~1200–3600 N/m² for stents anchored with hooks and barbs [131]; varying the radial force applied by stents against the vascular wall has little impact on the required extraction force.) Such shear forces, if imposed unidirectionally by large numbers of closely-packed co-ambulating nanorobots for time periods of >10³ sec, may induce significant changes in shape, orientation, and physiological function in the underlying endothelial cell population. If instead these forces are applied in randomized directions varying over short time periods (<1 hour; Section 7.4) by vasculoid nanorobots, then mechanically-induced modulation of endothelial phenotype and function should not occur.

All shear forces must not be eliminated, however. A nanorobot aggregate that shields vascular cells from fluid shear for an extended time may induce those cells to revert to their flow-unstressed phenotype or to undergo apoptosis. Endothelial cells cultured in the absence of shear stress tend to become dedifferentiated [132]. In one study [133], after blood shear was artificially reduced near a wound lesion for 24 hours the local endothelial cells became less elongated, contained fewer central microfilament bundles, and exhibited a slower repair process. In another study [134], vein grafts removed from the higher-shear arterial circulation and reimplanted in the lower-shear venous circulation of the same animal showed regression of intimal hyperplasia and medial rethickening in 14 days, apparently due to induction of smooth muscle cell apoptosis by a reduction in pressure or flow forces.

Endothelial cells can also respond to persistent static overstretching in many ways, up to and including apoptosis. For instance, hypertension caused by hydrostatic edema can induce apoptosis in capillary EC [135].

Additionally, vascular wall cells respond to lateral stretch forces due to cyclical blood vessel expansion *in vivo*. For example, in one experiment [188] bovine aortic endothelial cells were seeded to confluence on a flexible membrane to which cyclic strain was then applied at 1 Hz (0.5 sec strain, 0.5 sec relaxation) for 0–60 min. After 15 minutes of this cyclic stretching, there was an increase in adenylyl cyclase (AC), cAMP, and protein kinase A (PKA) activity of 1.5–2.2 times at 10% average strain as compared to unstretched cells, but there was no activity increase at 6% strain – evidently, cyclic strain activates the AC signal transduction pathway in endothelial cells by exceeding a strain threshold, thus stimulating the expression of genes containing cAMP–responsive promoter elements. Stretch–activated cation channels in bovine aortic EC are inhibited by $GdCl_3$ at 10 μM [125]. Human umbilical EC subjected to a 3–sec stretch pulse show an intracellular rapid–increase Ca^{++} spike, followed by a (ryanodine–inhibitable) slow–decline, due to Ca^{++} entry into the cell through stretch–activated channels; Mn^{++} also permeates mechanosensitive channels (but not Ca^{++} channels) and enters the intracellular space immediately after an application of mechanical stretch [110]. Cyclic strains of 10% at 1 Hz induce intracellular increases in Ca^{++} [136], diacylglycerol [137, 138], inositol trisphosphate [136–138] and protein kinase C (PKC) [137] in peak response times of 10–35 sec, often sustained for up to ~500 sec, and induce transcription factor activation over response times ranging from 0.25–24 hours [100–105]. Several endothelial cytokines are induced by cyclic mechanical stretch [139], and cyclic mechanical strain modulates tissue factor activity differently in endothelial cells originating from different tissues [140].

Similarly, bovine aortic smooth muscle cells (SMCs) seeded on a silastic membrane and subjected to cyclic strains up to 24% enhanced SMC proliferation at any strain level [141], although SMC under high strain (7–24%) showed more proliferation than SMC at low strain (0–7%) in this experiment. High–strained SMC aligned themselves perpendicular to the strain gradient, whereas low–strained SMC remained aligned randomly; PKA activity and CRE (cAMP response element) binding protein levels increased for highly strained cells, compared to low–strained cells [141]. Other experiments have found that small mechanical strains of 1–4% at 1 Hz applied to human vascular smooth muscle cells can inhibit intracellular PDGF– or TNF α –induced synthesis of matrix metalloproteinase (MMP)–1 [189]; that saphenous vein SMC distention by 0.5 atm pressure subsequently elevates cell apoptosis [142]; that cyclic mechanical strain at normal physiological levels decreases the DNA synthesis of vascular smooth muscle cells, holding SMC proliferation to a low level [143]; that 1 Hz, 10% cyclic strain on SMC activate tyrosine phosphorylation and PKC, PKA, and cAMP pathways over response times from 10 sec to 30 min [141, 144]; and that vascular SMC exhibited stretch–induced apoptosis when subjected to cyclic 20% elongation stretching at 0.5 Hz for 6 hours [196]. Consequently, medical nanorobot aggregates which shield the vasculature from normal cyclical strains might elicit excess growth of vascular smooth muscle cells, which growth is normally held in check by the rhythmic stretching from the arterial pulse [143]. Intravascular nanorobot aggregates that apply cyclic mechanical strains exceeding a few percent might encourage increased SMC proliferation and activate mechanosensitive and stretch–activated channels in EC, along with cellular realignment and subsequent SMC apoptosis at the highest strain levels.

In 2002 it was unknown whether high frequency (>KHz) cyclic mechanical strains likely to be employed by vasculomobile medical nanorobots ([8] and [4], Section 9.4.3.5) would have biological effects similar to or different from those described above for low–frequency cyclic strains, excepting certain specialized

mechanoreceptor cells such as the cochlear stereocilia [145, 146], other hair cells [147–149], and somatosensory neurons [150–152], since most mechanical cell stimulation experiments have been conducted at low frequencies.** Unrecognized effects that might be triggered by high–frequency cyclic strains cannot be ruled out. However, given the relative safety of procedures involving intravascular ultrasound [153–162] with its low complication rate (e.g., only 1.1%, including spasms, vessel dissection and guidewire entrapment [156]) using frequencies as high as 10–20 MHz [153–155], it seems improbable that KHz or MHz acoustic waves of the intensities that might be employed by medical nanorobots for communication ([4], Section 7.2.2) or power supply ([4], Section 6.4.1) will damage the luminal vascular walls. Continuous low–power ultrasound exposures exceeding $\sim 10^4$ sec are considered safe ([4], Figure 6.8), but there are few studies on the safety of long–duration chronic exposures. (Interestingly, relatively high–intensity intravascular ultrasound has been used to dissolve occlusive platelet–rich thrombi safely and effectively in myocardial infarctions [158] and in restenosed stents [161].) If necessary, large wave motions and pressure patterns that are characteristic of normal blood flow can in principle be simulated by the vasculoid plate array by a combination of motile ciliary activity and periodic manipulations of interplate bumpers.

It is likely that the vasculoid appliance will need to control smooth muscle cell proliferation [163–170], in the simplest case releasing specific cytokines into the vasculoid–endothelial space.*** Such factors may include known SMC proliferation promoters [171, 172] such as thrombin (esp. alpha–thrombin), PDGFs (esp. PDGF–AA), FGF (esp. basic FGF), HBEGF (heparin binding epidermal growth factor), TGF β (transforming growth factor–beta) at low concentrations, angiotensin II, thrombospondin–1 (stretch/tension), and known SMC proliferation inhibitors [220, 173–178] such as heparin/heparan sulfate, TGF β (transforming growth factor–beta) at high concentrations, nitric oxide, prostaglandins, calcium antagonists, agonists that activate guanylate and adenylate cyclases, inhibitors of angiotensin–converting enzyme, interferon gamma, 18–beta–estradiol, sodium salicylate, and the topoisomerase I inhibitor topotecan. Adult arterial walls contain both differentiated and immature SMCs [179]. R. Bradbury notes that further research is needed regarding how SMCs handle conflict resolution between “divide” and “don’t divide” signals that it may be receiving from both internal and external sensors. Given the large number of signals that SMCs currently respond to, it seems highly likely that the vasculoid can “manage” them, along with other secretion products of SMCs that play important roles in the prevention of vascular disease, such as extracellular superoxide dismutase [180].

* For laminar fluid flow in cylindrical tubes of radius R and length L through a pressure differential of DP, the fluid shear stress [19] is $\tau = DP/2L$.

** Specifically, between 0.05–5 Hz ([4], Section 9.4.3.2.1) and more recently at: 0.01 Hz [181], 0.05 Hz [182, 198], 0.1 Hz [181, 186], 0.2 Hz [183], 0.3 Hz [184–187], 0.4 Hz [194], 0.5 Hz [195–198], 1 Hz [187–193], 3 Hz [187], 4 Hz [199], 5 Hz [200], 6 Hz [194], 4/10/20/50 Hz [199], and DC–100 Hz [201].

*** Other approaches, though less desirable, might also work. R. Bradbury notes that overproliferating SMC could be induced to undergo apoptosis, perhaps at the cost of telomere shortening in any SMC stem cells that might be present as they proliferate to replace those being eliminated by the vasculoid. ECs play a role in attracting and regulating SMCs [202], so controlling the ECs could indirectly control the SMCs; indeed, all SMCs could be lost with minimal effects beyond changes in nutrient diffusion times, and could possibly reduce the body’s O₂ and glucose demand. Once there is no heartbeat, SMCs are no longer strictly required for day–to–day vasculoid operations but would still be necessary to preserve reversibility of vasculoid installation if the patient’s physician desires to avoid having to reseed the SMC from stem cells.

4.1.2 Vascular Response to Stenting

Mechanical biocompatibility must also be demonstrated by intravascular nanorobots that are intended to remain in long-term near-contact with blood vessel walls. A related medical analog is the vascular stent – a flexible metal coil or open-mesh tube that is surgically inserted into a narrowed artery, expanded, and pressed into the vascular wall at up to 10–20 atm pressure, in order to ensure long-term local vascular patency by providing a scaffold to hold the artery open. Within 4 days, SMC begin to appear in the intima [203]. After a few months the stent is completely overgrown with new endothelium, forming a neointima, although the media is usually compressed with smooth muscle cell atrophy in all stented regions; stenosis is prevented in vessels 10 mm or greater in diameter but is not precluded in vessels smaller than 6 mm [204]. Histologically, in-stent restenosis appears to derive almost exclusively from neointimal hyperplasia [205, 206], which appears more abundant following stent implantation than balloon angioplasty and in stents of greater stent length and smaller vessel caliber (or inadequate stent expansion) [207]. Restenosis occurs in 22–46% of all stents emplaced within 6–12 months [208–213]), in some cases requiring the insertion of a second stent into the first [214], and varies according to the material used. In one experiment [215], the thickness of the neointimal layer formed over wire-mesh stents placed in canine aortas was 83.9 microns thick for gold, 103.6 microns for stainless steel, 115 microns for Teflon, 209.6 microns for silicone, and 228.6 microns for silver; a copper stent produced severe erosion of the vessel wall, marked thrombus formation, and aortic rupture. Stent surface coating and texture also affects leukocyte-platelet aggregation and platelet activation [216].

Improved prospects are reported for diamondoid stents ([3], Section 15.3.9.3). For instance, diamond-coated stents produced by Phytis Corp [217] are inserted at 16 atm pressure (vs. 2–3 atm normally for stents) and yet do not dislodge surface (thrombogenic) antigens and selectins: “The results show that in none of the control systems (systems without stents) [could] a change in glycoprotein expression (i.e. all antigens) ... be detected. With the exception of one measurement also the structural epitopes (CD 41a, CD 42b) show no significant changes during the test period. The reason is most probably that the shearing strength of the system was too weak or the expression of the antigens was too strong. Whereas for the thrombocyte activation, remarkable difference in the expression of CD 62p and CD 63 could be detected. The thrombocyte activity marker CD 62p is reduced in diamond-like coated stents and diamond-like coated stents with heparin compared with uncoated stents.”

However, stent devices are far from ideally mechanocompatible with blood vessel walls. For example, stents placed endovascularly in dog aorta for 4–45 weeks and then examined histologically show medial atrophy, intimal hyperplasia (tissue ingrowth), and proliferation of the vasa vasorum (the microvasculature of the aorta) more prominently for covered stents than for bare stents, probably due to hypoxia in the aortic wall [218]. Cellular proliferation is highest when the artery wall is most hypoxic [219]; but vasculoid nanorobot aggregates (e.g., basic plates) that entirely cover the vascular endothelium can precisely regulate oxygenation of the underlying tissue (using data from oxygen sensors in the plate wall contacting the endothelium), thus largely eliminating the possibility of hypoxia. Stentlike vascular-coating structures also may be able to inhibit stenosis due to vascular smooth muscle proliferation, migration, and neointima formation, without inducing apoptosis, by releasing the topoisomerase I SMC-proliferation inhibitor topotecan in a localized 20-min exposure [220], or by using other similar drugs.

4.1.3 Nanorobotic Destructive Vasculopathies

The physical configurations or activities of medical nanorobotic aggregates could in some circumstances be destructive of vascular tissue [221]. Owens and Clowes [222] point out that the severity of arterial injury is important in determining the ultimate pathophysiologic response and describe a classification system [223] based on the immediate histologic effect of the injury:

Type I injuries involve no significant loss of the vessel's basic cellular architecture, although there may be a slight change in endothelial architecture and associated cellular adhesion. Examples include the fatty streak (an early atherosclerotic lesion), hemodynamic factors and flow disturbances which produce, at most, only a modification of the established cellular architecture.

Type II injuries involve loss of the endothelial layer, perhaps inducing platelets to adhere and begin forming a thrombus at the area of loss, but the internal elastic lamina remains intact and there is little or no damage to the media. Examples include injuries incurred during simple arterial catheterization, endovascular procedures, vein graft preparation, or gentle filament-induced endothelial denudation of the carotid artery in a rat model [224].

Type III injuries involve transmural damage in which the endothelium is removed, the internal elastic lamina is often disrupted, and a significant portion of the medial cells are killed [224, 225]; platelets deposit and a thrombus forms at the site of endothelial loss, and an inflammatory response (vasculitis) including intimal hyperplasia [222] is initiated within the vessel wall. Examples include spontaneous vascular dissection and various forms of surgical repair or reconstruction such as balloon angioplasty, endarterectomy and atherectomy.

Medical nanorobot device and mission designs should always seek to avoid Type II and Type III injuries, although in some special circumstances the potential even for Type III injuries may be inescapable. Destructive mechanical vasculopathies that might be caused by vasculoid nanorobots may be classified as ulcerative (4.1.3.1), lacerative (4.1.3.2), or concussive (4.1.3.3).

4.1.3.1 Nanorobotic Ulcerative Vasculopathy

Pressure ulcers are normally caused by a prolonged mechanical pressure against epidermal tissues (e.g., the skin of a person who is lying down; decubitus ulcer, or bedsores), typically at sites over bony or

cartilaginous prominences including sacrum, hips, elbows, heels and ankles. The combination of pressure, shearing forces, friction and moisture [226, 227] leads to tissue death due to a lack of adequate blood supply; if untreated, the ulcer progresses from a simple erosion to complete involvement of the dermal deep layers, eventually spreading to the underlying muscle and bone tissue [228]. In rare cases [229], mechanical frictional stimulation of the skin can precipitate systemic cutaneous necrosis and calciphylaxis, a state of induced tissue sensitivity characterized by calcification of tissues. Stercoral ulcers [230–232] are caused by the necrosis of intestinal epithelium due to the pressure of impacted feces. Fluid mattresses can greatly reduce pressure ulcers in long–duration surgeries [233] and pressure–relieving surfaces have been investigated for surgical patients [234, 235], wheelchair users [236–239], and for other circumstances [240–242].) It is generally recommended that the interior surface should employ materials having roughly the same mechanical properties as the enclosed tissue [243–246], and the applied interfacial pressures should be reduced to below 1 psi [237] or ~ 50 mmHg.

Similarly, a macroscale nanorobot aggregate such as a vasculoid appliance may cause luminal vascular ulceration by prolonged mechanical pressure against intimal tissues, similar to epithelial pressure ulcers, necrotizing vasculitis, or pressure necrosis. For example, mechanical stretch induces apoptosis in mammalian cardiomyocytes [247] and hypertension caused by hydrostatic edema can induce apoptosis in capillary endothelial cells [135]. Another example is IUD–induced metrorrhagia (nonmenstrual uterine bleeding), wherein the IUD (intra–uterine device) elicits a vascular reaction most pronounced in the endometrium adjacent to the device and includes increased vascularity, degeneration with defect formation, congestion, and poor hemostatic responsiveness to increased vascular permeability and damage, leading to interstitial hemorrhage due to vascular damage from mechanical stress transmitted by the IUD through the endometrium to its vascular network [248].

Indwelling catheters can rest very snugly against the vascular walls without complication for brief periods [249]. A biological–like interface may reduce ulceration in longer–term missions. In one study, a stented aortic graft was placed endovascularly in the native aorta of male sheep, and a histological examination 6 months later found good incorporation of the graft with no pressure necrosis, although there was a foreign body reaction around the graft and an organized blood clot was noted between the graft and the aortic wall [250] (the inner, but not the outer, aortal surfaces would be expected to have clotting–suppressive properties).

However, long–duration nanoaggregates (such as vasculoid plates) that must maintain close contact with endothelium should employ a mechanically compliant coating having properties similar to extracellular matrix. All such linkages should be not just immunocompatible (Section 4.3) but also mechanocompatible, possessing equivalent elasticity or mechanical compliance [251] as the underlying tissue to which attachment must be secured. With conventional implants, compliance design may include assessments of circumferential compliance (measurement of changes in vessel diameter over a complete cardiac cycle, including pressure–radius curves [252], dynamic compliance [253], and mechanical hysteresis effects) [251], longitudinal compliance (elasticity of selected lengths of the vascular system, including any localized stiffening) [254], tubular compliance (impairity of elasticity between a prosthetic conduit and the native artery, elastic energy reservoiring, and pulsatile energy losses due to interfacial impedance mismatches) [255], and anastomotic compliance (suture line anastomotic compliance mismatch and the para–anastomotic hypercompliance zone [256, 257], localized regions of excessive mechanical stress [258–260], and cyclic stretch effects on replication of vascular SMC and extracellular matrix [259, 262]). A mismatch in mechanical properties between relatively compliant arteries and less–compliant metallic stents [263] and tissue grafts has been thought to influence patency [258] and pseudointimal hyperplasia [259–261]. Larger more central arteries are more compliant than the distal small caliber arteries [264], wall shear stress from blood flow differs on either side of a curving vessel and the stress is out of phase with the pulsing

circumferential stretch strain [265], and compliance mismatch between host artery and prosthetic graft may promote subintimal hyperplasia [256]. Analogous compliance issues may be assessed once the static and dynamic stress patterns in the vasculoid transport system are more precisely known.

Post-installation vascular conditioning can be maintained on a permanent basis because the vasculoid appliance exercises precise control over the transport of most metabolic and cellular traffic – e.g., of cholesterol, leukocytes and platelets, the principal participants in the arteriosclerogenic process, or of various circulating pluripotent stem cells and their activating factors.

4.1.3.2 Nanorobotic Lacerative Vasculopathy

Individual vasculomobile nanorobots or nanorobotic aggregates may occasionally scratch, scrape, or gouge the vascular luminal surface, causing partial or complete loss of local endothelium (Type II damage), a form of mechanical vasculitis or capillaritis, particularly during installation of the vasculoid appliance (Section 7). Since the typical dimensions of nanorobotic vasculoid components approximate the endothelial thickness, transmural Type III damage to the media is unlikely. Turnover studies of rat endothelium show that (a) injured endothelium can recover an area one cell wide ($\sim 1000 \text{ micron}^2$) in ~ 3 hours [266], (b) the natural loss rate is $\sim 0.1\%$ of endothelial cell area per day ($\sim 1 \text{ micron}^2/\text{day}$) [267], and (c) the steady-state vascular denudation area is $\sim 0.125 \text{ micron}^2/\text{cell}$ [268].

Smooth nanorobot hulls, boundary layer effects and low fluid flow velocity throughout most of the vasculature during installation (Section 7) should ensure that major “sandblasting” type erosion [269, 270] is unlikely to occur inside human blood vessels even at the highest nanocrits consistent with continuous flow. Free-floating nanorobots that collide with blood vessel walls (given the no-slip condition at the wall) produce minimal shear forces, on the order of $< \sim 0.1 \text{ N/m}^2$ ([4], Section 9.4.2.2) – this is less than the $1.0\text{--}2.6 \text{ N/m}^2$ shear forces normally encountered in arteries and capillaries due to normal blood flow and the $0.14\text{--}0.63 \text{ N/m}^2$ shear forces in veins, but may be sufficient to cause a small biological response from the vascular endothelium (Section 4.1.1). Applying the maximum possible bloodstream velocity of 1 m/sec to the impact-scratch relation ([4], Section 9.5.3.6, Eqn. 9.96), it is clear that particle-wall collisions should produce only harmless submicron nicks even in the most turbulent arteries.

Nevertheless, some caution is warranted because natural endothelial cell wounding of $\sim 1\text{--}18\%$ of all cells, possibly erosionally-derived, has been observed in rat aorta [271]. Erosion of cultured fibroblast monolayers (simulating the vascular endothelium) using MHz ultrasound at acoustic pressures of $\sim 10^6 \text{ N/m}^2$ is enhanced by the presence of a microbubble (particulate) contrast agent [272]. Injection of crystalloid cardioplegic solutions into canine hearts at pressures $> 110 \text{ mmHg}$ and at peak flow rates $> 25 \text{ ml/sec}$ also causes a higher incidence of mechanical-physical trauma to the vascular endothelium and the endocardium [273]. In another unusual case, intravenous self-injection by a drug abuser of dissolved tablets containing microcrystalline cellulose as filler material produced numerous microcrystalline cellulose pulmonary emboli, intravascular foreign body granulomas, focal necrosis and edema of the pulmonary parenchyma, and fatal vascular destruction [274].

Endothelial abrasion alone may not stimulate neointimal thickening [275] but inevitably must involve some endothelial cell loss [276] and other biological responses. For example, mechanically scraping cultured endothelial cells causes growth factor to be released within 5 minutes, not abating for at least 24 hours thereafter, due to plasma membrane disruption [277]. In the case of vascular dissection, a piece of the endothelium peels up, making an intimal flap that defines regions of true and false lumina, and sometimes may induce an intramural hematoma in the aortic wall [153]. Endothelial cells mechanically damaged with a razor blade activate extracellular-signal-regulated kinases within ~300 sec, releasing fibroblast growth factor (FGF-2) which in turn induces intimal hyperplasia [278]. Nanorobots which detect FGF-2 are alerted that mechanical endothelial injury has taken place; by absorbing the cytokine using molecular sorting rotors, the hyperplasia signal may be suppressed by a nanorobot, if desired ([4], Section 7.4.5.4). However, shear-induced endothelial denudation of healthy canine arterial endothelium appears not to occur at shear stresses up to at least 200 N/m² [279]. The role of erythrocyte collisions with vascular walls on the detachment rate of endothelial cells is just starting to be seriously investigated [280].

K. Clements suggests that some provision might be also be made for emergency plate disconnects in certain unusual accident situations, e.g., where the user has irreversibly caught his hand in a machine applying superior force, and now risks not just amputation of the original biological limb, but also faces either (1) forcible extraction of the diamondoid appliance from the remaining biological tissues, or (2) progressive amputation of additional biological tissues because the vasculoid network has become caught in the machine.

4.1.3.3 Nanorobotic Concussive Vasculopathy

If a patient experiences significant external crushing or concussive forces, resident medical nanorobots that are present in small numbers can simply move out of the way, as described previously by Freitas [4, 6, 281] in connection with the risks of dental grinding (e.g., [4], Section 9.5.1). In the case of macroscale intravascular nanoaggregates, there are several additional risks that should be avoided in specific appliance designs.

First, there is the possibility that a sudden mechanical external tissue compression could push macroscale nanorobotic aggregates through the soft tissues, causing deep tissue penetrations, perforations, or other serious mechanical trauma. Similarly, because the vasculoid materials may have higher density than the surrounding biological tissues, very high accelerations (Section 8.8) could produce effects on those tissues that would be not unlike pushing gelatin through a metal wire strainer. Simple activities such as hand clapping or fistfights are unlikely to produce the high accelerations required for serious damage, but this risk should be quantified in future studies. Possibly relevant analogies in the medical literature include:

- (1) ulnar artery erosion, thromboemboli, digital ischemia and skin necrosis from a glass foreign body in a patient's hand [282];
- (2) tantalum coil stent damage that was induced or aggravated by intravascular ultrasound inside a coronary artery [157].

(3) a chronic indwelling catheter that led to erosion and rupture of the anterior wall of the right ventricle, producing a near–exsanguinating hemorrhage [283];

(4) cardiac perforation by a subclavian catheter [284];

(5) pulmonary artery catheter–induced right ventricular perforation during coronary artery bypass surgery [285];

(6) an ICD patch that migrated and perforated the right ventricular cavity [286];

(7) a stent that migrated to an oblique position across the aorta, producing a 7–cm pseudoaneurysm after 3 years [287];

(8) catheter–induced pulmonary artery rupture (a well–recognized complication of invasive monitoring) that often leads to fatal hemorrhage [288–290];

(9) femoral artery catheterization trauma producing hematoma, pseudoaneurysms and arteriovenous fistulas of the femoral vessels [291];

(10) iatrogenic subclavian artery injury due to central venous catheterization [292];

(11) repeated and prolonged vein catheterization that led to subsequent stenosis (presumably due to luminal vascular mechanical damage) [293];

(12) high–pressure injection injury that induced inflammation and foreign body granulomatous reaction, progressing to necrosis [294];

(13) mechanical tearing of arteries due to overstretching [295]; and

(14) spontaneous coronary artery dissection (mechanical arterial wall failure) [296].

(Most of these cases pertain to injury from objects much stiffer and larger than vasculoid components, or are due instead to intrinsic vessel dysfunction (as in spontaneous arterial dissection.)

Second, a sudden external tissue compression could force nanorobotic aggregates into physical contact with neighboring nanoaggregates, possibly causing major structural damage or fragmentation of the devices. This risk increases as the nanodevices become more densely packed, especially along the crushing axis. Nanoorgans (as well as looser aggregates) can be crushed if sufficient force or mechanical shock is applied. Again, a few possibly relevant analogies from the medical literature include:

(1) external compression of emplaced stents that produced premature stenosis [297];

(2) a transabdominal teflon stent that broke intraperitoneally during tuboplasty procedure [298];

(3) a strongly–beating heart that sheared off a pericardial drainage catheter [299];

(4) a Hickman catheter that suffered rupture and embolization during normal use [300];

(5) an indwelling catheter that fractured and a distal remnant embolized to the right ventricular outflow tract and main pulmonary artery, precipitating cardiopulmonary near-collapse [301];

(6) a catheter embolism that was produced when a catheterized patient engaged in power training exercises, externally crushing the catheter, although no symptoms or complications accompanied this event [302];

(7) spontaneous fracture of indwelling venous catheter, leading to vascular leakage [303]; and

(8) other instances of catheter fracture and embolism [304–307], including one case that led to cardiac arrest [308].

(Here, too, many of these cases might differ substantially from the vasculoid, since the catheters were made from a bulk material that depended on its integrity for function while the vasculoid would consist of a large number of semi-independent components capable of restoring functional connections on their own.)

Third, there is a small risk that poor device design, poor mission design, or a loss of control might cause nanoaggregates to operate in a dangerous manner, causing macroscale concussive injury to biological tissues. For example, iatrogenic vascular trauma caused by intra-aortic balloon pumps is well-known [309]. In one case, balloon expansion during angiography ruptured the pulmonary artery [310]. In a canine model [311], an aortic valve balloon dilation to 5–12 atm pressure produced valve leaflet connective-tissue injury and hemorrhage. In an experiment with canine intestine, excessive lymph pressures ($>850\text{--}1630\text{ N/m}^2$) produced artificially in the central lacteals caused fluid to leak out of the villi and caused intestinal epithelial cells to be shed into the intestinal lumen [312]. These risks can be largely avoided or at least minimized by good design and experience with related systems, initially in animal models.

4.1.4 Mechanical Interactions with Glycocalyx

Endothelial cells are surrounded by a well-developed extracellular glycocalyx [313]. If this outer margin is traumatized, receptor sites and fibronectin may be exposed [314, 315] which could then become available for bacterial adhesion [316, 317]. Nanorobots that rely upon absorption of local oxygen and glucose for their power supply ([4], Section 6.3.4) or whose missions include extensive small-molecule exchanges with the environment [3] may have $\sim 10^4\text{--}10^5$ molecular sorting rotors ([4], Section 3.4.2) embedded in their exterior surfaces [2, 6]. These spinning sorting rotors are unlikely to cause direct physical damage to cell surfaces for several reasons. First, rotors are atomically smooth and recessed into the housing, reducing physical contact with colliding surfaces and eliminating potential nucleation sites that may trigger thrombogenesis, gas embolus formation, or foaming. Second, only a small fraction of all available sorting rotors may be actively spinning at one time, further reducing the likelihood of physical trauma. And such limited contact, when it occurs, should be relatively benign: Maximum rotor rim velocity of 2.6 mm/sec is less than 1% of mean aortic blood velocity and lies only slightly above maximum capillary flow speed ([4], Table 8.2).

Many disease processes are known that involve damage to the glycocalyx [318–329], including some bacteria that phagocytose [330] or otherwise destroy [331–334] the cellular glycocalyx during an infection. Damage to the glycocalyx creates conditions that favor the binding of immune complexes, complement activation, and intravascular coagulation, with loss of gradients between blood and parenchyma [335]; desialylated glycocalyx of endothelium also allows an increased rate of endothelial cell detachment from arterial walls [336]. Could the glycocalyx strands present at all tissue and nontissue cells surfaces get trimmed, even by a recessed sorting rotor? Nanorobot sorting rotor binding sites for small molecules (<20 atoms) involve pockets measuring <2.7 nm in diameter ([7], Section 13.2.1.a), too small to physically accommodate the 10–20 nm thick plasma membrane or the main body of the glycocalyx projections typically measuring 5–8 nm thick and 100–200 nm long [337], consisting of glycoproteins comprised of 10,000 atoms or more. While an occasional sugar residue may get clipped, binding sites can be designed for maximum steric incompatibility with glycocalyx glycoproteins and proteoglycans, further minimizing the opportunities for trimming. Note that clipping a covalent C–C, C–O, or C–N bond probably requires a clipping energy >500 zJ/molecule ([7], Table 3.8), but sorting rotors designed to pump against pressures of ~30,000 atm can only apply ~100 zJ/molecule (i.e., per binding site) so an accidentally–bound glycocalyx moiety seems more likely to jam the rotor than to be clipped off by the rotor. If this happens, the result may be a glycocalyx–tethered nanorobot, in which case a rotor–dejamming protocol* will be required to free the trapped nanorobot.

Natural rates of glycocalyx damage are just starting to be quantified [338, 339], and many tissue cells replace their glycocalyx or are retired in times ranging from 10^3 – 10^6 sec. For example: Schistosome parasites can shed some tegument–bound complexes in only ~1200 sec [340] to 3600 sec [341]; plasma membrane turnover rate is ~1800 sec for macrophage [342] and ~5400 sec for fibroblast [343]; cholesterol turnover rate in RBC membrane is ~7200 sec [344]; membrane phospholipid half–life averages ~10,000 sec [345]; neutrophil lifespan in blood is ~11,000 sec [346]; enterocyte glycocalyx is renewed in 14,000–22,000 sec, as vesicles with adhered bacteria are expelled into the lumen of small and large intestine [347]; some schistosome membrane antigen turnover may require from 68,000 [348] to 160,000–430,000 sec [349]; typical protein turnover half–life is ~200,000 sec [345, 350]; cell turnover time is ~86,000 sec in gastric body, ~200,000 sec for duodenal epithelium, ~240,000 sec for ileal epithelium, and ~400,000 sec for gastric fundus [351]; neutrophil lifespan in tissue is ~260,000 sec [346]; glycocalyx turnover in rat uterine epithelial cells is ~430,000 sec [352]; and platelet lifespan is ~860,000 sec [353].

As the cell coat is a secretion product incorporated into the plasma membrane that undergoes continuous renewal, any trimmed glycocalyx glycoproteins from tissue cells would be rapidly replaced via biosynthesis in the ribosomes of the endoplasmic reticulum, followed by final assembly with the oligosaccharide moiety in the Golgi complex and subsequent export to the plasma membrane [354]. Glycoprotein strands or stray sugar residues released into the extracellular medium as a consequence of such trimming are nonimmunogenic and would be quickly metabolized, although it is possible that nearby parasites could absorb this released material onto their surface, affording themselves some camouflage protection against natural host immune defenses [355] but little protection against vasculoid defenses since parasite antigens should still be visible at cell surfaces.

* One obvious backflushing procedure would use follower rods to affirmatively push unwanted ligands out of the binding pocket. Additionally, some molecular sorting rotor designs ([7], Section 13.2.1.d) assume a compliant mechanical coupling that permits the rotor to spin backward a short distance as if in free rotational diffusion, thus allowing improperly bound ligands to be freed.

4.2 Interruption of Plasmatic Water and Lymphatic Flows

A nanorobotic aggregate covering a macroscale area of the capillary luminal surface may reduce the normal flow of plasma water [356] and other substances that leaves the circulation via ultrafiltration, unless the necessary water is replaced by the nanosystem. The plasma water flow helps to remove waste products from the extracellular spaces around tissue cells, a function that could be compromised by the shielding presence of the nanoaggregate unless the aggregate replaces this flow with water transported through or around the device, by various means. Consequently, both lymph volume and the gross water flows between tissues may be affected by vasculoidization, given that the vasculoid substitutes encapsulated fluid transport in place of bulk-flow and diffusive fluid transport in the principal global materials distribution system of the human body. More specifically, ~20 liters/day ($0.23 \text{ cm}^3/\text{sec}$) of plasma water exit the natural circulation via ultrafiltration through leaky capillaries, of which 18 liters/day are reabsorbed after passing through the lymphatic capillaries and back into the venous loops [4], leaving a net flow of ~2 liters/day to pass onward through the lymphatic system.

The maximum vasculoid water transport rate has been scaled to $0.60 \text{ cm}^3/\text{sec}$ or ~52 liters/day, which is the most that the water tanker subsystem can handle (Section 2.1.2). Under normal conditions only ~4% of the water tanker fleet is in use, which still allows the transit of at least $0.024 \text{ cm}^3/\text{sec}$ or ~2.1 liters/day of water which if not re-imported by the vasculoid on the venous side of the capillary bed is forced to enter the lymphatic system, maintaining normal flow and volume. This flow should be sufficient because the direct removal from the intercellular fluids of pure waterborne electrolytes, solutes, and other physiological substances by the vasculoid (through the plates) can create pericellular concentration gradients sufficient to ensure injection and removal of such substances from the vicinity of the bathed cells. This should greatly reduce the gross intercellular fluid flow rate required to maintain proper physiological conditions.*

One minor additional concern might arise because lymph is moved primarily by peristaltic one-way valving. Envasculoided tissues adjacent to lymphatic capillaries may have slightly higher mechanical stiffness, hence may transmit somewhat less peristaltic action resulting in reduced lymphatic flow rates. But lymph fluids transport solutes at far below maximum concentration – for example, lymph normally contains $\sim 0.003 \text{ gm}/\text{cm}^3$ NaCl, two orders of magnitude less than the $\sim 0.36 \text{ gm}/\text{cm}^3$ maximum solubility at 310 K [4] – and bacterial entry will be largely precluded by the appliance, so small reductions in lymph flow rates are probably tolerable. Lymphatic venules do exhibit small-amplitude pulsations on their own, and it may be desirable for other reasons (e.g., Section 4.1.1, Section 7) to simulate the stiffness and motion (including motion resulting from blood flow) of pre-vasculoid tissue. Lymph movement also may be replaced by an optional “lymphovasculoid” appliance (Section 8.5).

Similar considerations and conclusions apply to other fluid spaces within the body that communicate, directly or indirectly, with the blood, including the choroid plexus and cerebrospinal fluid, as well as the pericardial, pleural, peritoneal, synovial, and intraocular fluid spaces.

* If it proves necessary to maintain gross intercellular fluid flow rates at original physiological levels, in principle the entire 20 liter requirement may be supplied by local counterflows of tankers moving from the venous loops back through the capillaries. Transporting the needed $\sim 0.2 \text{ cm}^3/\text{sec}$ of water across a distance of $\sim 1 \text{ mm}$ (typical capillary length; [4], Table 8.1), taking account of the $\sim 10 \text{ sec}$ tanker discharge time at docking bays (Section 2.4.1), requires only an additional ~ 2.7 trillion water tankers (adding $\sim 60\%$ to the basal active water tanker fleet; Section 2.1.2) – about 140 new water tankers per capillary, or only $\sim 0.6\%$ of capillary wall surface area committed to this special function.

4.3 Immune System Interactions

CVD (chemical vapor deposition) diamond coatings are said to have “low immunoreactivity” [357] and there were no reports of diamond immunogenicity in the medical literature as of 2001. Indeed, diamond is often used as an experimental control because it is so chemically inert and biologically inactive [358]. Pure sapphire also appears fairly nonimmunogenic, although similar hydrophilic surfaces do adsorb immunoglobulin IgG [359]; single-crystal sapphire has excellent biological inertness and chemical stability [360, 404]. However, both diamond nanoparticles [361] and various soluble aluminum salts (e.g., alum, aluminum hydroxide, aluminum phosphate [362]) have been shown to serve as adjuvants which enhance vaccines or immune system responses to foreign antigens.

Exposed to water, the polished single-crystal α -alumina (0001) surface elicits a hydration reaction, with a water vapor pressure of $\sim 1 \text{ torr}$ sufficient to fully hydroxylate the surface [363]. Alumina is corrosion-resistant because it exists in the highest oxidation state that aluminum metal can possess, and has the potential for microstructural control of the interface (with tissue) without formation of toxic corrosion products [364]. Yet it is also known that α -alumina is very slightly soluble in highly acidic or alkaline aqueous environments ([4], Section 9.3.5.3.6). Since Al^{+++} ions can produce “dialysis dementia” [365–367] and are generally considered toxic [368–372], it is of interest to determine whether or not these ions can leach into the body from alumina implants or sapphire nanorobots. Early studies in the 1970s found no movement of known contaminants into the surrounding tissue from sintered alumina implants inserted into the iliac crests (hip bones) and mandibles of rabbits [373]. During the 1980s and 1990s, small increases in blood aluminum concentrations were demonstrated in smelter workers [374], though the potential exposure level is several orders of magnitude greater for body uptake of more soluble aluminum compounds used as food additives [375], as antacid medication [374], or from food packaging materials and cooking utensils [376]. In 1990, Lewandowska-Szumiel and Komender [377] investigated aluminum release from an alumina bioceramic during standardized biocompatibility testing in an animal experiment. Alumina implants introduced into rat femurs and guinea-pig mandibles and then removed 6–8 months later were found to be well tolerated, and no changes in the surfaces of the removed implants were observed under SEM examination. The researchers decided to compare the aluminum content of the femurs of experimental and control rats using atomic absorption spectroscopy, and discovered that the level of aluminum was higher in the bones of the experimental animals. In 1991, Arvidson et al [404] investigated the corrosion resistance of single-crystal sapphire implants with respect to the release of aluminum ions, and found no ions in the test solutions. The next year, Christel [378] reported that alumina exhibited greater bioinertness than all other implant materials currently available for joint replacement, and that no lymphocyte or plasma-cell infiltration into joint implants is observed “because of the absence of soluble component release.” However, two studies in the early 1990s [379, 380] found some detectable aluminum ion release, so more research is clearly required on

this issue. In any case, a thin veneer of diamond on sapphire [381] should suffice to prevent aluminum ion release in vivo.

An allergic reaction or “hypersensitivity” is an acquired and abnormal immune system response to a substance, called an allergen, that normally does not cause a reaction. An allergy requires an initial exposure to an allergen which produces sensitization to it; subsequent contact with the allergen then results in a broad range of inflammatory responses. Sapphire or alumina ceramic [382–384] is considered nonallergenic – ceramic coatings are used to eliminate metal allergies on implant surfaces [385, 386], and hypersensitivity to oral ceramic is reported only rarely [387–390]. There are no reports of allergenicity for diamond, sapphire, fullerenes, or other probable diamondoid nanorobot exterior materials and such allergenicity appears unlikely, but experiments should be done to positively confirm this expectation. The immune system could also react to small subcomponents like cilia, especially if they form aggregates with proteins, possibly requiring clonal deletion or tolerization to deal with such issues ([3], Section 15.3.3).

4.4 Inflammation

Could the vasculoid surface in contact with the vascular endothelium trigger general inflammation in the human body? One early experiment [391] to determine the inflammatory effects of various implant substances placed subdermally into rat paws found that an injection of 2–10 mg/cm³ (10–20 micron particles at 10⁵–10⁶ particles/cm³) of natural diamond powder suspension caused a slight increase in volume of the treated paw relative to the control paw. However, the edematous effect subsided after 30–60 minutes at both concentrations of injected diamond powder employed. Another experiment [392] at the same laboratory found that intraarticular injection of diamond powder was not phlogistic (i.e., no erythematous or edematous changes) in rabbit bone joints and produced no inflammation. Diamond particles are traditionally regarded as biologically inert and noninflammatory for neutrophils [393–396] and are typically used as experimental null controls [392]. CVD diamond [397] and DLC diamond [398] surfaces elicit minimal or no inflammatory response, and atomically smooth diamond may perform even better. Diamond particles are said to have little or no surface charge [395, 399] but unmodified graphene ([4], Section 2.3.2) surfaces readily acquire negative charges in aqueous suspension [400, 401], so experiments are needed to determine if negatively charged fullerenes or other diamondoid substances can contact-activate Hageman factor or kallikrein and trigger an inflammation reaction.

Experiments with sapphire have generally found no serious inflammation in soft tissues [402–405] or bony tissues [406–408], or only mild reactions [409], though there are a few modest exceptions [410, 411] including a brief acute inflammatory response [412, 413].

4.5 Thrombogenesis

Blood coagulation involves a complex series of reactions in which various proteins are enzymatically activated in a sequential manner, transforming liquid blood into a gel-like clot which is then stabilized to form a thrombus (clot) consisting of platelets, fibrin, and red cells. The series of reactions is classically divided into two pathways – extrinsic and intrinsic – involving more than a dozen factors that converge on a single common final pathway, resulting in clot formation [346, 414–420]. Since these factors are carried by the blood, the vasculoid can regulate their local concentration and thus prevent thrombogenic pathways from proceeding to completion.

Additionally, platelets must undergo adhesion and activation for coagulation to occur. The adhesion of platelets to exposed collagen in injured blood vessels is mediated by a bridging molecule called von Willebrand's factor [421] that is secreted by endothelial cells into plasma, which prevents platelets from detaching under the high shearing stresses developed near vessel walls. The activation of normally quiescent platelets is a complex phenomenon that includes changes in cell shape, increased movement, release of the contents of their granules (containing nucleotidyl phosphates, serotonin [422], various factors, enzymes and plasma proteins), and aggregation. The most potent activator of platelets *in vivo* is thrombin [423], which interacts with a receptor on the platelet plasma membrane, followed by transmembrane signaling and subsequent activation of the cell. Collagen [424] is the other most important platelet activator; ADP can stimulate aggregation but not granule release. In principle, the blood-contacting surfaces of a nanoorgan, or of nanorobots in sufficient bloodstream numbers and concentrations, could activate platelets (and thus either of the two coagulation pathways), but careful choices of materials and of allowable mechanical motions should reduce or eliminate inherent nanodevice thrombogenicity. For example, DLC diamond-coated stents [425, 426], heart valves [427, 428] and other blood-contacting LVAD surfaces [429–432] or substrates [433, 434] generally show reduced thrombogenicity and no platelet activation [434]. Sapphire (alumina ceramic) has low thrombogenicity [435–437] and both platelet adhesion [438] and activation [437] are low. Hemolysis is near-zero for diamond [434, 439] and alumina [439] powders. Additionally, in the vasculoid plateletogenesis and release of platelets could be actively regulated and reduced to minimal levels.

Future experiments must determine if ordinary diamondoid surfaces will have to be supplemented with additional antithrombogenic coatings in order to achieve vasculoid performance objectives. If such coatings are required, one simple possibility is surface-immobilized heparin, a ~15 kD straight-chain anionic (acidic) mucopolysaccharide (glycosaminoglycan) that forms polymers of various lengths. Heparin, first discovered in 1916 [440], is produced naturally by human liver mast cells and basophil leukocytes, and inhibits coagulation primarily by accelerating the interaction between antithrombin and thrombin. Nanorobot exteriors can be “heparinized” [441–450], and thereby rendered thromboresistant by immobilized heparin on all blood-contacting surfaces at ~monolayer surface concentration (e.g., 7–10 pmol/cm² [450]). Cellulose membranes coated with 3.6 pmol/cm² of endothelial-cell-surface heparan sulphate show complete inhibition of platelet adhesion [451]. If satisfactory passive nonthrombogenic surfaces cannot be found, nanorobots might employ any of several active strategies to prevent iatrogenic coagulation ([3], Section 15.3.5).

4.6 Regulation of Angiogenesis and Vasculogenesis

During development and after physical injury, new blood vessels may originate from pre-existing blood vessels by angiogenesis or from endothelial cell precursors (angioblasts) by a process called vasculogenesis; both processes are mediated by paracrine growth factors [452–457]. In certain circumstances, such as wound

healing, post-ovulation capsule repair, and exercise-related capillary formation to support development of new skeletal muscle [458–460], angiogenesis is critical in the adult human body and its lack has been associated with chronic renal failure [461] and other pathological conditions. Without the ability to incorporate vasculoid plates into new capillary vessels, masses of new non-ensculoided tissue would accumulate around the original (ensculoided) tissues over time, reducing the effectiveness of the appliance. In principle, vasculoid can support angiogenesis and vasculogenesis by extending itself into the newly-formed space. Watertight multicomponent metamorphic surfaces have been described by Freitas [4], Section 5.3), but special techniques will be required to extend a new vascular branch while maintaining continuous watertightness. An angiogenesis event can be detected by monitoring concentrations of angiopoietin-2, VEGF, and other relevant factors. Conversely, detection of tumor angiogenesis factors could induce a vasculoid-mediated reduction in oxygen supply, increased local delivery of antibodies, refusal to deliver angiogenesis factors, and optional intervention such as delivery of chemotherapeutic drugs or external signaling to call for targeted therapeutic intervention.

It is envisioned that self-repair capabilities (Section 2.5) via active replacement of damaged components (from onboard inventories of spare parts including spare plates; Sections 7.6 and 8.3) will be an important feature of the complete vasculoid system design. These capabilities may be extended to support angiogenesis. When angiogenesis is not desired (for example, near tumors), local concentrations of angiogenic factors can be regulated by the vasculoid appliance to minimize vessel formation, and the vasculoid can refuse to deliver nutrients to the undesired tissues even if ersatz capillaries form. Attention must also be paid to the removal and disposal (or temporary onboard warehousing; Section 8.3) of damaged plates. In rare cases, traumatic events may damage plates (rather than simply causing them to separate temporarily), and radiation damage may cause rare failures. A capillary damaged beyond repair (e.g., in a severe contusion) may be abandoned and dismantled by the body; in such a case the vasculoid should cease delivery to that region and remove the plates.

Damaged endothelial cells can be detected based on sensory data indicating localizing chemical imbalances, and new stem cells or endothelial precursor cells (Section 2.2.1) can be transported to the vicinity of the damaged site to help restore the natural vascular integrity. Such restoration in some cases may require repositioning of a few plates using the motive cilia (Section 7.4), but the description of detailed specific angiogenic response, plate replacement or vascular repair activities are beyond the scope of this paper.

4.7 Vascular Patency and Relaxation

One important function of fluid flow in blood vessels is to ensure vascular patency. But replacing bulk fluid with a vasculoid appliance is unlikely to cause the smaller vessels to collapse because the buckling force is increased by up to several orders of magnitude by the addition of the plates in the capillaries and related small vessels, even in the absence of bulk fluid (Section 8.8). The largest vessels such as the aorta will lose significant luminal support (even if filled with gas), but – in addition to the external muscular and elastic support from the surrounding tunica media and tunica adventitia layers – such vessels also possess an extensive capillary vasculature which, greatly stiffened and at typical capillary densities, should provide adequate replacement support. Intravascular (cross-luminal) spring-loaded diamondoid scaffolding could also be added at need.

Arterioles in the natural vascular system perform extensive regulatory functions. These and related functions (including vasoconstriction and vasodilation) can be controlled, in turn, by the vasculoid (e.g., by monitoring local NO concentrations; Section 2.1.7). The underlying vascular musculature will probably be maintained in the relaxed state if this maximizes tissue stability and simplicity of control, although further research of this question is warranted.

5. Control Systems and Computational Requirements

Numerous local, intermediate-scale, and global control systems and protocols will be required to ensure the proper autonomic operation of the vasculoid appliance. Special communications subsystems for local plate configuration maintenance, cargo traffic control, and fast systemic response to large-scale external stimuli must be designed. An interplate packet-switching network for long-range communications, and to support real-time autogenous user control, should be considered. System control might be simplified using local computing centers throughout tissues, directing immune, angiogenetic, and trophic functions. Besides the interplate network, trans-tissue sonic or optical communication in principle could be employed between spatially close but topologically distant portions of the vasculoid network. Precise knowledge of the functions of various cytokines and other substances will enable the vasculoid to respond appropriately to sensor data reporting local extravascular concentrations of signaling molecules. Complexity of stimulation patterns must mirror physiological conditions as much as possible. Highly responsive and user-friendly graphic user interfaces may be useful to allow the patient to communicate quickly and easily with his or her appliance; several aspects of such interfaces have been described elsewhere ([4], Section 7.4), but considerably more work remains to be done [3]. The computational requirements of directed container switching/routing by the ciliary system should be investigated further.

A great number of software and computational architectural issues are as yet unresolved, including a detailed molecular routing logic for each substance to be transported, comprehensive details of nanorobot control protocols, container traffic flow patterns (e.g. flow lensing, lane definition, congestion waves and gridlock, flow viscosity, etc. [86]), and software requirements including software complexity for large-scale control issues, a discussion of which are beyond the scope of this paper. (For example, it might be interesting to apply existing vehicular traffic simulations to transport in fractal structures.) Only since the mid-1990s have multirobot control issues begun to be seriously addressed by the broader research and technical community [462-469]. Computation for vasculoid accident recovery and repair will be considerably more intensive than computation for maintenance or installation, and must also be deferred to another paper.

However, a few basic observations may be made here regarding vasculoid materials transport computation requirements. Concentrations of water and glucose are normally maintained by the appliance near typical serum levels, using simple feedback loops driven by concentration sensors located on the tissue side of the vasculoid device. Oxygen and carbon dioxide are similarly controlled using sensors capable of measuring

partial pressures, though the precise triggering thresholds may be modified in special circumstances (e.g. high altitudes, deep sea diving, hyperbaric chambers). A simple rate-control mechanism driven by sensor data compiled once every second, employing ~1000 distinguishable concentration levels requires ~10 bits/sec per molecular type, or ~40 bits/sec for all four molecules. Most of the time, entire rotor banks are engaged using a single command. Ciliary motions, largely stereotypical, likely require a similarly small computational budget.

Establishing or maintaining appropriate concentrations of mixed-cargo molecules is far more computationally complex. These other molecules include minerals, vitamins, lipids and waste products, but the most numerous and difficult to coordinate are the blood proteins and sterols including control molecules such as insulin, leptin, gastrin, resistin, estrogen, or testosterone; synaptic transmitters and other neural biochemicals such as acetylcholine, adrenalin, dopamine, nitric oxide, or serotonin; cytokines and other signaling molecules such as follicle stimulating hormone, epidermal growth factor, or tumor necrosis factor; and many thousands of specific antibodies that reflect the body's unique learned recognition of specific antigens. (Embedded analytical units scattered throughout the vasculoid surface can test for rising concentrations of hitherto unrecognized nonmetabolizable molecules, and configure a set of programmable binding sites ([4], Section 3.5.7.4) to rotor these molecules out of the tissues as well, though this should be a relatively rare occurrence.) Since the human genome contains ~40,000 genes, most of which may encode several proteins each, we assume there may be on the order of ~100,000 distinct biomolecules that must be recognized, monitored, transported, and regulated at the docking bays. This is likely a generous estimate, given that most of the proteins produced remain intracellular, but our conclusions do not depend sensitively upon the precise figure chosen.

Upon receipt of any tanker, each docking bay scans the tanker manifest before offloading the contents. In the case of gas, water, and glucose tankers, the manifest is extremely brief, since only one or two molecules are involved. This content information can be encoded in as little as 15 bits. A precise molecule count of up to 3×10^{10} molecules per tanker requires an additional 35 bits, but in most cases a precise molecule will not be necessary and a range figure requiring fewer bits should suffice. At the maximum rate of one tanker unloading every 20 seconds (Section 2.4.1), the manifest-reading bit rate is at most ~2.5 bits/sec.

In the case of mixed-cargo tankers, 17 bits uniquely specify the identity of each of 100,000 distinct molecules; each tanker can hold a total mixed-cargo molecule count of $\sim 10^9$, requiring up to 30 bits per item to ensure an exact count. Based on existing human physiology, we posit a specification that each vascular cell must have access to at least 5% of all ~100,000 molecular types during one blood circulation time, ~60 sec. Since each cell is supplied by two mixed-cargo docking bays, then restricting tankers to a maximum of 834 different molecules per load fulfills our specification, requiring in the worst case a 39,198 bit manifest to be read in 20 seconds, a maximum bit rate of ~2,000 bits/sec. Again assuming ~10 bits/sec per molecular type for rate-control of rotor mechanisms, rotor control will require a maximum ~8,340 bits/sec. (One design alternative is to allow stochastic mixing and transport of the low-concentration molecules which would mimic the natural process, reduce the computational needs, and impose only a very small burden on the transport capacity.)

In sum, docking bay process control appears to require ~10,000 bits/sec of computation. Cellulock control requires reading manifests of up to ~1000 cells of at most ~1000 different types, which is ~20 bits/cell type or ~20,000 bits/manifest. Cellulocks unloading one boxcar every 60 seconds (Section 2.4.2) will require a bit rate of ~333 bits/sec. Other control tasks will add only fractionally to the ~10,000 ops/sec budget previously

estimated for individual docking bays (Section 2.4.1), a capacity that can be used for other purposes between docking events.

6. Overall System Reliability

A detailed assessment of vasculoid system reliability also lies beyond the scope of this paper, especially given the possibility for prompt and severe damage if the robot is subjected to extreme accelerative loads or unplanned segmentations. However, if we assume normal gravitational loading and ignore catastrophic accidents, we find that the vasculoid promises an annual survival probability well in excess of “six nines” (failure probability $< 10^{-6}$) at least against radiation damage if all major subsystems incorporate tenfold redundancy as specified in Section 2.

Adopting Drexler's [7] radiation damage model for the first part of this analysis and applying it to a system comprised of N components, with each component comprised of n redundant parts, the probability P that the system remains operational after T years is approximated by: $P = \exp[-N(1-p)^n]$, where p = the probability that an individual part remains operational; $p \sim \exp(-10^{-15} Dm)$, where m = mass of the part in kg and D = radiation dose in rads $\sim 0.5 T$ for normal background radiation in the terrestrial environment. As a further simplifying assumption for this analysis, we shall presume that all vasculoid modular “parts” are similar in mass to the $\sim 4,000,000$ -atom robotic manipulator device described in [7], after which the vasculoid cilium is patterned (Section 2.3.1). From the above formulae, $p \sim 0.999960$ for each such cilium-like part, per year, even with no internal redundancy within the part.

The vasculoid ciliary subsystem (Section 2.3) includes a minimum requirement of $N = 300$ trillion cilia incorporating a redundancy of $n = 10$, giving a total of 3000 trillion cilia. From the above, the annual probability of failure of the ciliary subsystem is $< 10^{-29}$; assuming a redundancy of only $n = 5$, failure probability is still $< 10^{-7}$.

Each vasculoid plate is $\sim 2 \text{ micron}^3$ in volume. Given that there are ~ 150 trillion plates, with zero redundancy among them, then to be assured of a complete plate subsystem annual failure rate $< 10^{-6}$, the annual probability of failure per plate must be reduced to $\sim 10^{-20}$. This is achieved for plates comprised of a total of $\sim 88,000$ “parts” as described above, with a redundancy of ~ 6 among such parts. However, in this study we have specified a more generous (i.e., safer) redundancy of 10 among such parts (Section 2.4.1).

Each vasculocyte repair robot is $\sim 10^{-14}$ kg in mass. Given that there are ~ 200 billion active vasculocytes, and assuming zero redundancy among them, then to be assured of a vasculocyte subsystem annual failure rate $< 10^{-6}$, the annual probability of failure per robot must be reduced to $\sim 10^{-17}$. This is achieved for robots

comprised of a total of ~125,000 “parts” as described above, with a redundancy of ~5 among such parts; we have again assumed a more generous redundancy of 10 among such parts (Section 2.5).

Non-radiation failure mechanisms have not been examined in the above analysis. Software failure modes have been ignored, and even plate computers may be complex enough to host intentionally disruptive programs such as computer viruses. Many other more subtle or second-order difficulties also have been ignored in the present paper, such as the potentially destabilizing effects of dynamic oscillations and resonances among the various moving components which would require a detailed design before undertaking a comprehensive analysis. For instance, we should try to avoid Per Bak’s notion of self-organized criticality [470–474] when complex systems are pushed too close to their design limits, as in car traffic simulations. Numerous specific failure modes have not yet been exhaustively analyzed, including complete single-plate failures and the seizing or locking of individual cilia while a transfer operation is in progress, e.g., near a capillary entrance where such failures could prove most troublesome. However, the vasculocyte fleet has been scaled to accommodate a reasonable repair mission requirement (Section 2.5). A discussion of possible autogenous and autonomic repair behaviors in response to major device trauma has also been deferred to subsequent papers.

Vasculoid tankers are micron-size compressed-gas containers which may rupture explosively – though this event is extremely improbable, since tankers with rupture strength exceeding 40,000 atm are loaded to only 1000 atm pressure (Section 2.1.1). If this unlikely rupture event occurs in a large vessel such as the aorta, the possible failure modes may resemble those involved in a detachment avalanche (Section 2.3.1), but the low tanker mass should preclude any serious direct infrastructural damage. However, if the explosive event occurs within a smaller vessel such as a capillary, the risk of breach is considerably greater. However, the maximum overpressure that can be explosively applied to the appliance walls is limited to the ~1000 atm compression pressure of the tanker contents (Section 2.1.1), which likely does not exceed the theoretical rupture strength ([4], Eqn. 10.14) of the vasculoid walls in capillaries which may be crudely estimated as $p_{\max} \sim 3300\text{--}33,000$ atm, taking vasculoid plate tube thickness $t_{\text{wall}} = 1$ micron, capillary tube radius $R \sim 3$ microns ([4], Table 8.1), and working stress $s_w \sim 10^{10}$ N/m² ([4], Table 9.3) for solid tube walls or maximum interbumper working stress $s_w \sim 10^9$ N/m² ([4], Section 5.4.3) for more realistic plated walls jointed with bumper interconnects. Whether such explosive events will occur with sufficient frequency to warrant explicit corrective protocols (beyond conventional vasculoid self-repair activities; Section 2.5) deserves further study. A shockwave cascade failure (such as recently occurred at the Super Kamiokande neutrino detector facility, wherein the initial implosion of a single photomultiplier tube (PMT) during refilling of the water tank triggered a runaway cascade, destroying 6,665 of the 11,146 PMTs in a few seconds [475]) seems unlikely in the vasculoid but also should be investigated theoretically.

In practice, one should expect that a few contaminant molecules will make their way into the vasculoid, perhaps from local strain that exceeds the adjustment capabilities of the metamorphic bumpers, accidental spills, and so forth. A molecule that is small enough to be mobile at room temperature is small enough to be captured by a sorting rotor. Larger molecules can be physically handled by vasculocytes. A specialized class of vasculocyte, also measuring several microns in size and moving at ~1 cm/sec, can employ a 0.25-mm-wide chemotactic detector bank on each mobile nanorobot to search for, bind, and remove large molecules – a complete sweep of the entire vasculoid luminal surface once a minute requires the activity of only 1% of the total active vasculocyte fleet. The motion of the tankers creates a net motion of the nitrogen atmosphere that can sweep molecules toward centrally placed filters. Thus a combination of internal sorting rotors, filters, and vasculocyte activity can quickly extract contaminants from the vasculoid volume. Once contaminants are trapped, they may be dealt with in ways suggested previously (e.g., Section 8.3; [4], Section 10.4.2; etc.). The volumetric capacity of the appliance to deal with internal contamination must be

scaled according to anticipated applications and event scenarios, which should be studied further but are beyond the scope of this paper.

7. Hypothetical Vasculoid Installation Scenarios

Installation of the vasculoid involves, at the least, complete exsanguination of a sedated patient and an intricate vascular plating operation. Two hypothetical installation scenarios are presented. The first scenario (Sections 7.1 to 7.7) is a detailed description of a procedure that would be feasible using the technology available in 2002. This is to demonstrate that vasculoid installation can in principle be carried out without violating any well-established medical or physical limits. However, the authors are aware that by the time a vasculoid-class device can be built, medical technology will have advanced significantly. We therefore also briefly sketch out a highly speculative second scenario (Section 7.8) which, if practicable in some future era, might be considerably more convenient and up to 100 times faster. This second procedure would be unduly aggressive by today's standards but might be feasible and safe, given the supporting technology available in a nanotechnology-rich medical environment.

The principal installation scenario involves complete exsanguination of a sedated and hypothermic patient, replacement of the natural circulatory fluid with various installation fluids, followed by mechanical vascular plating, defluidization, and finally activation of the vasculoid and rewarming of the patient. Installation takes ~6.5 hours from start to finish and requires a peak ~200-watt power draw midway through the procedure. (By comparison, present-day kidney dialysis treatments require 4–12 hours and the equipment also draws a few hundred watts.)

Our discussion first considers the lifespan of cells temporarily denied access to external molecular transport mechanisms (Section 7.1). We next describe the details of vasculoid installation including patient preparation (~24 hours; Section 7.2), vascular washout (~4 hours; Section 7.3), vascular plating (~1 hour; Section 7.4), defluidization (~0.3 hour; Section 7.5), and initialization and cold start (~1.2 hours; Section 7.6). We conclude with a brief discussion of vasculoid removal (Section 7.7).

The hypothetical installation protocol described below has been selected for maximum comfort, reversibility, and reliability. The correct performance of the system is verified at every step, providing a plateau of safe operation before moving on to the next step. Since the entire procedure is intended to be fully reversible at each step, any step which fails or does not proceed in a manner acceptable to the installing physician may be quickly abandoned with a retreat to the previous plateau of established safety, after which a decision may be made to try again or to abort the installation.

Patients must be made aware that they are about to undergo a major medical procedure which involves replacing ~8% of their body mass with complex nanomachinery. They must be psychologically prepared to deal with the personal implications of this.* From the turn-of-the-century perspective, vasculoid installation appears massively intrusive especially when compared to other superficially related procedures with which we are commonly familiar such as intubation, kidney dialysis, blood transfusion and blood replacement therapies, installation of pacemakers or artificial organs, and coronary angioplasty or fiberoptic endoscopy. However, in a future era when nanomedical systems are widely employed and generally accepted as standard treatment, vasculoid installation may be regarded with considerably less trepidation than it would today.

* One recent recipient of an artificial heart reports [476] that living with an artificial heart entails adjusting to some strange new sensations: “The biggest thing is getting used to not having a heartbeat, except a whirring sound...”

7.1 Cellular Ischemispecific Limits

In classical medicine, “ischemia” refers to a local inadequate blood supply which is usually caused by a mechanical arterial obstruction (e.g. clot), a spasm wherein a blood vessel pinches shut, arterial narrowing (e.g. arteriosclerosis), or cessation of cardiac activity. The principal clinical outcome of local ischemia is a shortage of oxygen. Because of the high continuous biological power density of nerve cells, neurons and the brain succumb most rapidly to oxygen starvation. The precise survival limit of human brain tissue under hypoxic conditions (after which time some decline begins to occur) depends on many factors. Traditionally this has been reported as ~4 minutes (240 sec), although more recently it has been shown that 10 minutes of warm ischemia (even followed by another 10 minutes of trickle-flow CPR) is reversible without neurological deficit if followed by mild hypothermia when normal blood flow is restarted [477], and even modest advances in technology will likely extend this still further. Much longer periods of cold ischemia are tolerable – for example, survival with complete functional and histologic cerebral recovery has been achieved with brain temperature at 5–10 °C during 1 hour of circulatory arrest [478], and stable spontaneous circulation has restored after water ice submersion of up to 90 minutes [479].

In nanomedicine, where it is possible to achieve precise control of human physiology at the cellular and molecular levels, ischemia may refer to an interruption in the extracellular mass transport of any vital molecular species within the human body. Failure to adequately import a particular nutrient, or to adequately export a specific harmful waste product, or to properly regulate the transport of a particular signaling molecule, may produce some of the classical symptoms of cellular ischemia. Since the entire bloodflow must be interrupted during the vasculoid installation process (producing whole-body ischemia), it is useful to estimate how long tissue cells can maintain normal metabolism and avoid toxemia after cellular access to the bloodflow is denied. This time period – the ischemispecific limit – varies with each important cytomolecular molecule, as summarized below. (The limit also varies by cell type; a more detailed study would likely reveal specific tissues where ischemic sensitivity is higher than average for a given metabolite.)

Oxygen. The average (20 micron)³ tissue cell consumes $\sim 10^7$ molecules/sec of O₂ at the basal (resting) rate of ~ 30 picowatts. The cytosol of such a cell can dissolve up to $\sim 6 \times 10^8$ O₂ molecules at 310 K. If suddenly cut off from all external supply, the average cell has only enough O₂ in inventory to survive ~ 60 sec at the basal metabolic rate.

Glucose. Assuming $\sim 50\%$ energy conversion efficiency [35] and $\sim 10^{-3}$ gm/cm³ glucose in the cytosol ([4], Appendix B), then $\sim 3 \times 10^{10}$ glucose molecules are available in the average tissue cell. For a power demand of 30 picowatts, ~ 4800 zJ/glucose molecule, and $\sim 50\%$ energy conversion efficiency, then the basal glucose consumption rate is 1.25×10^7 glucose molecules/sec and the basal cellular ischemispecific limit for glucose is ~ 2400 sec.

Carbon Dioxide. The metabolic “combustion” of one molecule of glucose with six molecules of O₂ produces six molecules of CO₂, hence the average tissue cell produces $\sim 10^7$ molecules/sec of CO₂ at the basal rate. The cytosol of an average cell should normally dissolve up to $\sim 10^{10}$ molecules of CO₂ at 310 K (assuming working tissue P_{CO2} = 54 mmHg ([6], Table 1) and applying the Henry's law constant for CO₂ ([4], Table 9.2)), an estimate which compares favorably with the measured ~ 5 millimoles/kg intracellular CO₂ concentration (2.4×10^{10} molecules/cell assuming an 8000 micron³ cell) in various frog tissue cells at 302 K [480]. Hence the cellular ischemispecific limit for CO₂ is ~ 1000 sec, consistent with maximum physiological cellular and plasma pH levels. It may be possible to dissolve more CO₂ but this will lower pH, leading to toxic acidosis of the cell. (Acidosis has two major components, CO₂ and lactic acid. The absence of oxygen blocks electron transport and stalls the Krebs cycle, halting CO₂ production, so glucose is shunted to lactic acid in anoxia.) Additional amounts of CO₂ may be stored in combination with plasma proteins as carbamate.

Lactate. Under anaerobic conditions, lactic acid is produced during the metabolism of glucose (glycolysis) in most cells [481], glycogenolysis in muscle [482] and glucolysis [483]; two molecules of lactic acid are produced per molecule of glucose metabolized. Thus at the basal rate the average anaerobic tissue cell can produce at most 2.5×10^7 lactate molecules/sec – though this is an overestimate by perhaps a factor of 2 [484] because in most cells the pyruvate (the immediate precursor of lactic acid) formed at the end of glycolysis enters the TCA cycle and is further oxidized by mitochondria [484, 485]. The maximum normal blood concentration of lactate ([4], Appendix B) equates to $\sim 1.1 \times 10^{10}$ molecules/cell, potassium channel openings are induced by 2–20 nM lactate ($0.96\text{--}9.6 \times 10^{10}$ molecules/cell) applied to the cytosol of rabbit ventricular myocytes [486], and the brain lactate threshold for cerebral ischemic damage is 17 mmol/gm [487] or $\sim 8.1 \times 10^{10}$ molecules/cell, so the ischemispecific range for lactate is $\sim 380\text{--}3800$ sec.

Nitrogenous Waste Products. Urea is the principal mammalian waste product due to protein, purine, and pyrimidine nitrogen metabolism, constituting $\sim 85\%$ of human nitrogen excretion. However, urea is formed in the human liver through reactions of the Krebs ornithine cycle, a process not available to tissue cells denied access to the circulation. Ammonia [488] is the chief byproduct of protein and amino acid metabolism in the cell, with one molecule of ammonia produced per molecule of amino acid broken down. The daily RDA for protein represents an upper limit on the breakdown rate of $\sim 5 \times 10^5$ amino acid molecules per cell–sec, assuming mean amino acid MW ~ 100 Da, implying a maximum ammonia generation rate of $\sim 5 \times 10^5$ molecules/cell–sec. Given the maximum observed concentration of ammonia of $\sim 6 \times 10^8$ NH₃ molecules/cell in whole blood cells ([4], Appendix B), the ischemispecific limit for nitrogenous wastes is ~ 1200 sec.

Acetate. Acetic acid (MW = 60 Da) is the simplest possible fatty acid having an even number of carbon atoms. It is most notably produced during the breakdown of acetaldehyde (the second step in the metabolism of alcohol), bacterial fermentation in the gut, and in other circumstances. The typical human intracellular production of acetic acid has been roughly estimated from rat studies [489] as $\sim 8 \times 10^6$ molecules/cell–sec. This chemical is highly metabolizable in vivo, but assuming a maximum nontoxic limit of $\sim 10^{-4}$ gm/cm³ (vs. $\sim 4 \times 10^{-3}$ gm/cm³ for all esterified fatty acids in cells) or $\sim 10^{10}$ molecules/cell, then the ischemispecific limit for acetic acid is ~ 1300 sec.

Ketones. Absent circulatory removal and in cases of low glucose levels, the metabolism of fats may produce abnormal amounts of toxic ketones including primarily beta–hydroxybutyric and acetoacetic acids (and their decarboxylation product acetone) which may be present up to $\sim 6 \times 10^8$ molecules/cell assuming MW ~ 86 Da for ketones. Given the RDA for lipids of $\sim 7 \times 10^{-7}$ kg/sec (Section 2.1.6), and since one palmitic acid (typical lipid) molecule (MW = 256 Da) would convert to ~ 3 molecules of acetoacetic acid (MW = 86 Da), the maximum natural ketone generation rate is $\sim 5 \times 10^5$ molecules/cell–sec and the minimum ischemispecific limit for ketones is >1200 sec.

Summary of Cellular Ischemispecific Limits. If the average human tissue cell is denied access to all extracellular molecular transport systems, the major byproducts of normal cellular metabolism may build to near–toxic levels from a near–zero initial concentration in $\sim 10^3$ sec. Glucose reserves last $>10^3$ sec, but oxygen runs short in $\sim 10^2$ sec without external resupply. These theoretical limits appear crudely consistent with the concept of the “Golden Hour” in traditional trauma care [490–495]. For instance, ischemia induced by aortic cross–clamping in dogs has been survived for up to 20–60 minutes without inducing paraplegia [496] (though decline of spinal cord electrical function is detected in the ~ 20 – 30 minute range for dogs and rabbits [497–499]). Cardiac ischemia induced by aortic cross–clamping in dogs is survived for 30 minutes during normothermic (37 °C) cardioplegia [500], 45 minutes during mild hypothermic (28–30 °C) cardioplegia [501, 502], and 90 minutes using potassium verapamil during profound hypothermic cardioplegia at 8–10 °C [503]. The duration of cold ischemic tolerance is enhanced by the administration of excess insulin [504] and other pretreatments [505–507], possibly involving gene products [508] that will be well–known in a future nanomedical era in which vasculoid installation is commonplace. (Interestingly, wood frogs can endure freezing for >2 weeks with no breathing, no heart beat or blood circulation, and with up to 65% of their total body water as ice [509].)

7.2 Patient Preparation (~24 hours)

Before the vasculoid may be installed, the patient must be prepared as follows:

(1) Vascular Conditioning. The day before the installation, the patient receives an injection containing a treatment dosage (~ 1 cm³) of vascular repair nanorobots [8], or ~ 70 billion individual devices. These 8–picogram, 7 micron³ mobile legged artery–walking nanodevices clean out all fatty streaks, plaque deposits, complex atherosclerotic lesions, infections, vascular wall tumors, and parasites, and repair all other vascular

lesions as required in less than 24 hours, in a multistep process described elsewhere in detail [8]. As one additional task, these nanorobots inject each of the $\sim 10^{12}$ endothelial cells lining the human vascular tree (a) with cytokine blockers to at least partially inhibit the cells' natural surface pressure and shear force responses [510–515], and (b) with adhesion–inducing glycoproteins to forestall cell migration during the installation procedure by encouraging firm anchoring. All vascular repair devices are then exfused before vasculoid installation begins; the results of their vascular reconnoiter protocol may be downloaded to an external computer and used to prepare a detailed map of the patient's vascular tree to improve efficiency during plating (Section 7.4) and plate initialization (Section 7.6). The patient may be started on a diuretic (e.g. furosemide) to reduce blood volume a few hours before the installation procedure begins.

(2) Sedation. On the day of the operation, the patient arrives at the installation facility and is administered a preoperative sedative such as sodium pentobarbital an hour before the procedure is to begin, to encourage drowsiness.

(3) Cannulation. A standard closed–chest cardiopulmonary bypass [479] (aka. heart–lung machine support) or CPB is employed. Usually this involves a combination of femoral and thoracic vessel cannulation, but in this case a fem–fem bypass (cannulation of the vena cava and aorta via the femoral vein and artery) might suffice. This procedure, by definition, continuously supplies the equivalent of resting cardiac output through the femoral vessels and the blood pump–oxygenator circuit – typically a $50\text{--}70\text{ cm}^3/\text{sec}$ flow rate during hypothermic CPB [516], allowing the entire human blood volume can be exchanged about once every few minutes. Fresh oxygenated blood flows retrograde up the femoral artery into the aorta, and oxygen–depleted blood flows retrograde down the vena cava to return to the heart lung machine via the femoral vein. The leg inferior to the cannulation point is supplied by collateral vessels. At this point in the procedure, the patient's own blood continues to circulate through the body. (Note that the above “manual cannulation” scenario is included for illustrative purposes only. In an era when advanced medical nanotechnology is available, self–directing nanocannulators [3] will make it easy to quickly and safely establish flow–regulated channels into any desired artery or vein, up to and including the aorta and vena cava, so much higher flow rates than the conservative figures used in this Section are theoretically available if required.)

(4) Heparinization. Heparin and streptokinase are injected (a) to prevent clotting and promote lysis of hemostatic fibrin, (b) to break up axial red cell rouleaux that form spontaneously at low blood flow shear rates, and (c) to help ensure patency of the catheters throughout the procedure. The conventional cocktail of drugs given to patients placed on bypass leading up to a cold circulatory arrest procedure is rather complicated and will not be elaborated further here, but there are established procedures in conventional medical practice for cooling patients and diluting their blood for work at very cold temperatures [517].

(5) Cytoactivity Restraint. The installing physician next administers: (a) an erythropoietin antagonist to maximally suppress erythrocyte production; (b) agents to temporarily suppress all leukocyte production, reversibly depress leukocyte intracellular metabolism and cytokine sensitivity, and briefly reduce or block antigen reactivity; (c) agents to temporarily suppress platelet production, reversibly depress platelet intracellular metabolism and cytokine sensitivity, and temporarily toughen the platelet cytomembrane to reduce the likelihood of shear damage; (d) minute traces of normal bloodstream hormones, cytokines, and other control biochemicals designed to minimize production of natural secretions such as insulin, adrenalin and testosterone, glucose and cholesterol, sebum and semen, etc., as well as angiogenesis inhibitors to halt the development of new capillaries; and (e) broad–spectrum antibiotics or programmable nanobiotics such as

microbivores [2] designed to prevent microbial attack during the brief period of immunological vulnerability. For example, one element of this complex and as yet incompletely specified biochemical cocktail might be dexamethasone, the most powerful anti-inflammatory and immunosuppressive adrenocortical steroid; another element might be anti-CD18, an antibody known to prevent leukocytes from sticking to blood vessel walls in the brain. (Some of these and related restraints may not be absolutely essential, since the processes in question are quite slow compared to the time course of installation.)

The patient is now ready for vascular washout.

7.3 Vascular Washout (~4 hours)

Vascular washout (to prepare the patient for vasculoid plating) may be performed as follows:

(1) General Anesthesia. A general anesthetic such as propofol is administered by the installing physician at sufficient dosage (~90 mg) to establish a condition of surgical anesthesia.

(2) Respirocyte Infusion. Over a period of 3 hours, the patient's entire blood volume is replaced with a suspension of fully charged respirocytes (1 micron³ spherical O₂/CO₂ 1000-atm pressure vessels [5, 6]) in an isotonic aqueous 0.01 M glucose solution (double the natural serum concentration) also containing most of the cytoactivity restraint substances described in Section 7.2 and additionally a mixture of appropriate electrolytes and other components commonly found in hypothermal blood substitutes [520–522]. A 5% (by volume) respirocyte suspension, containing ~10¹¹ respirocytes/cm³, is sufficient to provide oxygen and carbon dioxide transport equivalent to the entire human red cell mass for ~10⁴ sec (almost 3 hours) after the cessation of respiration. The respirocyte fleet generates ~17 watts of waste heat while supplying oxygen at the human basal rate, producing at most a negligible ~0.1 °F rise in core body temperature. Typically ~20 liters of infusant is required to completely clear the vessels of all natural blood components. Exfused blood cells are removed, collected and saved for emergency reperfusion, if required.

It is true that the reduction of cerebral blood flow by 50% can produce marked disturbances in brain metabolism [523], and at 20% of normal flow the neurons can depolarize with rapid loss of intracellular potassium into extracellular spaces [524]. But the infusant composition can be adjusted to maintain physiological electrolyte (esp. Na⁺, K⁺, and Ca⁺⁺) concentrations and osmotic balances, and to extract any excitotoxins that might be released [525] – or else respirocyte-class phamacyte nanorobots [3, 4] can be employed to similar effect. Since blood cells have been removed, leukocyte plugging and other forms of neutrophil-related damage [526] cannot occur. The basal metabolism remains sufficiently active throughout the procedure so that tissue cells suffer minimal ischemic damage. The infusant constitutes an adequate temporary replacement for the natural blood which is being removed. This is based on an established medical technology: It is well-known that the entire blood supply of a human being can be replaced with cell-free blood substitute at a low temperature, with the patient then reperfused with blood and recovered, as was first demonstrated clinically 30 years ago as a treatment modality for hepatic coma [527].

(3) Cooldown. Once the entire blood volume has been completely exchanged with the respiration-infusant described in (2) in the unconscious patient on CPB (as in conventional medical settings), control of perfusate temperature will suffice to control body temperature. Core temperature follows the perfusate temperature fast and close, with any perfusate/core temperature difference decaying with a ~10 minute half-life. The heat capacity of the body is so large that the 200 watts of power dissipated by vasculoid installation over an hour or so would heat the patient by only a couple of degrees, which is tolerable. (By comparison, external cooling of a body in circulatory arrest is so inefficient that even placing the patient in an ice water bath would yield surface-to-core temperature differences decaying with a half-life of hours.) The patient's average core temperature is reduced from 310 K (37 °C) to 280–290 K (7–17 °C) in ~1 hour, a cooldown rate of ~0.5 °C/minute. This cooldown schedule is qualitatively similar to hypothermic schedules commonplace in current resuscitation medicine [528] and hypothermic CPB procedures [517]. Mivacurium, rocuronium, or older agents such as vecuronium or metubine (recently withdrawn) may be administered to inhibit shivering and as a reversible nondepolarizing muscle relaxant; the effect of vecuronium bromide may be reversed by acetylcholinesterase inhibitors such as neostigmine or pyridostigmine.

B. Wowk notes that there are three broad categories of clinical hypothermia used in medicine. First, there is mild hypothermia (a few degrees below normal body temperature). This is very commonly used during cardiopulmonary bypass for open heart surgery, and often occurs as an incidental effect of general anesthesia during other surgeries. Second, there is deep hypothermia (15–20 °C). This is used when significant periods of circulatory arrest (up to 1 hour) are required for complex bloodless surgeries such as repair of cerebral aneurisms or congenital defects of the aortic arch. Hemodilution (partial blood substitution) is used during these surgeries, in part to avoid red blood cell agglutination at low temperatures. Third, there is profound (or ultraprofound) hypothermia (0–10 °C). Profound hypothermia does not yet have routine clinical use but is the subject of active investigation in relevant animal models [518–520] with an eye toward human use [529], and preliminary human clinical results recently have been reported [530–532]. Total blood substitution, as proposed in the vasculoid installation protocol, is the norm for profound hypothermia. Specialized perfusates such as hypothermosol [520–522] are necessary to overcome physiological problems with this temperature regime that ordinary plasma can't handle. Dogs have been held for three hours in profound hypothermia during perfusion of a blood substitute [519], and the record for profound hypothermic perfusion without neurological deficit is said to be ~6 hours; the record for profound hypothermic circulatory arrest (as distinct from continuous perfusion) in dogs at <5 °C is ~3 hours [533, 534].

(4) Cardioplegia. After the cooldown process has begun, the heart (already in bradycardia from the muscle relaxant) may be stopped by direct infusion of cold potassium chloride solution (reversible with atropine or digitalis) or other standard cardioplegic solution. However, if the target is ultraprofound hypothermia there is no need to stop the heart with drugs during this process because the heart will stop itself when the temperature falls below 15–20 °C.

In ~4 hours, washout, cooldown and cardioplegia are completed. Cytometabolic processes continue, but, at 280 K, with reduced metabolic requirements and hence reduced oxygen demand. This potentially allows infused respiocytes to provide complete respiratory gas maintenance for up to ~10⁵ sec (~1 day) before they would be exhausted after complete cessation of circulatory flow via the catheters, giving a significant safety margin for the next phase of the installation procedure. However, B. Wowk notes other risks of profound hypothermic circulatory arrest beyond mere hypoxia, including the failure of ion pumps (causing growing intra- and extracellular imbalances of calcium ions), the alteration of cell membrane permeability (allowing normally extracellular solutes to slowly leak into cells), and the decoupling of certain cellular metabolic

processes (which does not occur during mild hypothermia). The vasculoid installation process may fit within the circulatory arrest times achievable with the standard off-the-shelf deep hypothermic (not profound hypothermic) protocols of conventional medicine. Further study is required to determine the optimum temperature for hypothermic installation.

The anesthetized patient is finally ready for intravenous deployment of vasculoid components.

7.4 Vascular Plating (~1 hour)

The original 5% respirocyte suspension is replaced by a new suspension containing 1% fully-charged respirocytes and 10% cargo-bearing vasculocytes (plus cytoactivity inhibitors and glucose), creating a mixture whose viscosity and flow characteristics are roughly equal to normal-hematocrit human blood. At an ~11% nanocrit, partial plug flow might ensue in a few of the smallest capillaries, but complete plug flow (requiring much higher pumping power and pressure than laminar flow) can be avoided [4].

Each 3 micron³ vasculocyte grasps a single 2 micron³ plate, ready for installation, thus the new vasculo-infusant contains ~20 x 10⁹ vasculocytes/cm³. Installing ~150 x 10¹² basic plates thus demands a minimum of 7500 cm³ of vasculo-infusant, requiring ~3800 sec or ~1 hour assuming a very gentle flow rate of only ~2 cm³/sec.

Each vasculocyte drifts quietly in the flow until it encounters a vessel wall for the Nth time (N is an integer control variable), which activates it, causing it to attempt to release its cargo in a clear space. (Slowly increasing N during the installation process produces a crudely progressive plating pattern.) If the immediate area is already fully plated, the legged vasculocyte walks across the surface until it reaches a clear area to deposit its cargo. Corner registration of adjacent plates is verified prior to plate release, to ensure a maximally dense tiling pattern. Because of their small size, vasculocytes can enter even the narrowest capillaries and install plates by tiling motions (Section 2.4.4.3). This process may be loosely regarded as a robotically-guided variant of fluidic self-assembly, a well-known existing commercial process [535]. Special procedures must also be devised to handle encounters with nonendothelial materials (e.g., fibrin strands) or stray cells (e.g., adherent leukocytes) that may be blocking the endothelial surface, or denuded patches of vasculature lacking full endothelial cell coverage, although most of these defects should have been remedied during preoperative vascular conditioning (Section 7.2).

Once its cargo plate is in place, the vasculocyte releases back into the flowing fluid, powers down, and is eventually exfused from the body. Approximately 42 billion plates/sec are deposited during this 1-hour process. We generously assume that each 1–50 picowatt vasculocyte requires ~100 sec of active operation up to peak power to find a clear space to deposit its cargo before resuming its fluidborne dormancy – though early arrivers will spend less time searching for gaps in the structure than later arrivers. Thus there are at most ~4 trillion vasculocytes active at any moment and the total power released as waste heat by the vasculo-infusant is under ~200 watts, thermal energy which is easily carried off by the cold infusant. Given

that one plate is installed by one vasculocyte carrier that performs $\sim 10^6$ mechanical motions/sec during a ~ 10 sec install time, this implies $\sim 10^7$ motions/plate and allows an allocation of ~ 1800 motions per nanometer of plate perimeter during the installation of each plate, which seems sufficient.

The plates are not passive during the installation process. Besides the 20 cilia positioned atop each plate to provide tanker and boxcar mobility as part of the ciliary subsystem (Section 2.3), plates also possess “motive cilia” to assist in both installation and repair operations. Each motive cilium is fully retractable when not in use. Complete positional, rotational and translational control during installation (and functional redundancy) requires at least one motive cilium on each of the 4 sides and at least four on the underside to establish a stable tripod while walking. The motive cilia allow limited trans–endothelial cytoambulation by each plate (using adherent tool tips) and fine control of plate/plate jostling motions.

A working cilium consumes 0.1 picowatt during continuous operation at 1 cm/sec (Section 2.3.1), roughly the speed of jostling motions involving motions of $\sim 1\%$ plate width per microsecond. Even with all motive cilia operating at once, plate power is under ~ 1 picowatt; even with all 150 trillion jostling at once, maximum power would be under 150 watts – energy easily obtained from glucose and oxygen provided by the vasculo–infusant medium, and waste heat that is easily dissipated by thermal conduction. However, the motive ciliary power draw of the entire plate population normally should not exceed ~ 1 watt during installation because once properly positioned in a regular grid pattern (in < 1 sec) all local plate jostling ceases and the motive cilia are stowed.

The installation process may be made more efficient if plates are programmed to dynamically shift holes (in the plating pattern) upstream. This ensures that gaps are unlikely to persist in the developing vasculoid structure (except in cases of plate malfunction), and also ensures that shifted holes will arrive in a known region of the upper vascular tree where they are most convenient for vasculocytes to quickly find and fill. Out–of–register plate domains that collide during this dynamic repositioning process require a simple interaction protocol to allow them to mutually align correctly (such a protocol has not yet been devised). Once plates are in place, their surface cilia can be adjusted to provide variable drag on the circulating fluid. This can be used as a crude method of directing resources for more efficient construction.

Plates also assist the vasculocytes in system validation. Upon installation, plates briefly activate all subsystems to verify that everything is working properly. With all 18,750 sorting rotors spinning, individual plates momentarily draw up to ~ 2 picowatts (Section 2.4.1). Malfunctioning plates jettison themselves back into the fluid flow for ultimate removal, or if this is not possible, take other action to bring their condition to the attention of the circulating vasculocyte fleet so that they may be replaced at once.

Following supravascular positioning and subsystem validation, each plate inflates fluidtight metamorphic bumpers [4, 8] along its contact perimeter with its neighbors. This provides at least $\sim 14\%$ linear effective elasticity (1.6 microns vs. 1.4 microns, center–to–center, comparable to the usual stretch requirements of the elastic arteries during normal cardiac pumping) and permits plates to track lateral movements of the underlying tissue while avoiding any relative movement of the opposing surfaces. Ventral lipophilic anchors dropped into the lipid bilayer cytomembrane of the adjacent endothelial cells of the vascular wall serve as sensors to detect any such relative movement, providing continuous feedback to control bumper inflation – although with cardioplegia such wall movements will be quite small because infusant pressure may be held

nearly constant throughout the installation procedure. Neighboring plates lock their bumpers firmly together with reversible fasteners embedded in the bumpers.

Along vessels whose diameters change rapidly as a function of axial position, orthogonal plate alignment along a circumference can be maintained via bumper expansion. Once maximum bumper extension is reached, a further increase in vessel circumference is accommodated in the next row by deflating bumpers in the circumferential direction and inserting one additional plate. Incommensurate offsets are reconciled using multiple ports in the bumper structure. If bumpers can expand by up to 20%–30% [4], then the blood vessel being plated can change in width by 20%–30% before such a pattern discontinuity is required, so such discontinuities should be relatively uncommon in most of the plated vasculature. Computer modeling of the dynamic adjustments required to achieve continuous plating at blood vessel bifurcations and in tapered vessels would be useful.

As the natural vascular surface is covered by the growing vasculoid, individual plates that have completed self-testing procedures and are locked in place activate a sufficient number of rotors to begin providing full molecular transport services to the underlying tissues. Any plate malfunctions are corrected by the circulating vasculocytes, via plate changeout. Metabolism in the underlying cellular tissues continues normally, just as it did before these tissues were plated with the vasculoid. Rotors on the ventral plate face (away from the lumen) gain access to nutrients in the vascular infusant fluid via gated channels leading to the dorsal plate face (toward the lumen) which is directly exposed to the fluid; cellular waste products escape to the fluid by a similar route. Plate power requirements normally range from ~0.004 picowatt (basal rate) to ~0.09 picowatt (peak rate) plus ~0.6 pW for computation (Section 2.4.1). At 280 K the patient's cells would require only a fraction of the basal rate; after plating is complete and in the absence of significant computation, the entire population of 150 trillion installed plates might generate only ~1 watt.

Specific procedures for cellulock installation have not been examined in detail because these vasculoid components are relatively few in number (Section 2.4.2) and require a net installation rate of only ~9 million/sec (compared to 42 billion/sec for basic plates). To the extent cellulock placement can be governed by easily detected geometric factors such as vascular diameter (e.g., near capillary entrances), cellulock placement may occur similarly to plate deposition, but using vasculocytes programmed with specific geometric release criteria. Some modest number of cellulocks destined for specific vascular addresses may be installed after plate initialization (Section 7.6) using a combination of vasculocytes and now-active cargo cilia, by replacing temporary plates with cellulocks.

Nontubular vascular segments including flaps, valves, sphincters, portals, sinuses, plexuses, nodes, and discontinuous microvascular beds such as the red pulp of the spleen constitute only a tiny fraction of the vascular surface but may require special procedures by the vasculocytes whose description is beyond the scope of this paper. Vasculoid interaction with angiogenesis and related processes is briefly discussed in Section 4.7. Endothelial pressure/shear responses (Section 4.1.1) may be managed by continuous emission of appropriate blockers, inhibitors or cytokines; the response may be reversibly disabled or eliminated using a designed vector to insert a short segment of revised DNA into the cells' nucleus. The vasculoid also includes an explicit mechanism to inhibit the electrical output of the sinoatrial node, thus maintaining a permanent (but in theory reversible) state of cardioplegia.

After ~1 hour, the structure of the vasculoid is almost complete. All major components have been tested and are in good working order – indeed, the still–submerged vasculoid is already maintaining full cell metabolism in the tissue below. The patient is now ready for defluidization.

7.5 Defluidization (~0.3 hour)

At this stage, the 1–micron thick monolayer of nanorobotic plates forms a chemically inert, flexible sapphire liner on the luminal (interior) surface of the entire vascular tree. This liner may be made fluidtight and airtight to at least modest pressures. Vasculo–infusant fluid is purged from the body by introducing ~6 liters of oxygenated* pure anhydrous acetone** as a dehydrating rinse followed by pressurized dry air at 2 atm through the input catheters and allowing all lavage fluids to exit through the output catheters for ~15 minutes. If necessary, surface cilia may assist in the distribution of fluid or air flow to help ensure that no pockets of fluid remain trapped anywhere in the system, and to ensure that no respirocytes, inoperative or damaged vasculocytes, or other stray particles are left behind.

The upper limit for laminar flow (Reynolds number ~ 2000) of aqueous vasculo–infusant fluid passing through a smooth 9–mm diameter exit catheter occurs at ~1 m/sec. Assuming a constant laminar outflow velocity of 1 m/sec, flow volume through each of the two cannula is ~60 cm³/sec and the vasculoid lumen is emptied of all installation and rinse fluids in ~100 sec. (This step is easily reversed by re–introducing an aqueous oxygen–rich or respirocyte–laden nutrient solution.) Acetone viscosity is ~40% that of water [4], so pumping power may be reduced as the rinse proceeds.

Oxygen needed to sustain human life is slightly restricted for only ~100 sec*** during the pure acetone rinse, and thereafter is continuously available at the requisite concentration from the dry purge gas. A temporary supply of dry air with 20% O₂ at 2 atm puts 5×10^{22} O₂ molecules into the vasculoid lumen, which when burned with glucose at 50% efficiency in tissue cells produces ~20,000 joules, equivalent to ~2000 sec of power at the reduced metabolic rate of ~10 watts in a human body cooled to 280 K. The plate population consumes only an additional ~1 watt. As long as fresh purge gas continues to circulate, the oxygen requirements of both human and vasculoid can be satisfied indefinitely.

Cellular glucose reserves will last ~10⁵ sec at the reduced metabolic rate; subject to cautions noted earlier (Section 7.3), cellular waste products may not approach toxic levels for ~10⁴ sec. Vasculoid plates can also continue functioning in the temporary absence of glucose. Assuming a power requirement of ~0.6 pW/plate at the basal rate, then a ~1 hour supply of glucose may be stored in a small fuel tank inside each plate, representing only ~9% of the 2 micron³ plate volume.

* The oxygen should dissolve readily at normal atmospheric pressure. For instance, N₂ (a gas with solubilities similar to O₂) is 11 times more soluble in acetone than in water (177 ml gas per kg of acetone vs. 16 ml/kg of water at 298 K and ambient pressure [536]). Highly pressurized oxygenation, which might produce an explosive mixture, should not be required.

** Laboratory glassware rinses commonly consist of acetone, chloroform, ethanol, ether, water, or other solvents, but acetone is often considered superior when it is necessary both to solvate organic contaminants and to remove excess water [537]. Ether and acetone are more volatile than ethanol (hence are more quickly removed by aspiration) though more flammable [538]. Both ethanol (>1 mg/ml [4]) and acetone (>0.01–0.1 mg/ml [539–542]) have been found in human blood, often as common metabolites, and in acetonemia [543]. Toxicity effects are similar to within an order of magnitude – for example, lethal blood concentration is 0.55 mg/ml for acetone [544] vs. 4 mg/ml for ethanol [4]; and 10–20 ml of acetone have been taken by mouth without ill effect [545], though high vapor concentrations induce anesthesia [546]. Rinse solution alternatives for vasculoid installation should be analyzed in more detail.

*** If all 24 trillion docking bays have their buffer tanks fully charged with oxygen at the outset, then the docking bay system collectively holds $\sim 2.3 \times 10^{23}$ molecules of O_2 or ~ 28 times more than the active capacity of the entire natural human red blood cell mass, providing an additional margin of safety against the risk of ischemia during rinse.

7.6 Initialization and Cold Start (~1.2 hours)

The final steps of vasculoid installation include:

(1) Plate Initialization. To aid in injury response and medical diagnosis, each plate may be assigned a unique position and identity code which can be echoed upon interrogation. With 200 billion operational vasculocytes and 150 trillion plates to initialize, each active vasculocyte must contact and initialize ~ 750 plates. Traveling at a net velocity of 10 microns/sec across the vasculoid, a vasculocyte can traverse (and initialize) 750 plates in ~ 100 sec. The address block is 100 bits in length; 50 bits are sufficient to specify $2^{50} = 1000$ trillion unique objects in the system, but additional bits are required to specify each plate's branch level in the fractal vascular tree and 10 bits are reserved for self-correcting parity checks.

(2) Install Storage Vesicles. The vesicles are small storage garages containing reserves of mobile and cargo-carrying nanodevices, other auxiliary nanodevices, spare parts, replacement modules and repair materials, critical biochemical consumables, and compressed refuse. Vesicles may also incorporate nanoscale bioprocess plants to manufacture small quantities of artificial biochemicals not normally produced in the body. Each vesicle is $\sim 1 \text{ mm}^3$ in volume, providing enough space to store ~ 1 billion tankers, ~ 300 million vasculocytes, or 350,000 boxcars. Vesicles may be attached directly to the vasculoid surface using sapphire struts affixed to reinforced base plates, or may be attached to each other to build convenient three-dimensional configurations (e.g. “bunch of grapes” formations).

As an order-of-magnitude estimate of the total number of vesicles that might be required, the volume required to store a complete replacement for the entire mobile container population would include 166.2 trillion tankers (1 micron³/tanker) or 166.2 cm³, 32 billion boxcars (2827 micron³/boxcar) or 91.7 cm³, and 2 trillion backup vasculocytes for tenfold redundancy (3 micron³/vasculocytes) or 6 cm³, totaling ~264 cm³ of storage. Including additional space for bioprocess plants, spare parts, consumables and refuse storage may boost total vesicle volume to ~500 cm³, requiring ~0.5 million vesicles which would fill roughly the combined internal volume of the four cardiac chambers [4] which are no longer needed for pumping blood. However, conservative design principles would suggest that vesicles should be widely distributed throughout the body to maximize system survivability in the event of massive trauma.

Infusion of 500 cm³ through the two catheters at a modest infusion velocity of 1 cm/sec requires ~200 sec for infusion of all vesicle components and their contents. Each 3 mg (fully loaded) vesicle is installed by a team of ~3000 vasculocytes which can collectively apply ~30,000 nanonewtons of force (using only 10 active legs among the ~100 available on the ventral side of each vasculocyte) resulting in a vesicle acceleration of ~1 g (enough to overcome gravity in a supine patient, and easily increased if needed). Simultaneously installing all 500,000 vesicles requires the cooperative activity of ~1.5 billion 1–50 picowatt vasculocytes (Section 2.5) which consumes a total power of 1.5–75 milliwatts during the installation.

- (3) Install sealed carotid, jugular, or navel access port (Section 8.1), as required (~40 sec).
- (4) Activate ciliary distribution system (~10 sec). This should probably include a brief stereotypical self-cleaning protocol to further ensure that all particles and stray nonessential nanorobots have been removed from the appliance interior.
- (5) Introduce into the vasculoid interior the entire 257.9 cm³ operational tanker and boxcar population, requiring ~100 sec at a modest ~1 cm/sec dry infusion velocity.
- (6) Warm the patient (~1 hour) using heat generation from excess ciliary activation, energy from onboard thermogenerative systems or external heat sources imported via enhanced plate conductivity (Section 8.2), or simple electrical or rf heating. Restart normal respiration as soon as possible. (The heart remains permanently inhibited, although the endocardium is coated with vasculoid plates.)
- (7) Reverse cytoactivity inhibition that was initiated during patient preparation (Section 7.2), as appropriate.
- (8) Remove catheters and seal all vascular and dermal breaches.

The vasculoid is now fully operational and self-contained. The patient is warm and breathing. All essential metabolic and immunological systems have returned to normal function. Healthy vascular conditioning is

maintained on a permanent basis (post–installation) because the vasculoid exercises precise control over the transport of cholesterol, leukocytes and platelets, the principal participants in the arteriosclerogenic process. Skin and tissue suppleness may be controlled by adjusting the spring constants of linked bumpers between adjacent plates (Section 8.8).

A number of cosmetic issues must be addressed. For example, unpigmented tissues (e.g. the tongue and gums, fingernail dermae, the uvea and lacrimal apparatus of the eye, and brain tissue) will appear a pale, waxy translucent white owing to the complete absence of red cells; pigmented tissues (e.g. dark skin) should be largely unchanged. For more traditionalist users or for other aesthetic reasons, semi–natural coloration might be restored by retaining blue sapphire in venous channels but substituting red ruby (chemically similar to sapphire) in arterial plate materials. However, transmission and reflection properties of these substances may differ markedly, and such colors would likely require at least small numbers of potentially troublesome impurity atoms (10^{-3} – 10^{-4} of Fe, Ti, or Cr atoms; [4], Section 5.3.7) to be present. Alternatively, a thin diamondoid–veneered sublayer of organic chromophores of appropriate colors might be employed.

After a brief period of rest, postoperative checkout, and familiarization with user interfaces, the patient is released from the installation facility.

7.7 Vasculoid Removal

The procedures outlined above for vasculoid installation are designed to be fully reversible at every step. Thus, vasculoid removal may be accomplished by reversing the installation procedure, except that patient preparation should be performed first. If the patient has worn his or her vascular appliance for a considerable time, heart muscles [547–549], venous valves, splenic filtration systems and the erythroid marrow may have significantly atrophied, requiring remedial cellular repair [3]. (The conditions and procedures necessary for maintaining such tissues in a healthy state, post–installation, have not been thoroughly examined and require further study.) Homologous formed blood elements such as RBCs must also be premanufactured for postoperative infusion prior to vasculoid removal, and any genetically modified endothelial cells must be reprogrammed back to their original state.

7.8 Aggressive Installation Scenario

For our highly speculative second scenario, we briefly (and only superficially) describe an aggressive installation procedure that attempts to install the vasculoid into a fully metabolizing normothermic human body about 100 times faster than the hypothermic procedure detailed in the principal scenario. As discussed in Section 7.2, vascular conditioning and mapping should occur before installation, in part to allow the manufacture of a folded, pre–assembled custom appliance tailored to the patient’s unique vasculature which is then presented to the physician for installation. Our aggressive procedure involves three steps: (1)

pre-charging the body with respirocyte infusant and removal of bloodborne cells; (2) physical installation of vasculoid plates as continuous rolling sheets, coincident with removal of infusant fluid; and (3) configuration and permanent connection of the appliance, followed by removal of support structures and system activation. It is intended that all steps will be carried out within the $\sim 10^3$ sec (~ 15 min) ischemic time limit (Section 7.1) imposed by non-respiratory metabolite concentrations.

The aggressive procedure begins by accessing one or more large veins to permit rapid infusion and exfusion. The blood is quickly replaced, as it circulates, with an infusant solution containing electrolytes, glucose, and other essential substances, plus a sufficient nanocrit of respirocyte-class devices to provide respiratory support. The transfusion is speeded by using moderate numbers of “dragnet” style nanorobots as described in other contexts by Freitas [9, 550] – each such nanorobot manipulates an adjustable 1–100 micron diameter net in order to physically gather bloodborne cells that may be trapped in eddies near venous valves, vascular sinuses, and similar spaces. Within a few circulation times, perhaps ~ 200 sec, the vascular compartment is cleared of all free cells and most macromolecules. Exfused blood is retained until the procedure is complete, to facilitate reversal in the event of a medical emergency. The heart is now stopped. Respirocytes continue to provide oxygen and absorb carbon dioxide; even a modest 1% nanocrit can provide ~ 25 minutes of resting metabolism without recharging, perhaps slightly less in the most energy-intensive tissues such as the brain. But because fresh infusant can be introduced continuously, the patient can be parked in this state indefinitely if need be.

Next, the vasculoid is introduced into the arteriovenous vasculature directly through the heart via cardiopuncture or cardiocentesis [551–563]. Cardiocentesis involves the surgical puncture of the heart, most often used today *in utero* on developing fetuses [558–563] either to extract [559–561] or to insert [562, 563] fluids into the vasculature (e.g., blood transfusion [563]), or more rarely on adult organisms for related purposes [551–557]. Cardiocentric installation of the vasculoid is required because the human circulation consists of two independent arterial circuits (pulmonary and systemic) each containing their own capillary beds.

The appliance is installed as a continuously-everting concentric tube, a process called progressive fractal eversion that may be visualized as turning a glove inside out. Basic plates, docking bays and cellulocks are prefastened in the proper configuration to fit the various diameters and branchings of the blood vessels that they will coat. The necessary flexibility of this sheet of plates is provided by sophisticated watertight jointed interplate bumpers that have yet to be designed. Eversion may be powered by compressed gas, ciliary action between opposed plates, or by other appropriate means; the presence of pressurized gas (e.g., pure dry N_2) would also help to minimize the occurrence of leaks during installation. Each docking bay has an appropriate tanker already docked. As soon as the plate makes contact with the endothelial surface, the docking bay begins to work. Since the vasculoid contains a sufficient number of docking bays to accommodate peak metabolic loads, the preattached tankers can supply oxygen, glucose, and other nutrients, and accumulate wastes. Most critically, 5 trillion oxygen tankers are attached to all available respiratory-tanker docking bays, providing ~ 474 sec (~ 8 min) of oxygen at the basal rate. This sustainable duration is easily extended to ~ 1318 sec (~ 22 min) of basal oxygen supply by redesigning 13.9 trillion of the 24 trillion docking bays that are not needed for nonrespiratory transport (Section 2.1) to include the capacity for gas transfer during installation, since at the basal rate docking bays require only 67 active sorting rotors (Section 2.4.1).

Installation is initiated cardiocentrically as two primary segments imported via two cardiopuncture entry points through the relatively thin walls of the right atrium and the left atrium, respectively. Installation works outward from each chamber opening, usually in the natural direction of valve motion, moving towards the distal capillary beds. From the right atrial entry point, the unfolding right atrial appliance segment has four “fingers” and simultaneously plates: (1) the superior vena cava; (2) the inferior vena cava; (3) the coronary sinus (which receives cardiac veins from heart tissue); and moves through (and plates) the right atrial and ventricular chambers, thence to plate (4) the pulmonary artery. The right atrial segment also must plate all of the numerous Thebesian veins; these venules return blood from the myocardium without entering the venous current, and open directly into the right atrium. From the left atrial entry point, the unfolding left atrial appliance segment has five “fingers” and simultaneously plates: (1&2) the two left pulmonary veins (which frequently terminate by a common opening); (3&4) the two right pulmonary veins; and moves through (and plates) the left atrial and ventricular chambers, thence to plate (5) the aorta.

Additionally, a third vasculoid segment called the portal segment must be inserted through a third abdominal entry point in order most efficiently to plate the portal vein, which lies midway between the hepatic capillary beds and the intestinal capillary beds.

Advancing at 1 cm/sec (2 cm/sec internal speed between the installed surface and the inverted tube), the vasculoid requires only 70 sec to plate the maximum ~70-cm main arterial or venous course ([4], Table 8.1). Fluid and respirocytes are withdrawn through the center of the inverted tube. As the vasculoid reaches the capillaries, the progression of the eversion may slow to ~10 micron/sec of travel, requiring another ~100 sec to complete all capillary plating. Human capillaries contain ~14% of blood volume but comprise ~95% of the surface area of the vascular system ([4], Table 8.4), so most of the appliance’s plates are installed during this final ~100 seconds. If all 150 trillion plates are active throughout this process, the power draw is a physiologically-tolerable 150 watts (Section 7.4). Upon first contacting the endothelium, each 2 mm² plate has ~0.1414 seconds – time enough for 14,140 localized 100-nm movements at 1 cm/sec (100 KHz; Section 2.3.1) – to adjust its position and bumper configurations, and to clear away any detritus trapped beneath it (e.g., respirocytes, stray cells, etc.), before the next plate is placed. This seems sufficient.

Once the vasculoid has filled the capillaries, the arterial and venous branches are joined, detaching the internal fluid transfer channels running through the vasculoid lumen which are quickly retracted from the interior. The ciliary system can then be activated and tankers will begin to be delivered to and from the capillaries, starting ~200 sec after the first transcordial introduction of the vasculoid mechanism. Interior rinse is unnecessary because the luminal surface of the appliance was installed dry. Vesicle installation is performed post-installation via component injection, and assembled using vasculocytes, at leisure.

Since this advanced model of the vasculoid comes preassembled, it can continually report its status and monitor physiological indications of the patient during installation, via an interplate communication network ([4], Section 5.4.2). In the event of an unforeseen medical catastrophe during installation, the vasculoid may be evacuated using an emergency extraction protocol if the appliance itself has not suffered a major loss of integrity and the transfer channels are still attached. In the emergency extraction protocol, the vasculoid undergoes partial flattening with circumferential fission in the capillaries. Then the arterial and venous sides of the vasculoid are withdrawn as they were inserted, using a reverse-eversion process with progressively increasing velocities possibly reaching ~10 cm/sec in the largest arteries. During such an extraction, only a ~1.4-micron-wide annular ring will be moving at this high speed adjacent to tissue – the installed vasculoid does not move, and the moving vasculoid is surrounded by immobile vasculoid. As a result, installed

appliance plate–sheets may be pulled out by applying an extraction force to the fluid transfer channel structures that are still attached to the terminus of each capillary tube. Continuous pressurized return of respirocyte–charged infusant to the natural vasculature through these channels prevents pulling a vacuum behind the retreating tendrils of the appliance, which would cause the collapse of blood vessels as the appliance was removed. Thus in less than a minute, the patient has returned to the relative safety of the respirocyte–infused parked state from which the installation procedure was begun. In the context of a medical technology capable of manufacturing a vasculoid, the temporary bloodless state would not appear to be a cause for concern.

8. Vasculoid Optional Equipment

The following is a selection of a few additional devices, options, or subsystems that may be added to the basic vasculoid installation to achieve enhanced functionality.

8.1 External Ports

To facilitate physical communication with the external environment, the vasculoid may be equipped with mechanical external ports which permit the ready attachment of cables or peripheral equipment as an alternative to purely wireless (e.g. radio, optical) communication links. Vasculoid ports include an appropriate macroscopic connector receptacle in hard contact with the sapphire structure. Ports may include connections to the internal plate–to–plate acoustic communications network ([4], Section 7.3) or to docking bays and celllocks to permit access to the internal material flow and thus allow inserting or extracting: (1) molecules and cells; (2) fresh vasculocytes and spare parts; (3) bioprovisions including respiratory gases, water and energy supplies; and (4) nanomechanical or other waste material. Extracorporeal user control interfaces could also be connected via an external port, if needed. Convenient and aesthetic locations for external ports include the navel or the nape of the neck.

Respiratory gas and glucose transport requirements could be reduced by importing externally–supplied electrical energy – e.g., wall sockets (110 VAC at 0.9 amps equals the 100 watt human basal rate), backpack generators, solar collectors, nuclear batteries ([4], Section 6.3.7.1), etc. – to be distributed throughout the appliance via wiring in the plates. These sources could be used to power: (1) local recycling of CO₂ and H₂O waste back into O₂ and high–energy carbohydrate fuel (mimicking photosynthesis energized by light), (2) the reconstitution of amino acids and proteins from urea and other nitrogenous wastes (as found in ruminants [564] and in hibernating bears [565–567]), and (3) other “reversible nutrition” processes, converting the body of the envasculoided user into a more closed–cycle system with reduced dependence on certain material and energy inputs. However, this approach would correspondingly increase user dependence

on the chosen external power source and would require new in-plate or in-vesicle chemical processing plants without completely eliminating the need for any existing subsystem, hence may not be worth the added complexity.

8.2 Thermal Comfort Subsystem

Vasculoid installation leaves the user's gross thermal mass largely unchanged, as only ~4.4 kg of bloodborne water (~9% of the ~50 kg normally present in the human body) is removed and replaced with ~2 kg of sapphire vasculoid with a heat capacity equivalent to ~0.2 kg of water. Total passive aqueous heat capacity drops from 50.4 kcal/K down to 46.3 kcal/K.

Nevertheless, 20th century patients with extensive metallic implants (e.g. pins, plates, bolts and joints) occasionally report brief chilly sensations during periods of cold weather [568, 569] and in other circumstances [570], due to the high thermal conductivity of metal compared with natural biomaterials (Section 3) or with plastics [571]. Some organs such as the cornea are quite sensitive to sudden temperature changes – as little as a 0.3 K drop over a 0.785 mm² area for a duration of 0.9 sec (~700 nanojoules) is detectable by patients [572]. A thermally conductive sapphire or diamondoid-coated sapphire vascular implant could extend these unpleasant sensations throughout the entire body, even for activities as simple as manually grasping a cold object [573]. A targeted thermogenerative subsystem could help to eliminate this effect.

Perspiratory thermoregulation will continue as before. However, as explained in Section 3 the active heat transfer mechanism of blood will be completely disabled. Normal capillary vasoconstriction/vasodilation mechanisms may be at least partially suppressed to avoid unnecessary tensions at the vasculoid-vessel interface. Detection of these responses, or direct temperature measurement, may be used to adjust passive thermal conductivity over a wide range, as follows. Each plate abuts neighboring plates through metamorphic bumpers [4, 8], with optimal thermal contact along stripe-like diamondoid buttons. Within each bumper, we may place an opposed pair of diamondoid pistons, separated by vacuum when they are pulled apart. When pulled apart, heat can be conducted only through the sapphire infrastructure, or vacuum in the plate, or through a surrounding aqueous medium, and is thus very slow, almost the same as normal tissue. But when the two pistons are pressed tightly together against diamondoid bumper buttons that are in good thermal contact, heat conduction largely bypasses the poorly-conducting sapphire regions and flows almost exclusively through the diamondoid contact region. Thus with pistons apart, the envasculoided human body has near-normal thermal conductivity; with pistons in contact, the body's thermal conductivity becomes near-metallic, perhaps as conductive as stainless steel (Section 3). This transition is subject to user or program control, is switchable in microseconds, and may be directed only to specific volumes or pathways within the body if so desired*. A more complex system might employ thermal rectifiers [574], or, as J.S. Hall suggests, "heat pumps could be placed in the joints to make the whole phenomenon usefully controllable, augmented if necessary with tankers of ice and/or steam."

* For example, the brain has some special vascular supply, with venous blood in the nose and from the face providing additional cooling. During even the most strenuous exercise in hot environments, with

temperatures in the leg muscles reaching 44–45 °C, the brain remains at a balmy 38–39 °C, preventing heat stroke. This functionality may be replicated by the vasculoid appliance.

8.3 Internal Caching

Installation of a full vasculoid appliance permanently displaces ~4.2 liters of natural blood volume, freeing up ~1 gallon of internal storage volume. At least some of this volume may be used for containerized temporary caching of consumables including surplus glucose, fats, water, oxygen (e.g. a high–pressure nanolung [6]), minerals or other useful biomaterials, or various bio– and nano–wastes. For example, a 1–liter 1000–atm O₂ solid–walled cache holds ~34 hours of oxygen at the human basal metabolic rate or ~2 hours at the maximum rate [6].

The free ~4.2–liter volume could also be used to store a wide variety of useful equipment or tools including computers, computer memories, external communications or navigational devices, solar energy accumulators, weapons, spare vasculocytes and other special purpose nanorobots, spare parts, or useful tools. An entire spare vasculoid (~558 cm³) could even be stored in this volume.*

* New technologies are not always employed for sober purpose. The authors hesitate to note that 4.2 liters is exactly the volume of ethanol present in 14 metric (750 ml) bottles of 80–proof vodka, bringing new meaning to the idiom “hollow leg”.

8.4 Breathing in Low–Oxygen Environments

The vasculoid, like the micron–sized respirocites proposed elsewhere [5, 6], will offer the ability to breathe at low O₂ partial pressures. The vasculoid gas tanker fleet can hold ~20 minutes of oxygen at the basal metabolic usage rate, or up to ~100 minutes if most of the tanker fleet is diverted to respiratory gas carriage in lieu of other applications.

Vasculoid installed in underwater divers who are breathing pressurized air to modest depths should allow only enough nitrogen into the body to forestall mechanical tissue damage, then rotor it back out again as the diver surfaces to avoid decompression sickness. At 100% saturation the body absorbs ~10²¹ excess N₂ molecules per meter of depth. Each tanker could hold ~7.98 x 10⁹ nitrogen molecules (at 1000 atm), requiring the

storage capacity of 0.125 trillion tankers per each 1 meter of decompression. Given a reconfigurable fleet of ~166 trillion tankers, expedited decompressions from ~100 meters are probably achievable using the present design. To establish a greater vasculoid operating depth, in theory an auxiliary 1000-atm storage tank “nanolung” [6] installed in the vasculoid wall could provide ~9.43 cm³ N₂ storage capacity per each 100 meters of decompressible diving depth. However, nitrogen should not be used to hyperpressurize the tissues due to nitrogen narcosis [575]. It should also be noted that obesity is a risk factor in decompression sickness [576] because nitrogen is 5 times more soluble in fat than in water and because of reduced blood access to adipose tissue, and also compression and decompression are asymmetrical: a nitrogen load acquired in a few minutes may take hours to fully deplete purely by diffusion (and the extraction rate varies markedly by tissue type), so extravasculoid (Section 8.6) respirocyte-class nanorobots may be required for optimal results. Clearly the vasculoid can achieve a decompression rate comparable to breathing pure oxygen, but without the oxygen toxicity [575]. Helium may be useful for mixed-gas diving, but is prone to leakage ([4], Section 10.3.4); some will be lost from the body during use and cannot effectively be replaced from the environment.

8.5 Lymphovasculoid and Pathogen Disposal

The lymphatic system extends into all the same tissues as capillaries and is structurally similar to the venule network. However, since lymph vessels constitute a “cul-de-sac” system, not a “circulatory” system, it is unnecessary to install vasculoid systems in the lymphatics in order to achieve most of the positive benefits expected from an arteriovenous vasculoid. With the circulatory vasculoid in place, the workload of the natural lymphatic system may be greatly reduced – protein leakage from capillaries, entry of particulates into the tissues, and the presence of pathogens requiring immune system response all should be greatly reduced (Section 4.1).

More properly, lymphovasculoid should be regarded as optional equipment which may permit more precise control of the immune system in general and of lymphocyte traffic in particular. Total adult lymph flow is typically ~2 liters/day, so transport requirements within the lymphovasculoid should not be particularly severe (Section 4.2). If implemented, the lymphovasculoid would be emplaced as two distinct installations – a right lymphatic and a thoracic subsystem – following the natural division in the human body. Special lymph-recycling facilities may be required at the locations where the thoracic duct and the right lymphatic duct join the venous tree.

Pathogen disposal sites using an enzyme-based digest and discharge protocol [2] may be located near lymphoid tissues and organs (to permit immune system processing) and near excretory organs such as kidney, liver, gallbladder, and gut (to facilitate removal from the body). Specialization of this function at specific locations appears more efficient than on-site pathogen processing systems which would need to be numerous, widely distributed, and usually idle.

8.6 Extravasculoid Devices

It may be useful to deploy sensor probes which can leave the vasculoid and enter the surrounding tissues to detect and monitor remote events (such as angiogenesis, tumors, or pathogens) that otherwise might not be conveniently detected from within the vasculoid. Additionally, large blocks of tissue are only lightly vascularized or have no capillaries whatsoever, as for instance the synovial chambers in skeletal joints and the epidermis. Medical nanorobots capable of migrating through noncellular tissue might be useful both for repair purposes and for maintaining a disease-free condition in these tissues [3]. Extravasculoid devices may also constitute general-purpose mobile cell repair machines with even broader injury response and prevention capabilities.

8.7 Active Thermal Damage Suppression

Although the vasculoid itself is essentially fireproof (sapphire and ruby will not burn in oxygen), the overlying human tissue is not. Thus another optional upgrade to the basic vasculoid package is an active damage control subsystem that offers some protection from severe thermal burns. This optional subsystem would include installation of biocompatible sensor-tipped diamondoid or sapphire pores that pass from the epidermis through the dermis to the nearest envasculoided capillaries. The comparative human skin response to sapphire vs. fluid cooling has been studied experimentally [94].

Upon detection of a potentially harmful thermal event, sacrificial water is pumped from internal reservoirs into channels in the plates, and from there into the pores, eventually emerging as billions of aqueous microstreams. Touching a red hot object stimulates a nearly instantaneous emission of ablative water, producing a protective layer of heated water and steam between the hot object and the skin. Protection of the human hand ($\sim 150 \text{ cm}^2$) up to $\sim 1300 \text{ K}$ (\sim decomposition temperature of diamond) for a ~ 1 second exposure requires a 162 kilowatt/m^2 heat dissipation rate and a $\sim 1 \text{ cm}^3$ sacrificial water reservoir. Of course, this system could easily be overwhelmed if the user is exposed to intense IR radiation, such as inside burning buildings or near large explosions, and in any case the hair is not protected as well as the skin.

8.8 Active Resistance to Mechanical Damage

The overall static structure of the basic vasculoid appliance is an array of rigid plates, strongly fastened together, entirely covering a curved two-dimensional surface embedded in a three-dimensional space. The plates conform to ordinary movement, but may adequately resist certain kinds of destructive movement such as separation due to cutting, rapid accelerations or decelerations, and crushing injuries. Although local endothelial cells may be damaged during such sharp movements, an envasculoided tissue should be somewhat more resistant to gross damage.

For example, the critical buckling pressure of a hollow tube of circular cross-section deformed into an elliptical cylinder by external pressure is given by Freitas ([4], Eqn. 10.20) as $p_{crit} = (E h_{tube}^3) / (4 r_{tube}^3 (1 - c_{Poisson}^2))$ where E is Young's modulus ($\sim 10^6$ N/m² for vascular tissue and $\sim 10^{11}$ N/m² for sapphire ([4], Table 9.3)), h_{tube} is tube wall thickness (~ 1 mm for aorta, ~ 1 mm for capillary and for vasculoid plate-tube; [4], Table 8.1), r_{tube} is tube inner radius (~ 25.0 mm for aorta, ~ 8 mm for capillary, ~ 7 mm for vasculoid plate-tube; [4], Table 8.1), and $c_{Poisson}$ is the Poisson ratio for the material (~ 0.3 for vascular tissue, ~ 0.1 for diamondoid). Using this formula and the stated values, p_{crit} for aorta is ~ 59 N/m² and the vasculoid coating adds only negligible additional resistance to crushing, $p_{crit} \sim 0.002$ N/m². However, for the ubiquitous capillaries $p_{crit} \sim 540$ N/m² but adding the vasculoid coating can dramatically increase crushing resistance up to $\sim 7 \times 10^7$ N/m², or ~ 700 atm of overpressure. Since the mechanical coupling between plate bumpers is subject to both design and conscious user control ([4], Section 7.4.2), the crushing resistance of capillary beds can be autogenously varied over five orders of magnitude. Of course, high overpressures may seriously damage the underlying natural endothelium (Section 4.1.3.1) but this might nevertheless be acceptable over small areas during emergency situations. For instance, resistance to deep incision-slash wounds would be markedly improved. Crushing strength may be increased using thicker plates or stronger bumpers.

Similarly, the bending stiffness of a hollow tube is given by Freitas ([4], Section 9.3.1.2) as $k_{shaft} = 3p E (R_{tube}^4 - r_{tube}^4) / (4 L_{tube}^3)$, where the outside tube radius is $R_{tube} = r_{tube} + h_{tube}$ and the tube length is L_{tube} (~ 400 mm for aorta, ~ 1 mm for capillary; [4], Table 8.1). Using this formula and the stated values, the resistance to bending (stiffness) of the aorta increases 60-fold (to ~ 230 N/m) when coated with a single layer of vasculoid plates, but the stiffness of capillaries increases nearly 70,000-fold (to ~ 0.4 N/m) when coated with diamondoid plates. The buckling strength ([4], Eqn. 9.44) of coated vessels compared to natural vessels may exhibit similar orders-of-magnitude improvement, though in practical systems some of this potential will be lost because interbumper connection rupture strength may be only 10^7 – 10^9 N/m² ([4], Section 5.4.3), 1–3 orders of magnitude less than for solid diamondoid materials. The natural musculature may be too weak to move soft tissues that are thoroughly penetrated with ultrastiff capillaries, but selective autogenous control of plate bumper expansion and contraction should make possible any necessary macroscale voluntary movements, or on-demand mechanical rigidification of specific limbs or organs. Bumpers may be driven at \sim KHz frequencies ([4], Section 5.4.3), permitting positional adjustments on millisecond timescales. Such motions will require additional energy expenditure.

A complete examination of the acceleration tolerance of the envasculoided whole human body would have to take into account a wide variety of factors including differential density of body parts (e.g., lung, soft tissue, skeleton), magnitude and direction of the stress vector (e.g., positive or negative, axial or transverse, etc.), duration and timing of the stress vector (e.g., acute or chronic, linear or periodic), rate of onset and pulse shape of the acceleration, and the mechanical characteristics both of linked vasculoid components and of the vasculoid-endothelial interface – a major analysis that is quite beyond the scope of this paper. However, a simple order-of-magnitude estimate may be cautiously ventured, as follows.

A vasculoid appliance of differential density Dr_{vasc} relative to soft tissue and mean thickness h_{vasc} in contact with biological tissues that are subjected to a linear acceleration of $a = (a_G g)$, where $g = 9.81$ m/sec², pushes the vasculoid into the tissues with a pressure force of $P_{vasc} \sim h_{vasc} Dr_{vasc} g a_G$. Because the vasculoid tube has 2 opposed walls, each 1 mm thick, and because the tanker fleet covers 4%–55% of the surface of each of these opposed walls (Section 2.4.1) with tankers that are 1 mm thick, then the effective capillary thickness of pushed vasculoid under acceleration ranges from $h_{vasc} \sim 2.1$ – 3.1 microns. Tissue density is $r_{tiss} \sim 1050$ kg/m³ ([4], Table 8.12); sapphire tanker density is $r_{tank} \sim 993$ – 1738 kg/m³ if filled with vacuum or water at 310 K, and plate density is $r_{plate} \sim 2000$ kg/m³ (Table 1), giving an effective vasculoid density of $r_{vasc} \sim 1643$ – 1988 kg/m³ under various usage conditions. Hence $Dr_{vasc} = r_{vasc} - r_{tiss} \sim 593$ – 938 kg/m³ and so the maximum

tolerable G–force for envasculoided tissue is $a_G \sim P_{\text{vasc}} / (h_{\text{vasc}} D r_{\text{vasc}} g) = 24.4 P_{\text{vasc}} \sim 4880 \text{ G}$, taking $P_{\text{vasc}} \sim 200 \text{ N/m}^2$ as the tentative limit for acute vascular damage because this has been found experimentally not to cause gross injury or denudation of canine arterial endothelium by shear force [279].

However, endothelial transcription factor responses (protein expression) can be triggered by shear forces as low as $0.02\text{--}2 \text{ N/m}^2$ ($a_G \sim 0.5\text{--}48.8 \text{ G}$) (Section 4.1.1) and normal physiological blood shear forces are $0.14\text{--}2.6 \text{ N/m}^2$ ($a_G \sim 3.4\text{--}63.4 \text{ G}$), so the maximum chronic external acceleration indefinitely tolerable by an envasculoided human body probably may not exceed 50–100 G without producing altered, possibly pathological, cytochemical states. (The operational limit of the current vasculoid design is also $\sim 30\text{--}100 \text{ G}$; Sections 2.3.1 and 2.4.4.4.) This still would represent a substantial improvement over the natural acceleration tolerance of the unaided human body – the mean relaxed tolerance is $\sim 3.23 \text{ G}$ [577] and loss of brain blood flow occurs at $+G_z > 4.5 \text{ G}$ [578]. Consciousness has been retained for a maximum of 45 seconds at 9 G using G–protective equipment and straining maneuvers developed for the U.S. Air Force [579], and for 4 minutes at 12 G or 4 seconds at $\sim 16 \text{ G}$ using water immersion [580]. Severe impact injury to humans occurs from $+G_z$ accelerations of 30 G exceeding 100 millisecon or 100 G exceeding 2 millisecon [578] – the recordholding primate is evidently one of Colonel Stapp’s chimpanzee test subjects that survived ~ 1 millisecon of 247 G in the $-G_x$ direction on a rocket sled, suffering only “moderate” injuries [581]. Thus the basic vasculoid may improve maximum human acceleration tolerance by a factor of 10–20, or more, and higher–G–tolerant architectures can probably be devised.

With sufficient capability, the vasculoid structure could allow the non–local distribution of stress – for example, by spreading the force of an impact in a manner similar to a bulletproof vest, also helping to quickly close any vascular breaches that might occur. A common and significant personal injury mechanism is brain–skull impact, and a tough interwoven vascular support scaffolding could help to fix the brain within the skull, potentially reducing the danger of concussion for at least moderate decelerative loads. (Active suppression of rotational impact trajectories may enhance cerebral durability, as demonstrated using high–speed cinematograph films of woodpeckers which regularly survive 6–7 m/sec cranial impact velocities with $\sim 1000 \text{ G}$ decelerations [582, 583].) Positional information and selective sectioning could allow unavoidable partitions of tissue to occur along straight planes, producing a minimum of damage when compared with ordinary tearing injuries. Whether the vasculoid appliance would be a liability in explosive overpressure situations, where a fluid–filled vasculature might not (e.g., lethal effects in humans noted for 40 psi [584] to 50 psi [585] overpressure shockwave; 300 psi ($\sim 20 \text{ atm}$) record for successful deep water submarine escape [584]), deserves further study.

More speculative capabilities, such as temporary life support of sectioned tissue and repair of severe wounds, are beyond the scope of this paper.

9. Conclusions

This paper has presented a preliminary scaling study for a conceptual design of a single, complex, multisegmented nanotechnological robot that appears capable – with numerous caveats, as noted – of duplicating all essential thermal and biochemical transport functions of the blood, including circulation of respiratory gases, glucose, specialty biochemicals, waste products, and all bloodborne cellular elements. The vasculoid, a 2-kg ~200-watt intimate personal appliance, conforms to the shape of the existing vasculature and may serve as a complete replacement for natural blood while greatly improving the durability and functionality of the human body.

The authors are well aware that the device described in this paper would represent a most extreme intervention using a very advanced medical molecular nanotechnology. It also should be noted that our current knowledge of the biological functions of the circulatory system is incomplete, so the design presented here must be considered provisional at best. But the principal challenge of the present work was to advance a plausible argument that a nanomechanical whole-body thermal and biomaterials transport system would violate no known physical, engineering, or medical principles, could presumptively be made adequately safe for the user, and might confer some significant advantages over simpler whole-body systems exclusively employing unlinked populations of individual bloodborne and tissueborne nanorobots.

Ultimately, and from the standpoint of human-guided evolution, the body exists primarily to ensure the survival of the mind – not the replication of the genes, which was the ancient paradigm [586, 587]. It would seem that a somewhat more advanced and compact version of the proposed device could function independently of nearly all noncortical tissue. Thus the vasculoid is most fascinating because it may represent one last outpost of humanity at the final frontier of biological evolution.

References

1. Christopher J. Phoenix, "Early Nanotech Project: Replace Blood?" sci.nanotech posting on 14 June 1996; http://discuss.foresight.org/critmail/sci_nano/2273.html or http://crit.org/critmail/sci_nano/2273.html
2. Robert A. Freitas Jr., "Microbivores: Artificial Mechanical Phagocytes using Digest and Discharge Protocol," Zyvex preprint, March 2001; <http://www.zyvex.com/Publications/articles/Microbivores.html>. See also: Robert A. Freitas Jr., "Microbivores: Artificial Mechanical Phagocytes," Foresight Update No. 44, 31 March 2001, pp. 11–13; <http://www.imm.org/Reports/Rep025.html>
3. Robert A. Freitas Jr., Nanomedicine, Volume II: Systems and Operations, 2004. In preparation.
4. Robert A. Freitas Jr., Nanomedicine, Volume I: Basic Capabilities, Landes Bioscience, Georgetown, TX, 1999; <http://www.nanomedicine.com>
5. Robert A. Freitas Jr., "Respirocytes: High performance artificial nanotechnology red blood cells," NanoTechnology Magazine 2(October 1996):1, 8–13.
6. Robert A. Freitas Jr., "Exploratory design in medical nanotechnology: A mechanical artificial red cell," Artificial Cells, Blood Substitutes, and Immobil. Biotech. 26(1998):411–430; <http://www.foresight.org/Nanomedicine/Respirocytes.html>
7. K. Eric Drexler, Nanosystems: Molecular Machinery, Manufacturing, and Computation, John Wiley & Sons, Inc., New York, 1992; K. Eric Drexler, Engines of Creation: The Coming Era of Nanotechnology, Anchor Press/Doubleday, New York, 1986; <http://www.foresight.org/EOC/index.html>
8. Robert A. Freitas Jr., "Vasculocytes," unpublished document, 14 September 1996; <http://www.foresight.org/Nanomedicine/Gallery/Species/Vasculocytes.html>
9. Robert A. Freitas Jr., "Clottocytes: Artificial Mechanical Platelets," Foresight Update No. 41, 30 June 2000, pp. 9–11; <http://www.imm.org/Reports/Rep018.html>
10. Robert A. Freitas Jr., "Say Ah!" The Sciences 40(July/August 2000):26–31;

<http://www.foresight.org/Nanomedicine/SayAh/index.html>.

11. Robert A. Freitas Jr., "Robots in the bloodstream: the promise of nanomedicine," Pathways, The Novartis Journal 2(October–December 2001):36–41;
<http://www.novartis.com/pathways/content/artic3.html>,
<http://www.kurzweilai.net/meme/frame.html?main=/articles/art0410.html>
12. Amy L. Decatur, Daniel A. Portnoy, "A PEST-like sequence in listeriolysin O essential for *Listeria monocytogenes* pathogenicity," Science 290(3 November 2000):992–995.
13. S. Majumdar, H. Kaur, H. Vohra, G.C. Varshney, "Membrane surface of *Mycobacterium microti*-infected macrophages antigenically differs from that of uninfected macrophages," FEMS Immunol. Med. Microbiol. 28(May 2000):71–77.
14. P.M. Allen, D.I. Beller, J. Braun, E.R. Unanue, "The handling of *Listeria monocytogenes* by macrophages: the search for an immunogenic molecule in antigen presentation," J. Immunol. 132(January 1984):323–331; P.M. Allen, E.R. Unanue, "Antigen processing and presentation by macrophages," Am. J. Anat. 170(July 1984):483–490.
15. Cindy Belles, Alicia Kuhl, Rachel Nosheny, Simon R. Carding, "Plasma membrane expression of heat shock protein 60 in vivo in response to infection," Infect. Immun. 67(August 1999):4191–4200;
<http://iai.asm.org/cgi/content/full/67/8/4191?view=full&pmid=10417191>
16. Jason G. Cyster, "Chemokines and cell migration in secondary lymphoid organs," Science 286(10 December 1999):2098–2102.
17. Yaneer Bar–Yam, "Dynamic Medicine," New England Complex Systems Institute, manuscript, 2002; see also <http://necsi.org/guide/examples/hiv.html>
18. Arthur C. Clarke, Profiles of the Future, Harper and Row Publishers, New York, 1962.
19. Michael LaBarbera, "Principles of design of fluid transport systems in zoology," Science 249(31 August 1990):992–1000.

20. S. Nielsen, J. Frokiaer, D. Marples, T.H. Kwon, P. Agre, M.A. Knepper, "Aquaporins in the kidney: from molecules to medicine," *Physiol. Rev.* 82(January 2002):205–244.
21. L. Bankir, N. Bouby, M.M. Trinh–Trang–Tan, "The role of the kidney in the maintenance of water balance," *Baillieres Clin. Endocrinol. Metab.* 3(August 1989):249–311.
22. E. Kristal–Boneh, J.G. Glusman, C. Chaemovitz, Y. Cassuto, "Improved thermoregulation caused by forced water intake in human desert dwellers," *Eur. J. Appl. Physiol. Occup. Physiol.* 57(1988):220–224.
23. A.K. Hemal, A. Goel, M. Kumar, N.P. Gupta, "Evaluation of laparoscopic retroperitoneal surgery in urinary stone disease," *J. Endourol.* 15(September 2001):701–705.
24. P. Tombolini, M. Ruoppolo, C. Bellorofonte, C. Zaatar, M. Follini, "Lithotripsy in the treatment of urinary lithiasis," *J. Nephrol.* 13(November–December 2000):S71–S82.
25. E. Minevich, "Pediatric urolithiasis," *Pediatr. Clin. North. Am.* 48(December 2001):1571–1585.
26. A. Dascalu, A. Peer, "Effects of radiologic contrast media on human endothelial and kidney cell lines: intracellular pH and cytotoxicity," *Acad. Radiol.* 1(October 1994):145–150.
27. W.A. Morgan, Y. Dingg, P.H. Bach, "The relationship between sodium chloride concentration and bile acid cytotoxicity in cultured kidney cells," *Ren. Fail.* 20(May 1998):441–450.
28. D.M. Cohen, S.R. Gullans, "Urea induces Egr–1 and c–fos expression in renal epithelial cells," *Am. J. Physiol.* 264(April 1993):F593–F600.
29. M. Hanelt, M. Gareis, B. Kollarczik, "Cytotoxicity of mycotoxins evaluated by the MTT–cell culture assay," *Mycopathologia* 128(December 1994):167–174.
30. S.Y. Chou, J.G. Porush, P.F. Faubert, "Renal medullary circulation: hormonal control," *Kidney Int.* 37(January 1990):1–13.

31. M.J. McKinley, "Common aspects of the cerebral regulation of thirst and renal sodium excretion," *Kidney Int. Suppl.* 37(June 1992):S102–S106.
32. C. De Rouffignac, "Multihormonal regulation of nephron epithelia: achieved through combinational mode?" *Am. J. Physiol.* 269(October 1995):R739–R748.
33. M. Meyer, C.G. Stief, A.J. Becker, M.C. Truss, A. Taher, U. Jonas, W.G. Forssmann, "The renal paracrine peptide system – possible urologic implications of urodilatin," *World J. Urol.* 14(1996):375–379.
34. G.A. Quamme, C. de Rouffignac, "Epithelial magnesium transport and regulation by the kidney," *Front. Biosci.* 5(1 August 2000):D694–D711.
35. James A. Wilson, *Principles of Animal Physiology*, Macmillan Publishing Company, New York, 1972.
36. T. Tozawa, "Enzyme-linked immunoglobulins and their clinical significance," *Electrophoresis* 10(August–September 1989):640–644.
37. F. Balli, S. Gentilini, "Asymptomatic hypertransaminasemia," *Pediatr. Med. Chir.* 18(July–August 1996):363–364. In Italian.
38. M. Monfort–Gouraud, A. Hamza, K. Nacer, G. Barjonnet, V. Tranie, M. Devanlay, G. Sauvageon, "Hypertransaminasemia in an adolescent," *Arch. Pediatr.* 6(November 1999):1191–1192. In French.
39. U. Pohl, C. De Wit, T. Gloe, "Large arterioles in the control of blood flow: role of endothelium–dependent dilation," *Acta Physiol. Scand.* 168(April 2000):505–510.
40. S. Ferlito, "Physiological, metabolic, neuroendocrine and pharmacological regulation of nitric oxide in humans," *Minerva Cardioangiol.* 48(June 2000):169–176.
41. J.S. Clegg, P. Seitz, W. Seitz, C.F. Hazlewood, "Cellular responses to extreme water loss: the water–replacement hypothesis," *Cryobiology* 19(June 1982):306–316.

42. J.S. Clegg, E.P. Gordon, "Respiratory metabolism of L-929 cells at different water contents and volumes," *J. Cell Physiol.* 124(August 1985):299-304.
43. J.L. Mansell, J.S. Clegg, "Cellular and molecular consequences of reduced cell water content," *Cryobiology* 20(October 1983):591-612.
44. J.S. Clegg, S.A. Jackson, K. Fendl, "Effects of reduced cell volume and water content on glycolysis in L-929 cells," *J. Cell Physiol.* 142(February 1990):386-391.
45. S. Eskelinen, P. Saukko, "Effects of glutaraldehyde and critical point drying on the shape and size of erythrocytes in isotonic and hypotonic media," *J. Microsc.* 130(April 1983):63-71.
46. Charles A. Linker, "Chapter 12. Blood," in Lawrence M. Tierney, Jr., Stephen J. McPhee, Maxine A. Papadakis, eds., *Current Medical Diagnosis and Treatment*, 35th Edition, Appleton and Lange, Stamford, CT, 1996, pp.434-488.
47. Willie R. Koen, "Chapter 34. Circulating Stem Cells: A Fourth Source for the Endothelialization of Cardiovascular Implants," in Peter Zilla, Howard P. Greisler, eds., *Tissue Engineering of Prosthetic Vascular Grafts*, R.G. Landes Company, Austin TX, 1999, pp. 371-378.
48. P. Carmeliet, A. Luttun, "The emerging role of the bone marrow-derived stem cells in (therapeutic) angiogenesis," *Thromb. Haemost.* 86(July 2001):289-297.
49. Manuela Martins-Green, "Chapter 3. The Dynamics of Cell-ECM Interactions with Implications for Tissue Engineering," in Robert P. Lanza, Robert Langer, William L. Chick, eds., *Principles of Tissue Engineering*, R.G. Landes Company, Georgetown TX, 1997, pp. 23-46.
50. Ivars Peterson, "From microdevice to smart dust," *Science News* 152(26 July 1997):62-63.
51. Martin L. Lenhardt, Ruth Skellett, Peter Wang, Alex M. Clarke, "Human ultrasonic speech perception," *Science* 253(5 July 1991):82-85. See also: <http://www.flantech.com/neuropho.htm>
52. NCT Group, <http://www.nctgroupinc.com>; Jeffrey N. Denenberg, "Noise cancellation: Quietening the environment," *Noise Cancellation Technologies*, <http://doctord.dyn.dhs.org:8000/Pubs/POTENT.htm>; Ron

Kurtus, "Noise cancellation," 9 November 2000, <http://www.school-for-champions.com/science/noise.htm>.

53. K. Holmberg, U. Landstrom, B. Nordstrom, "Annoyance and discomfort during exposure to high-frequency noise from an ultrasonic washer," *Percept. Mot. Skills* 81(December 1995):819–827.

54. A. Wright, I. Davies, J.G. Riddell, "Intra-articular ultrasonic stimulation and intracutaneous electrical stimulation: evoked potential and visual analogue scale data," *Pain* 52(February 1993):149–155.

55. A.R. Williams, J. McHale, M. Bowditch, D.L. Miller, B. Reed, "Effects of MHz ultrasound on electrical pain threshold perception in humans," *Ultrasound Med. Biol.* 13(May 1987):249–258.

56. C. Bruce Wenger, James D. Hardy, "Chapter 4. Temperature Regulation and Exposure to Heat and Cold," in Justus F. Lehmann, ed., *Therapeutic Heat and Cold*, Fourth Edition, Williams & Wilkins, Baltimore, MD, 1990, pp. 150–178.

57. W.C. Duckworth, "Hyperglycemia and cardiovascular disease," *Curr. Atheroscler. Rep.* 3(September 2001):383–391.

58. P.V. Vaitkevicius, M. Lane, H. Spurgeon, D.K. Ingram, G.S. Roth, J.J. Egan, S. Vasan, D.R. Wagle, P. Ulrich, M. Brines, J.P. Wuerth, A. Cerami, E.G. Lakatta, "A cross-link breaker has sustained effects on arterial and ventricular properties in older rhesus monkeys," *Proc. Natl. Acad. Sci. (USA)* 98(30 January 2001):1171–1175; <http://www.pnas.org/cgi/content/full/98/3/1171>

59. S. Vasan, P.G. Foiles, H.W. Founds, "Therapeutic potential of AGE inhibitors and breakers of AGE protein cross-links," *Expert Opin. Investig. Drugs* 10(November 2001):1977–1987.

60. F. Pomeroy, A. Molinar Min, M. La Selva, A. Allione, G.M. Molinatti, M. Porta, "Benfotiamine is similar to thiamine in correcting endothelial cell defects induced by high glucose," *Acta Diabetol.* 38(2001):135–138.

61. K. Asahi, K. Ichimori, H. Nakazawa, Y. Izuhara, R. Inagi, T. Watanabe, T. Miyata, K. Kurokawa, "Nitric oxide inhibits the formation of advanced glycation end products," *Kidney Int.* 58(October 2000):1780–1787.

62. S. Yamagishi, S. Amano, Y. Inagaki, T. Okamoto, K. Koga, N. Sasaki, H. Yamamoto, M. Takeuchi, Z. Makita, "Advanced glycation end products-induced apoptosis and overexpression of vascular endothelial growth factor in bovine retinal pericytes," *Biochem. Biophys. Res. Commun.* 290(25 January 2002):973-978.
63. Una S. Ryan, ed., *Endothelial Cells, Vols. I-III*, CRC Press, Boca Raton, FL, 1988.
64. Ralph C. Merkle, "Reversible electronic logic using switches," *Nanotechnology* 4(1993):21-40; J. Storrs Hall, "Nanocomputers and reversible logic," *Nanotechnology* 5(1994):157-167; Michael P. Frank, Tom Knight, Norm Margolus, "Reversibility in optimal scalable computer architectures," in Calude, Casti, Dineen, eds., *Unconventional Models of Computation (Proceedings of the First International Conference on Unconventional Models of Computation, January 1998)*, Springer, NY, 1998, pp. 165-182.
65. D.L. Brutsaert, "The endocardium," *Annu. Rev. Physiol.* 51(1989):263-273.
66. D.L. Brutsaert, L.J. Andries, "The endocardial endothelium," *Am. J. Physiol.* 263(October 1992):H985-H1002.
67. D.L. Brutsaert, G.W. De Keulenaer, P. Franssen, P. Mohan, G.L. Kaluza, L.J. Andries, J.L. Rouleau, S.U. Sys, "The cardiac endothelium: functional morphology, development, and physiology," *Prog. Cardiovasc. Dis.* 39(November-December 1996):239-263.
68. C. Garlanda, E. Dejana, "Heterogeneity of endothelial cells. Specific markers," *Arterioscler. Thromb. Vasc. Biol.* 17(July 1997):1193-1202; <http://atvb.ahajournals.org/cgi/content/full/17/7/1193>
69. A. Ager, "Regulation of lymphocyte migration into lymph nodes by high endothelial venules," *Biochem. Soc. Trans.* 25(May 1997):421-428.
70. J.P. Girard, F. Amalric, "Biosynthesis of sulfated L-selectin ligands in human high endothelial venules (HEV)," *Adv. Exp. Med. Biol.* 435(1998):55-62.
71. U.H. von Andrian, C. M'Rini, "In situ analysis of lymphocyte migration to lymph nodes," *Cell Adhes. Commun.* 6(1998):85-96.

72. S.R. Watson, L.M. Bradley, "The recirculation of naive and memory lymphocytes," *Cell Adhes. Commun.* 6(1998):105–110.
73. C.C. Michel, C.R. Neal, "Openings through endothelial cells associated with increased microvascular permeability," *Microcirculation* 6(March 1999):45–54.
74. J.L. Salyer, J.F. Bohnsack, W.A. Knape, A.O. Shigeoka, E.R. Ashwood, H.R. Hill, "Mechanisms of tumor necrosis factor–alpha alteration of PMN adhesion and migration," *Am. J. Pathol.* 136(April 1990):831–841.
75. K. Aoshiba, A. Nagai, Y. Ishihara, J. Kagawa, T. Takizawa, "Effects of alpha 1–proteinase inhibitor on chemotaxis and chemokinesis of polymorphonuclear leukocytes: its possible role in regulating polymorphonuclear leukocyte recruitment in human subjects," *J. Lab. Clin. Med.* 122(September 1993):333–340.
76. D.E. Van Epps, B.R. Andersen, "Streptolysin O inhibition of neutrophil chemotaxis and mobility: nonimmune phenomenon with species specificity," *Infect. Immun.* 9(January 1974):27–33; "Suppression of chemotactic activity of human neutrophils by streptolysin O," *J. Infect. Dis.* 125(April 1972):353–359.
77. A. Perianin, M.A. Gougerot–Pocidallo, J.P. Giroud, J. Hakim, "Diclofenac sodium, a negative chemokinetic factor for neutrophil locomotion," *Biochem. Pharmacol.* 34(1 October 1985):3433–3438.
78. P. Sacerdote, P. Massi, A.E. Panerai, D. Parolaro, "In vivo and in vitro treatment with the synthetic cannabinoid CP55,940 decreases the in vitro migration of macrophages in the rat: involvement of both CB1 and CB2 receptors," *J. Neuroimmunol.* 109(22 September 2000):155–163.
79. S.B. Carter, "Cell movement and cell spreading: A passive or an active process?" *Nature* 255(1970):858–859.
80. A.K. Harris, P. Wild, S. Stopak, "Silicone rubber substrata: A new wrinkle in the study of cell locomotion," *Science* 208(1980):177–179.
81. J.P. Trinkaus, *Cells Into Organs: The Forces That Shape The Embryo*, Prentice–Hall, Englewood Cliffs, NJ, 1984.

82. Thomas K. Hunt, J. Englebert Dunphy, *Fundamentals of Wound Management*, Appleton–Century–Crofts, New York, 1979.
83. Attributed to Atchison Robertson by John Harvey Kellogg, *The New Dietetics, Modern Medicine Publishing Co., Battle Creek MI, 1927*, p. 150.
84. A.G. Harris, T.C. Skalak, D.L. Hatchell, “Leukocyte–capillary plugging and network resistance are increased in skeletal muscle of rats with streptozotocin–induced hyperglycemia,” *Int. J. Microcirc. Clin. Exp.* 14(May–June 1994):159–166.
85. Y. Kinukawa, M. Shimura, M. Tamai, “Quantifying leukocyte dynamics and plugging in retinal microcirculation of streptozotocin–induced diabetic rats,” *Curr. Eye Res.* 18(January 1999):49–55.
86. J. Storrs Hall, “Utility Fog: A Universal Physical Substance,” in *Vision–21*, Westlake, OH, NASA Conference Publication 10129, 1993, pp. 115–126; “Discrete Laminar Flow in Robotic Fluids,” lecture delivered at NASA/Ames Research Center, Moffett Field, CA, December 1997.
87. L.A. Geddes, S.F. Badylak, “Power capability of skeletal muscle to pump,” *ASAIO Trans.* 37(January–March 1991):19–23.
88. S.G. Williams, G.A. Cooke, D.J. Wright, W.J. Parsons, R.L. Riley, P. Marshall, L.B. Tan, “Peak exercise cardiac power output; a direct indicator of cardiac function strongly predictive of prognosis in chronic heart failure,” *Eur. Heart J.* 22(August 2001):1496–1503.
89. I.M. Sauer, J. Frank, A. Spiegelberg, E.S. Bucherl, “Ovalis TAH: development and in vitro testing of a new electromechanical energy converter for a total artificial heart,” *ASAIO J.* 46(November–December 2000):744–748.
90. C. Bruce Wenger, James D. Hardy, “Chapter 4. Temperature Regulation and Exposure to Heat and Cold,” in Justus F. Lehmann, ed., *Therapeutic Heat and Cold, Fourth Edition*, Williams & Wilkins, Baltimore, MD, 1990, pp. 150–178.
91. Y.S. Touloukian, R.W. Powell, C.Y. Ho, P.G. Klemens, eds., *Thermal Conductivity: Nonmetallic Solids, Thermophysical Properties of Matter, Volume 2*, IFO/Plenum, NY, 1970.

92. Y.S. Touloukian, ed., Thermophysical Properties of High Temperature Solid Materials, Volume 4, The Macmillan Company, NY, 1967.
93. Dwight E. Gray, ed., American Institute of Physics Handbook, Third Edition, McGraw–Hill Book Company, New York, 1972.
94. B. Anvari, T.E. Milner, B.S. Tanenbaum, J.S. Nelson, “A comparative study of human skin thermal response to sapphire contact and cryogen spray cooling,” IEEE Trans. Biomed. Eng. 45(July 1998):934–941.
95. R.W. Pryor, Lanhus Wei, P.K. Kuo, R.L. Thomas, T.R. Anthony, W.F. Banholzer, “Thermal wave measurement of isotopic effects in polycrystalline and bulk diamond materials,” in Russell Messier, Jeffrey T. Glass, James E. Butler, Rustom Roy, eds., New Diamond Science and Technology, Proc. Second Intl. Conf., Materials Research Society, Pittsburgh, PA, 1991, pp. 863–868.
96. Donald T. Morelli, G.W. Smith, J. Heremans, W.F. Banholzer, T.R. Anthony, “Thermal properties of diamond single crystals with varying isotopic composition,” in Russell Messier, Jeffrey T. Glass, James E. Butler, Rustom Roy, eds., New Diamond Science and Technology, Proc. Second Intl. Conf., Materials Research Society, Pittsburgh, PA, 1991, pp. 869–873.
97. Richard W. Hughes, Ruby & Sapphire. BWH Publishing, Boulder CO, 1997.
98. “Diamond Research at the Walter Schottky Institut”;
<http://www.wsi.tu-muenchen.de/E25/research/nebel/diamond/diamond.htm>
99. Christoph E. Nebel, “Nano–electronics on hydrogenated diamond surfaces,” Diploma Thesis, Walter Schottky Institute, Experimental Semiconductor Physics II – Nano electronics on diamond;
http://www.wsi.tu-muenchen.de/E25/available_pos/diamond%20nano%20electronics.htm
100. Q. Lan, K.O. Mercurius, P.F. Davies, “Stimulation of transcription factors NF kappa B and AP1 in endothelial cells subjected to shear stress,” Biochem. Biophys. Res. Commun. 201(15 June 1994):950–956.
101. L.M. Khachigian, N. Resnick, M.A. Gimbrone Jr., T. Collins, “Nuclear factor–kappa B interacts functionally with the platelet–derived growth factor B–chain shear–stress response element in vascular endothelial cells exposed to fluid shear stress,” J. Clin. Invest. 96(August 1995):1169–1175.

102. W. Du, I. Mills, B.E. Sumpio, "Cyclic strain causes heterogeneous induction of transcription factors, AP-1, CRE binding protein and NF- κ B, in endothelial cells: species and vascular bed diversity," *J. Biomech.* 28(December 1995):1485-1491.
103. N. Resnick, M.A. Gimbrone Jr., "Hemodynamic forces are complex regulators of endothelial gene expression," *FASEB J.* 9(July 1995):874-882.
104. J.N. Topper, M.A. Gimbrone Jr., "Blood flow and vascular gene expression: fluid shear stress as a modulator of endothelial phenotype," *Mol. Med. Today* 5(January 1999):40-46.
105. N. Resnick, H. Yahav, S. Schubert, E. Wolfowitz, A. Shay, "Signalling pathways in vascular endothelium activated by shear stress: relevance to atherosclerosis," *Curr. Opin. Lipidol.* 11(April 2000):167-177;
106. R.M. Nerem, D.G. Harrison, W.R. Taylor, R.W. Alexander, "Hemodynamics and vascular endothelial biology," *J. Cardiovasc. Pharm.* 21(1993):S6-S10.
107. P.F. Davies, "Flow-mediated endothelial mechanotransduction," *Physiol. Rev.* 75(July 1995):519-560.
108. Ira Mills, Bauer E. Sumpio, "Chapter 39. Mechanical Forces and Cell Differentiation," in Peter Zilla, Howard P. Greisler, eds., *Tissue Engineering of Prosthetic Vascular Grafts*, R.G. Landes Company, Austin TX, 1999, pp. 425-438.
109. B.L. Langille, "Arterial remodeling: relation to hemodynamics," *Can. J. Physiol. Pharmacol.* 74(July 1996):834-841.
110. K. Naruse, M. Sokabe, "Involvement in stretch-activated ion channels in Ca²⁺ mobilization to mechanical stretch in endothelial cells," *Am. J. Physiol.* 264(April 1993):C1037-C1044.
111. R.F. Viggers, A.R. Wechezak, L.R. Sauvage, "An apparatus to study the response of cultured endothelium to shear stress," *J. Biomech. Eng.* 108(November 1986):332-337.
112. A. Suciu, G. Civelekoglu, Y. Tardy, J.J. Meister, "Model for the alignment of actin filaments in endothelial cells subjected to fluid shear stress," *Bull. Math. Biol.* 59(November 1997):1029-1046.

113. C.G. Galbraith, R. Skalak, S. Chien, "Shear stress induces spatial reorganization of the endothelial cell cytoskeleton," *Cell Motil. Cytoskeleton* 40(1998):317–330.

114. S.P. Olesen, D.E. Clapham, P.F. Davies, "Haemodynamic shear stress activates a K⁺ current in vascular endothelial cells," *Nature* 331(14 January 1988):168–170.

115. M. Nakache, H.E. Gaub, "Hydrodynamic hyperpolarization of endothelial cells," *Proc. Natl. Acad. Sci. (USA)* 85(March 1988):1841–1843.

116. S.L. Diamond, S.G. Eskin, L.V. McIntire, "Fluid flow stimulates tissue plasminogen activator secretion by cultured human endothelial cells," *Science* 243(17 March 1989):1483–1485.

117. P.F. Davies, "Mechanical sensing mechanisms: shear stress and endothelial cells," *J. Vasc. Surg.* 13(May 1991):729–731; see also *News Physiol. Sci.* 4(1989):22 et seq.

118. J.N. Topper, J. Cai, G. Stavrakis, K.R. Anderson, E.A. Woolf, B.A. Sampson, F.J. Schoen, D. Falb, M.A. Gimbrone Jr., "Human prostaglandin transporter gene (hPGT) is regulated by fluid mechanical stimuli in cultured endothelial cells and expressed in vascular endothelium in vivo," *Circulation* 98(1 December 1998):2396–2403.

119. A.M. Malek, S. Izumo, "Mechanism of endothelial cell shape change and cytoskeletal remodeling in response to fluid shear stress," *J. Cell Sci.* 109(April 1996):713–726.

120. H. Tseng, T.E. Peterson, B.C. Berk, "Fluid shear stress stimulates mitogen-activated protein kinase in endothelial cells," *Circ. Res.* 77(November 1995):869–878.

121. M.U. Nollert, S.G. Eskin, L.V. McIntire, "Shear stress increases inositol trisphosphate levels in human endothelial cells," *Biochem. Biophys. Res. Commun.* 170(16 July 1990):281–287.

122. A. Bhagyalakshmi, F. Berthiaume, K.M. Reich, J.A. Frangos, "Fluid shear stress stimulates membrane phospholipid metabolism in cultured human endothelial cells," *J. Vasc. Res.* 29(November–December 1992):443–449.

123. J. Hoyer, R. Kohler, A. Distler, "Mechanosensitive Ca²⁺ oscillations and STOC activation in endothelial cells," *FASEB J.* 12(March 1998):359–366.
124. M. Ohno, J.P. Cooke, V.J. Dzau, G.H. Gibbons, "Fluid shear stress induces endothelial transforming growth factor beta-1 transcription and production. Modulation by potassium channel blockade," *J. Clin. Invest.* 95(March 1995):1363–1369.
125. A.M. Malek, J. Zhang, J. Jiang, S.L. Alper, S. Izumo, "Endothelin-1 gene suppression by shear stress: pharmacological evaluation of the role of tyrosine kinase, intracellular calcium, cytoskeleton, and mechanosensitive channels," *J. Mol. Cell. Cardiol.* 31(February 1999):387–399.
126. R.V. Geiger, B.C. Berk, R.W. Alexander, R.M. Nerem, "Flow-induced calcium transients in single endothelial cells: spatial and temporal analysis," *Am. J. Physiol.* 262(June 1992):C1411–C1417.
127. D.L. Fry, "Acute vascular endothelial changes associated with increased blood velocity gradients," *Circulation Res.* 22(1968):165–197.
128. G.W. Schmid-Schonbein, Y.C. Fung, B.W. Zweifach, "Vascular endothelium-leukocyte interaction," *Circulation Res.* 36(1975):173–184.
129. A. Kamiya, R. Bukhari, T. Togawa, "Adaptive regulation of wall shear stress optimizing vascular tree function," *Bull. Math. Biol.* 46(1984):127–137.
130. C.K. Zarins, M.A. Zatina, D.P. Giddens, D.N. Ku, S. Glagov, "Shear stress regulation of artery lumen diameter in experimental atherogenesis," *J. Vasc. Surg.* 5(March 1987):413–420.
131. M. Malina, B. Lindblad, K. Ivancev, M. Lindh, J. Malina, J. Brunkwall, "Endovascular AAA exclusion: will stents with hooks and barbs prevent stent-graft migration?" *J. Endovasc. Surg.* 5(November 1998):310–317.
132. B.J. Ballermann, M.J. Ott, "Adhesion and differentiation of endothelial cells by exposure to chronic shear stress: a vascular graft model," *Blood Purification* 13(1995):125–134.

133. S. Vyalov, B.L. Langille, A.I. Gotlieb, "Decreased blood flow rate disrupts endothelial repair in vivo," *Am. J. Pathol.* 149(December 1996):2107–2118.
134. M.G. Davies, G.J. Fulton, E. Svendsen, P.O. Hagen, "Time course of the regression of intimal hyperplasia in experimental vein grafts," *Cardiovasc. Pathol.* 8(May–June 1999):161–168.
135. N. Gotoh, K. Kambara, X.W. Jiang, M. Ohno, S. Emura, T. Fujiwara, H. Fujiwara, "Apoptosis in microvascular endothelial cells of perfused rabbit lungs with acute hydrostatic edema," *J. Appl. Physiol.* 88(February 2000):518–526.
136. O.R. Rosales, C.M. Isales, P.Q. Barrett, C. Brophy, B.E. Sumpio, "Exposure of endothelial cells to cyclic strain induces elevations of cytosolic Ca²⁺ concentration through mobilization of intracellular and extracellular pools," *Biochem. J.* 326(1 September 1997):385–392.
137. O.R. Rosales, B.E. Sumpio, "Changes in cyclic strain increase inositol trisphosphate and diacylglycerol in endothelial cells," *Am. J. Physiol.* 262(April 1992):C956–C962.
138. L. Evans, L. Frenkel, C.M. Brophy, O. Rosales, C.B. Sudhaker, G. Li, W. Du, B.E. Sumpio, "Activation of diacylglycerol in cultured endothelial cells exposed to cyclic strain," *Am. J. Physiol.* 272(February 1997):C650–C656.
139. M. Okada, A. Matsumori, K. Ohno, Y. Furukawa, T. Shioi, A. Iwasaki, K. Matsushima, S. Sasayama, "Cyclic stretch upregulates production of interleukin-8 and monocyte chemoattractant protein-1 in human endothelial cells," *Arterioscler. Thromb. Vasc. Biol.* 18(June 1998):894–901.
140. M.D. Silverman, V.G. Manolopoulos, B.R. Unsworth, P.L. Lelkes, "Tissue factor expression is differentially modulated by cyclic mechanical strain in various human endothelial cells," *Blood Coagul. Fibrinolysis* 7(April 1996):281–288.
141. I. Mills, C.R. Cohen, K. Kamal, G. Li, T. Shin, W. Du, B.E. Sumpio, "Strain activation of bovine aortic smooth muscle cell proliferation and alignment: study of strain dependency and the role of protein kinase A and C signaling pathways," *J. Cell Physiol.* 170(March 1997):228–234.
142. J. Galea, J. Armstrong, S.E. Francis, G. Cooper, D.C. Crossman, C.M. Holt, "Alterations in c-fos, cell proliferation and apoptosis in pressure distended human saphenous vein," *Cardiovasc. Res.* 44(November

1999):436–448.

143. A. Hipper, G. Isenberg, “Cyclic mechanical strain decreases the DNA synthesis of vascular smooth muscle cells,” *Pflugers Arch.* 440(May 2000):19–27.

144. M.G. Davis, S. Ali, G.D. Leikauf, G.W. Dorn 2nd, “Tyrosine kinase inhibition prevents deformation–stimulated vascular smooth muscle growth,” *Hypertension* 24(December 1994):706–713.

145. Y.N. Shvarev, B. Canlon, “Receptor potential characteristics during direct stereocilia stimulation of isolated outer hair cells from the guinea–pig,” *Acta Physiol. Scand.* 162(February 1998):155–164.

146. G.K. Yates, D.L. Kirk, “Cochlear electrically evoked emissions modulated by mechanical transduction channels,” *J. Neurosci.* 18(15 March 1998):1996–2003.

147. M.C. Gopfert, H. Briegel, D. Robert, “Mosquito hearing: sound–induced antennal vibrations in male and female *Aedes aegypti*,” *J. Exp. Biol.* 202(October 1999):2727–2738.

148. G.P. Bailey, W.F. Sewell, “Calcitonin gene–related peptide suppresses hair cell responses to mechanical stimulation in the *Xenopus* lateral line organ,” *J. Neurosci.* 20(1 July 2000):5163–5169.

149. J. Esther, C. Wiersinga–Post, S.M. van Netten, “Temperature dependency of copular mechanics and hair cell frequency selectivity in the fish canal lateral line organ,” *J. Comp. Physiol. A* 186(October 2000):949–956.

150. H. Bester, V. Chapman, J.M. Besson, J.F. Bernard, “Physiological properties of the lamina I spinoparabrachial neurons in the rat,” *J. Neurophysiol.* 83(April 2000):2239–2259.

151. E. Salinas, A. Hernandez, A. Zainos, R. Romo, “Periodicity and firing rate as candidate neural codes for the frequency of vibrotactile stimuli,” *J. Neurosci.* 20(15 July 2000):5503–5515.

152. Y. Kawakami, M. Miyata, T. Oshima, “Mechanical vibratory stimulation of feline forepaw skin induces long–lasting potentiation in the secondary somatosensory cortex,” *Eur. J. Neurosci.* 13(January 2001):171–178.

153. A.R. Weintraub et al, "Intravascular ultrasound imaging in acute aortic dissection," *J. Am. Coll. Cardiol.* 24(August 1994):495–503.
154. G. Gorge, J. Ge, M. Haude, D. Baumgart, T. Buck, R. Erbel, "Initial experience with a steerable intravascular ultrasound catheter in the aorta and pulmonary artery," *Am. J. Card. Imaging* 9(July 1995):180–184.
155. P. Wong, J.S. Hung, N. Miyamoto, C.J. Wu, M. Fu, S. Kyo, R. Omoto, "Utility of 10 MHz ultrasound catheters in the intraaortic assessment of coronary artery ostial stenoses," *Am. J. Cardiol.* 77(15 April 1996):870–872.
156. B.W. Batkoff, D.T. Linker, "Safety of intracoronary ultrasound: data from a Multicenter European Registry," *Cathet. Cardiovasc. Diagn.* 38(July 1996):238–241.
157. A. Nicosia, W.J. van der Giessen, S.G. Airiian, C. von Birgelen, P.J. de Feyter, P.W. Serruys, "Is intravascular ultrasound after coronary stenting a safe procedure? Three cases of stent damage attributable to ICUS in a tantalum coil stent," *Cathet. Cardiovasc. Diagn.* 40(March 1997):265–270, 271 (comment).
158. C.W. Hamm, W. Steffen, W. Terres, J. De Scheerder, J. Reimers, D. Cumberland, R.J. Siegel, T. Meinertz, "Intravascular therapeutic ultrasound thrombolysis in acute myocardial infarctions," *Am. J. Cardiol.* 80(15 July 1997):200–204.
159. A. Chavan, D. Hausmann, C. Dresler, H. Rosenthal, K. Jaeger, A. Haverich, H.G. Borst, M. Galanski, "Intravascular ultrasound-guided percutaneous fenestration of the intimal flap in the dissected aorta," *Circulation* 96(7 October 1997):2124–2127.
160. R. Lopez-Palop et al, "Feasibility and safety of intracoronary ultrasound. Experience of a single center," *Rev. Esp. Cardiol.* 52(June 1999):415–421. In Spanish.
161. T. Rassin, W. Desmet, J. Piessens, U. Rosenschein, "Ultrasound thrombolysis in stent thrombosis," *Catheter Cardiovasc. Interv.* 51(November 2000):332–334.
162. S.E. Nissen, P. Yock, "Intravascular ultrasound: novel pathophysiological insights and current clinical applications," *Circulation* 103(30 January 2001):604–616.

163. W. Casscells, "Smooth muscle cell growth factors," *Prog. Growth Factor Res.* 3(1991):177–206.
164. T. Scott–Burden, A.W. Hahn, F.R. Buhler, T.J. Resink, "Vasoactive peptides and growth factors in the pathophysiology of hypertension," *J. Cardiovasc. Pharmacol.* 20(1992):S55–S64.
165. P.E. DiCorleto, "Cellular mechanisms of atherogenesis," *Am. J. Hypertens.* 6(November 1993):314S–318S.
166. P.A. D'Amore, S.R. Smith, "Growth factor effects on cells of the vascular wall: a survey," *Growth Factors* 8(1993):61–75.
167. T. Scott–Burden, P.M. Vanhoutte, "Regulation of smooth muscle cell growth by endothelium–derived factors," *Tex. Heart Inst. J.* 21(1994):91–97.
168. P.E. Chabrier, "Growth factors and vascular wall," *Int. Angiol.* 15(June 1996):100–103.
169. P. Delafontaine, "Growth factors and vascular smooth muscle cell growth responses," *Eur. Heart J.* 19(July 1998):G18–G22.
170. G.A. Stouffer, M.S. Runge, "The role of secondary growth factor production in thrombin–induced proliferation of vascular smooth muscle cells," *Semin. Thromb. Hemost.* 24(1998):145–150.
171. K.E. Bornfeldt, E.W. Raines, L.M. Graves, M.P. Skinner, E.G. Krebs, R. Ross, "Platelet–derived growth factor. Distinct signal transduction pathways associated with migration versus proliferation," *Ann. N.Y. Acad. Sci.* 766(7 September 1995):416–430.
172. M.K. Patel, J.S. Lynn, G.F. Clunn, A.D. Hughes, "Thrombospondin–1 is a potent mitogen and chemoattractant for human vascular smooth muscle cells," *Arterioscler. Thromb. Vasc. Biol.* 17(October 1997):2107–2114.
173. A.B. Dodge, X. Lu, P.A. D'Amore, "Density–dependent endothelial cell production of an inhibitor of smooth muscle cell growth," *J. Cell Biochem.* 53(September 1993):21–31.

174. D.V. Young, D. Serebryanik, D.R. Janero, S.W. Tam, "Suppression of proliferation of human coronary artery smooth muscle cells by the nitric oxide donor, S-nitrosoglutathione, is cGMP-independent," *Mol. Cell Biol. Res. Commun.* 4(July 2000):32-36.
175. M. Raicu, S. Florea, G. Costache, D. Popov, M. Simionescu, "Clotrimazole inhibits smooth muscle cell proliferation and has a vasodilator effect on resistance arteries," *Fundam. Clin. Pharmacol.* 14(September-October 2000):477-485.
176. M. Oberhoff, W. Kunert, C. Herdeg, A. Kuttner, A. Kranzhofer, B. Horch, A. Baumbach, K.R. Karsch, "Inhibition of smooth muscle cell proliferation after local drug delivery of the antimitotic drug paclitaxel using a porous balloon catheter," *Basic Res. Cardiol.* 96(May-June 2001):275-282.
177. K. Hayashi, H. Takahata, N. Kitagawa, G. Kitange, M. Kamuhogo, S. Shibata, "N-acetylcysteine inhibited nuclear factor-kappaB expression and the intimal hyperplasia in rat carotid arterial injury," *Neurol. Res.* 23(October 2001):731-738.
178. N. Ferri, L. Arnaboldi, A. Orlandi, K. Yokoyama, R. Gree, A. Granata, A. Hachem, R. Paoletti, M.H. Gelb, A. Corsini, "Effect of S(-) perillidic acid on protein prenylation and arterial smooth muscle cell proliferation," *Biochem. Pharmacol.* 62(15 December 2001):1637-1645.
179. S. Sartore, A. Chiavegato, R. Franch, E. Faggini, P. Paoletti, "Myosin gene expression and cell phenotypes in vascular smooth muscle during development, in experimental models, and in vascular disease," *Arterioscler. Thromb. Vasc. Biol.* 17(July 1997):1210-1215.
180. P. Stralin, S.L. Marklund, "Vasoactive factors and growth factors alter vascular smooth muscle cell EC-SOD expression," *Am. J. Physiol. Heart Circ. Physiol.* 281(October 2001):H1621-H1629.
181. M.D. Buschmann, Y.J. Kim, M. Wong, E. Frank, E.B. Hunziker, A.J. Grodzinsky, "Stimulation of aggrecan synthesis in cartilage explants by cyclic loading is localized to regions of high interstitial fluid flow," *Arch. Biochem. Biophys.* 366(1 June 1999):1-7.
182. T. Chano, M. Tanaka, S. Hukuda, Y. Saeki, "Mechanical stress induces the expression of high molecular mass heat shock protein in human chondrocytic cell line CS-OKB," *Osteoarthritis Cartilage* 8(March 2000):115-119.

183. M. Tagil, P. Aspenberg, "Cartilage induction by controlled mechanical stimulation in vivo," *J. Orthop. Res.* 17(March 1999):200–204.
184. D.B. Saris, A. Sanyal, K.N. An, J.S. Fitzsimmons, S.W. O'Driscoll, "Periosteum responds to dynamic fluid pressure by proliferating in vitro," *J. Orthop. Res.* 17(September 1999):668–677.
185. H.S. Lee, S.J. Millward–Sadler, M.O. Wright, G. Nuki, D.M. Salter, "Integrin and mechanosensitive ion channel–dependent tyrosine phosphorylation of focal adhesion proteins and beta–catenin in human articular chondrocytes after mechanical stimulation," *J. Bone Miner. Res.* 15(August 2000):1501–1509.
186. D.M. Salter, W.H. Wallace, J.E. Robb, H. Caldwell, M.O. Wright, "Human bone cell hyperpolarization response to cyclical mechanical strain is mediated by an interleukin–1beta autocrine/paracrine loop," *J. Bone Miner. Res.* 15(September 2000):1746–1755.
187. D.A. Lee, T. Noguchi, S.P. Frean, P. Lees, D.L. Bader, "The influence of mechanical loading on isolated chondrocytes seeded in agarose constructs," *Biorheology* 37(2000):149–161.
188. C.R. Cohen, I. Mills, W. Du, K. Kamal, B.E. Sumpio, "Activation of the adenylyl cyclase/cyclic AMP/protein kinase A pathway in endothelial cells exposed to cyclic strain," *Exp. Cell Res.* 231(25 February 1997):184–189.
189. J.H. Yang, W.H. Briggs, P. Libby, R.T. Lee, "Small mechanical strains selectively suppress matrix metalloproteinase–1 expression in human vascular smooth muscle cells," *J. Biol. Chem.* 273(13 March 1998):6550–6555.
190. B. Chaqour, P.S. Howard, E.J. Macarak, "Identification of stretch–responsive genes in pulmonary artery smooth muscle cells by a two arbitrary primer–based mRNA differential display approach," *Mol. Cell Biochem.* 197(July 1999):87–96. See also: B. Chaqour, P.S. Howard, C.F. Richards, E.J. Macarak, "Mechanical stretch induces platelet–activating factor receptor gene expression through the NF–kappaB transcription factor," *J. Mol. Cell Cardiol.* 31(July 1999):1345–1355.
191. D. Kaspar, W. Seidl, C. Neidlinger–Wilke, A. Ignatius, L. Claes, "Dynamic cell stretching increases human osteoblast proliferation and CICP synthesis but decreases osteocalcin synthesis and alkaline phosphatase activity," *J. Biomech.* 33(January 2000):45–51. See also: D. Kaspar, W. Seidl, A. Ignatius, C. Neidlinger–Wilke, L. Claes, "In vitro cell behavior of human osteoblasts after physiological dynamic stretching," *Orthopade* 29(February 2000):85–90. In German.

192. G.C. Bett, F. Sachs, "Whole-cell mechanosensitive currents in rat ventricular myocytes activated by direct stimulation," *J. Membr. Biol.* 173(1 February 2000):255–263.
193. H. Iwasaki, S. Eguchi, H. Ueno, F. Marumo, Y. Hirata, "Mechanical stretch stimulates growth of vascular smooth muscle cells via epidermal growth factor receptor," *Am. J. Physiol. Heart Circ. Physiol.* 278(February 2000):H521–H529.
194. C. Orizio, R.V. Baratta, B.H. Zhou, M. Solomonow, A. Veicsteinas, "Force and surface mechanomyogram frequency responses in cat gastrocnemius," *J. Biomech.* 33(April 2000):427–433.
195. M.O. Jortikka, J.J. Parkkinen, R.I. Inkinen, J. Karner, H.T. Jarvelainen, L.O. Nelimarkka, M.I. Tammi, M.J. Lammi, "The role of microtubules in the regulation of proteoglycans synthesis in chondrocytes under hydrostatic pressure," *Arch. Biochem. Biophys.* 374(15 February 2000):172–180.
196. M. Cattaruzza, C. Dimigen, H. Ehrenreich, M. Hecker, "Stretch-induced endothelin B receptor-mediated apoptosis in vascular smooth muscle cells," *FASEB J.* 14(May 2000):991–998.
197. R.D. Graff, E.R. Lazarowski, A.J. Banes, G.M. Lee, "ATP release by mechanically loaded porcine chondrons in pellet culture," *Arthritis Rheum.* 43(July 2000):1571–1579.
198. M.J. Ryan, T.A. Black, K.W. Gross, G. Hajduczuk, "Cyclic mechanical distension regulates rennin gene transcription in As4.1 cells," *Am. J. Physiol. Endocrinol. Metab.* 279(October 2000):E830–E837.
199. S.N. Airapetian, R.S. Stepanian, G.S. Airapetian, N.A. Mikaelian, "Effect of mechanical oscillations in physiological solution on the contractile activity of the snail heart," *Biofizika* 44(September–October 1999):923–928. In Russian.
200. I. Westbroek, N.E. Ajubi, M.J. Alblas, C.M. Semeins, J. Klein-Nulend, E.H. Burger, P.J. Nijweide, "Differential stimulation of prostaglandin G/H synthase-2 in osteocytes and other osteogenic cells by pulsating fluid flow," *Biochem. Biophys. Res. Commun.* 268(16 February 2000):414–419.
201. S.M. Tanaka, "A new mechanical stimulator for cultured bone cells using piezoelectric actuator," *J. Biomech.* 32(April 1999):427–430.

202. R.L. Vender, "Role of endothelial cells in the proliferative response of cultured pulmonary vascular smooth muscle cells to reduced oxygen tension," *In Vitro Cell Dev. Biol.* 28A(June 1992):403–409.
203. J. Thyberg, K. Blomgren, U. Hedin et al, "Phenotypic modulation of smooth muscle cells during the formation of neointimal thickenings in the rat carotid artery after balloon injury: an electronic–microscopic and stereological study," *Cell Tissue Res.* 281(1995):421–428.
204. F. Castaneda, S.M. Ball–Kell, K. Young, R. Li, "Assessment of a polyester–covered Nitinol stent in the canine aorta and iliac arteries," *Cardiovasc. Intervent. Radiol.* 23(September–October 2000):375–383.
205. G.J. Becker, "Intravascular stents. General principles and status of lower–extremity arterial applications," *Circulation* 83(1991):1122–1136.
206. G.S. Mintz, J.J. Popma, M.K. Hong et al, "Intravascular ultrasound to discern device–specific effects and mechanisms of restenosis," *Am. J. Cardiol.* 78(1996):18–22.
207. C.R. Narins, S.G. Ellis, "Prevention of in–stent restenosis," *Semin. Interv. Cardiol.* 3(June 1998):91–103.
208. A. Witkowski et al, "High–pressure bail–out coronary stenting without anticoagulation: Early outcome and follow–up results," *J. Invasive Cardiol.* 10(March 1998):83–88.
209. L.A. Mattos et al, "Safety and efficacy of coronary stent implantation. Acute and six month outcomes of 1,126 consecutive patients treated in 1996 and 1997," *Arq. Bras. Cardiol.* 73(July 1999):23–36.
210. A. Betriu et al, "Randomized comparison of coronary stent implantation and balloon angioplasty in the treatment of de novo coronary artery lesions (START): a four–year follow–up," *J. Am. Coll. Cardiol.* 34(1 November 1999):1498–1506.
211. M. Yano et al, "Long–term follow–up of primary stenting with coil stent in acute myocardial infarction," *Angiology* 51(February 2000):107–114.
212. L. Maillard et al, "A comparison of systematic stenting and conventional balloon angioplasty during primary percutaneous transluminal coronary angioplasty for acute myocardial infarction. STENTIM–2

Investigators,” J. Am. Coll. Cardiol. 35(June 2000):1729–1736.

213. C. Le Feuvre et al, “Clinical outcome following coronary angioplasty in dialysis patients: a case–control study in the era of coronary stenting,” Heart 85(May 2001):556–560.

214. D. Antoniucci, R. Valenti, G. Moschi, M. Trapani, G.M. Santoro, L. Bolognese, E. Taddeucci, E. Dovellini, “Stenting for in–stent restenosis,” Catheter Cardiovasc. Interv. 49(April 2000):376–381.

215. N. Tanigawa, S. Sawada, M. Kobayashi, “Reaction of the aortic wall to six metallic stent materials,” Acad. Radiol. 2(May 1995):379–384.

216. A. Tarnok, A. Mahnke, M. Muller, R.J. Zotz, “Rapid in vitro biocompatibility assay of endovascular stents by flow cytometry using platelet activation and platelet–leucocyte aggregation,” Cytometry 38(15 February 1999):30–39.

217. Kai Gutensohn, “Flow Cytometric Analysis of Coronary Stent–Induced Alterations of Platelet Antigens in an In–Vitro Model,” 23 April 1998; <http://www.myltis.com/stent6.htm>

218. J.I. Sanada, O. Matsui, J. Yoshikawa, T. Matsuoka, “An experimental study of endovascular stenting with special reference to the effects on the aortic vasa vasorum,” Cardiovasc. Intervent. Radiol. 21(January–February 1998):45–49.

219. E.S. Lee, G.E. Bauer, M.P. Caldwell, S.M. Santilli, “Association of artery wall hypoxia and cellular proliferation at a vascular anastomoses,” J. Surg. Res. 91(1 June 2000):32–37.

220. B.R. Brehm, C. Bock, S. Wesselborg, S. Pfeiffer, S. Schuler, K. Schulze–Osthoff, “Prevention of human smooth muscle cell proliferation without induction of apoptosis by the topoisomerase I inhibitor topotecan,” Biochem. Pharmacol. 61(1 January 2001):119–127.

221. M.R. Nehler, L.M. Taylor Jr., J.M. Porter, “Iatrogenic vascular trauma,” Semin. Vasc. Surg. 11(December 1998):283–293.

222. Erik L. Owens, Alexander W. Clowes, “Chapter 22. Pathobiology of Hyperplastic Intimal Responses,” in Peter Zilla, Howard P. Greisler, eds., Tissue Engineering of Prosthetic Vascular Grafts, R.G.

Landes Company, Austin TX, 1999, pp. 229–240.

223. L.W. Kraiss, A.W. Clowes, “Response of the arterial wall to injury and intimal hyperplasia,” in A.N. Sidway, B.E. Sumpio, R.G. DePalma, eds., *The Basic Science of Vascular Disease*, Futura Publ. Co., Armonk NY, 1997, pp. 289–317.

224. J. Fingerle, Y.P.T. Au, A.W. Clowes, M.A. Reidy, “Intimal lesion formation in rat carotid arteries after endothelial denudation in absence of medial injury,” *Arteriosclerosis* 10(November–December 1990):1082–1087.

—

225. A.W. Clowes, M.A. Reidy, M.M. Clowes, “Kinetics of cellular proliferation after arterial injury. I. Smooth muscle growth in the absence of endothelium,” *Lab. Invest.* 49(September 1983):327–333.

226. G.D. Spoelhof, K. Ide, “Pressure ulcers in nursing home patients,” *Am. Fam. Physician* 47(April 1993):1207–1215.

227. L.F. Kanj, S.V. Wilking, T.J. Phillips, “Pressure ulcers,” *J. Am. Acad. Dermatol.* 38(April 1998):517–536.

228. Clayton L. Thomas, ed., *Taber's Cyclopedic Medical Dictionary*, 17th Edition, F.A. Davis Company, Philadelphia PA, 1989.

229. N. Sato, T. Teramura, T. Ishiyama, H. Tagami, “Fulminant and relentless cutaneous necrosis with excruciating pain caused by calciphylaxis developing in a patient undergoing peritoneal dialysis,” *J. Dermatol.* 28(January 2001):27–31.

230. H. Selye, G. Winandy, G. Gabbiani, “Production and prevention of stercoral ulcers in the rat,” *Am. J. Pathol.* 48(February 1966):299–303.

231. K.I. Maull, W.K. Kinning, S. Kay, “Stercoral ulceration,” *Am. Surg.* 48(January 1982):20–24.

232. C.A. Maurer, P. Renzulli, L. Mazzucchelli, B. Egger, C.A. Seiler, M.W. Buchler, “Use of accurate diagnostic criteria may increase incidence of stercoral perforation of the colon,” *Dis. Colon Rectum* 43(July 2000):991–998.

233. A.A. Chalian, S.H. Kagan, "Backside first in head and neck surgery: preventing pressure ulcers in extended length surgeries," *Head Neck* 23(January 2001):25–28.
234. S.A. Aronovitch, M. Wilber, S. Slezak, T. Martin, D. Utter, "A comparative study of an alternating air mattress for the prevention of pressure ulcers in surgical patients," *Ostomy. Wound Manage.* 45(March 1999):34–44.
235. D. Armstrong, P. Bortz, "An integrative review of pressure relief in surgical patients," *AORN J.* 73(March 2001):645–657 passim.
236. K.M. Eckrich, "A pneumatic bladder array for measuring dynamic interface pressure between seated users and their wheelchairs," *Biomed. Sci. Instrum.* 27(1991):135–140.
237. M.J. Rosenthal, R.M. Felton, D.L. Hileman, M. Lee, M. Friedman, J.H. Navach, "A wheelchair cushion designed to redistribute sites of sitting pressure," *Arch. Phys. Med. Rehabil.* 77(March 1996):278–282.
238. D.M. Brienza, P.E. Karg, "Seat cushion optimization: a comparison of interface pressure and tissue stiffness characteristics for spinal cord injured and elderly patients," *Arch. Phys. Med. Rehabil.* 79(April 1998):388–394.
239. D.M. Brienza, P.E. Karg, M. Geyer, S. Kelsey, E. Trefler, "The relationship between pressure ulcer incidence and buttock–seat cushion interface pressure in at–risk elderly wheelchair users," *Arch. Phys. Med. Rehabil.* 82(April 2001):529–533.
240. M.N. Pase, "Pressure relief devices, risk factors, and development of pressure ulcers in elderly patients with limited mobility," *Adv. Wound Care* 7(March 1994):38–42.
241. B. Klitzman, C. Kalinowski, S.L. Glasofer, L. Rugani, "Pressure ulcers and pressure relief surfaces," *Clin. Plast. Surg.* 25(July 1998):443–450.
242. J.B. Hardin, S.N. Cronin, K. Cahill, "Comparison of the effectiveness of two pressure–relieving surfaces: low–air–loss versus static fluid," *Ostomy. Wound Manage.* 46(September 2000):50–56.

243. C.R. Bragdon, D. Burke, J.D. Lowenstein, D. O'Connor, B. Ramamurti, M. Jasty, W.H. Harris, "Differences in stiffness of the interface between a cementless porous implant and cancellous bone in vivo in dogs due to varying amounts of implant motion," *J. Arthroplasty* 11(December 1996):945–951.
244. D.F. Williams, R. Roaf, *Implants in Surgery*, W.B. Saunders Company Ltd., London, 1973.
245. L.F.V. Vincent, *Structural Biomaterials*, Revised Edition, Princeton University Press, Princeton, New Jersey, 1990.
246. F.H. Silver, Y.P. Kato, M. Ohno, A.J. Wasserman, "Analysis of mammalian connective tissue: relationship between hierarchical structures and mechanical properties," *J. Long Term Eff. Med. Implants* 2(1992):165–198.
247. R.E. Shaddy, "Apoptosis in heart transplantation," *Coron. Artery Dis.* 8(October 1997):617–621.
248. S.T. Shaw Jr., L.K. Macaulay, W.R. Hohman, "Morphologic studies on IUD-induced metrorrhagia. I. Endometrial changes and clinical correlations," *Contraception* 19(January 1979):47–61.
249. P.K. Ng, M.J. Ault, M.C. Fishbein, "The stuck catheter: a case report," *Mt. Sinai J. Med.* 64(September–October 1997):350–352.
250. J.G. White, N.J. Mulligan, D.R. Gorin, R. D'Agostino, E.K. Yucel, J.O. Menzoian, "Response of normal aorta to endovascular grafting: a serial histopathological study," *Arch. Surg.* 133(March 1998):246–249.
251. Alexander M. Seifalian, Alberto Giudiceandrea, Thomas Schmitz–Rixen, George Hamilton, "Chapter 2. Noncompliance: The Silent Acceptance of a Villain," in Peter Zilla, Howard P. Greisler, eds., *Tissue Engineering of Prosthetic Vascular Grafts*, R.G. Landes Company, Austin TX, 1999, pp. 45–58.
252. S. Cavalcanti, A. Tura, "Hemodynamic and mechanical performance of arterial grafts assessed by numerical simulation: a design oriented study," *Artif. Organs* 23(February 1999):175–185.
253. S. Hsu, H. Kambic, "On matching compliance between canine carotid arteries and polyurethane grafts," *Artif. Organs* 21(December 1997):1247–1254.

254. M. O'Rourke, "Arterial compliance and wave reflection," *Arch. Mal. Coeur Vaiss.* 84(September 1991):45-48 (Spec. No. 3); E.D. Lehmann, "Elastic properties of the aorta," *Lancet* 342(4 December 1993):1417.
255. F. Giron, W.S. Birtwell, H.S. Soroff, R.A. Deterling, "Hemodynamic effects of pulsatile and nonpulsatile flow," *Arch. Surg.* 93(November 1966):802-810; D.E. Strandness, D.S. Summer, *Hemodynamics for Surgeon*, Grune & Stratton, New York, 1975.
256. J.E. Hasson, J. Megerman, W.M. Abbott, "Increased compliance near vascular anastomoses," *J. Vasc. Surg.* 2(May 1985):419-423.
257. W.M. Abbott, J.M. Megerman, "Adaptive responses of arteries to grafting," *J. Vasc. Surg.* 9(February 1989):377-379; T. Schmitz-Rixen, G. Hamilton, "Compliance: A critical parameter for maintenance of arterial reconstruction?" in R.M. Greenhalgh, L.H. Hollier, eds., *The Maintenance of Arterial Reconstruction*, W.B. Saunders, London, 1991, pp. 23-43.
258. W.M. Abbott, J.M. Megerman, J.E. Hasson, C.L. Italien, D.F. Warnock, "Effect of compliance mismatch on vascular graft patency," *J. Vasc. Surg.* 5(February 1987):376-382.
259. A.W. Clowes, M.M. Clowes, J. Fingerle, M.A. Reidy, "Kinetics of cellular proliferation after arterial injury. V. Role of acute distension in the induction of smooth muscle proliferation," *Lab. Invest.* 60(March 1989):360-364.
260. H.S. Bassiouny, S. White, S. Glagov, E. Choi, D.P. Giddens, C.K. Zarins, "Anastomotic intimal hyperplasia: mechanical injury or flow induced," *J. Vasc. Surg.* 15(April 1992):708-716, 716-717 (discussion).
261. W.M. Abbott, R.P. Cambria, "Control of physical characteristics (elasticity and compliance) of vascular grafts," in J.C. Stanley, ed., *Biological and Synthetic Vascular Prostheses*, Grune and Stratton, New York, 1982, pp. 189 et seq.
262. V.S. Sottiurai, S.L. Sue, E.L. Feinberg 2nd, W.L. Bringaze, A.T. Tran, R.C. Batson, "Distal anastomotic intimal hyperplasia: biogenesis and etiology," *Eur. J. Vasc. Surg.* 2(August 1988):245-256; H.G. Predel, Z. Yang, L. von Segesser, M. Turina, F.R. Buhler, T.F. Luscher, "Implication of pulsatile stretch on growth of saphenous vein and mammary artery smooth muscle," *Lancet* 340(10 October 1992):878-879.

263. C.M. Agrawal, H.G. Clark, "Deformation characteristics of a bioabsorbable intravascular stent," *Invest. Radiol.* 27(December 1992):1020–1024.
264. Joseph I. Zarge, Peter Huang, Howard P. Greisler, "Chapter 24. Blood Vessels," in Robert P. Lanza, Robert Langer, William L. Chick, eds., *Principles of Tissue Engineering*, R.G. Landes Company, Georgetown TX, 1997, pp. 349–364.
265. Y. Qiu, J.M. Tarbell, "Numerical simulation of pulsatile flow in a compliant curved tube model of a coronary artery," *J. Biomech. Eng.* 122(February 2000):77–85.
266. M.A. Reidy, S.M. Schwartz, "Endothelial regeneration. III. Time course of intimal changes after small defined injury to rat aortic endothelium," *Lab. Invest.* 44(April 1981):301–308.
267. S.M. Schwartz, E.P. Benditt, "Cell replication in the aortic endothelium: A new method for study of the problem," *Lab. Invest.* 28(June 1973):699–707; "Aortic endothelial cell replication. I. Effects of age and hypertension in the rat," *Circ. Res.* 41(August 1977):248–255.
268. Ronald L. Heimark, Stephen M. Schwartz, "Endothelial Morphogenesis," in Nicolae Simionescu, Maya Simionescu, eds., *Endothelial Cell Biology in Health and Disease*, Plenum Press, New York, 1988, pp. 123–143.
269. M.S. Clarke, C.R. Vanderburg, E.D. Hay, P.L. McNeil, "Cytoplasmic loading of dyes, protein and plasmid DNA using an impact-mediated procedure," *Biotechniques* 17(December 1994):1118–1125.
270. M. Horowitz, P. Purdy, T. Kopitnik, "Subarachnoid hemorrhage during arteriovenous malformation embolization as a result of vessel wall 'sandblasting'," *Surg. Neurol.* 50(November 1998):403–406, 406–407 (discussion).
271. Q.C. Yu, P.L. McNeil, "Transient disruptions of aortic endothelial cell plasma membranes," *Am. J. Pathol.* 141(December 1992):1349–1360.
272. A.A. Brayman, L.M. Lizotte, M.W. Miller, "Erosion of artificial endothelia in vitro by pulsed ultrasound: acoustic pressure, frequency, membrane orientation and microbubble contrast agent dependence," *Ultrasound Med. Biol.* 25(October 1999):1305–1320.

273. J.E. Molina, C.A. Galliani, S. Einzig, R. Bianco, T. Rasmussen, R. Clack, "Physical and mechanical effects of cardioplegic injection on flow distribution and myocardial damage in hearts with normal coronary arteries," *J. Thorac. Cardiovasc. Surg.* 97(June 1989):870–877.

274. M. Roger, T.O. Rognum, J. Ingum, G. Welle–Strand, "Intravenous abuse of crushed tablets. A case with fatal outcome," *Tidsskr. Nor. Laegeforen.* 110(20 June 1990):2080–2081. In Norwegian.

275. W.C. Grinstead, G.P. Rodgers, W. Mazur, B.A. French, D. Cromeens, C. Van Pelt, S.M. West, A.E. Raizner, "Comparison of three porcine restenosis models: the relative importance of hypercholesterolemia, endothelial abrasion, and stenting," *Coron. Artery Dis.* 5(May 1994):425–434.

276. I. Harich, M. Bohnke, J. Draeger, "Endothelium protective effect of the high viscosity substances hyaluronic acid and methylcellulose in mechanical damage," *Fortschr. Ophthalmol.* 87(1990):475–478. In German.

277. P.L. McNeil, L. Muthukrishnan, E. Warder, P.A. D'Amore, "Growth factors are released by mechanically wounded endothelial cells," *J. Cell Biol.* 109(August 1989):811–822.

278. G. Pintucci et al, "Mechanical endothelial damage results in basic fibroblast growth factor–mediated activation of extracellular signal–regulated kinases," *Surgery* 126(August 1999):422–427.

279. L.B. Langille, "Integrity of arterial endothelium following acute exposure to high shear stress," *Biorheology* 21(1984):333–346.

280. E. Sirois, J. Charara, J. Ruel, J.C. Dussault, P. Gagnon, C.J. Doillon, "Endothelial cells exposed to erythrocytes under shear stress: an in vitro study," *Biomaterials* 19(November 1998):1925–1934.

281. Robert A. Freitas Jr., "Nanodentistry," *J. Amer. Dent. Assoc.* 131(November 2000):1559–1566 (cover story); <http://www.ada.org/members/pubs/jada/0011/index.html> or <http://www.ada.org/prof/pubs/jada/archives/0011/index.html>.

282. J.R. Wendt, S.M. Ackley, "Vascular complications of a foreign body in the hand of an asymptomatic patient," *Ann. Plast. Surg.* 34(January 1995):92–94.

283. I.N. Nuno, K.A. Ashton, K.M. Uppal, P.W. Lee, V.A. Starnes, "Indwelling catheter-induced right ventricular rupture," *Ann. Thorac. Surg.* 68(September 1999):1085–1086.
284. L. San Vicente, M.E. Martinez, J. Codina, A. Maza, G. Lafuente, E. Rotellar, "Cardiac perforation from a subclavian catheter," *Nephron* 35(1983):276.
285. D. Karakaya, S. Baris, A. Tur, "Pulmonary artery catheter-induced right ventricular perforation during coronary artery bypass surgery," *Br. J. Anaesth.* 82(June 1999):953.
286. F. Siclari, H. Klein, J. Troster, "Intraventricular migration of an ICD patch," *Pacing Clin. Electrophysiol.* 13(November 1990):1356–1359.
287. G. Dorros, M.R. Jaff, A. Parikh, R. Sehgal, V. Thota, K. Ramireddy, R.E. Carballo, "In vivo crushing of an aortic stent enables endovascular repair of a large infrarenal aortic pseudoaneurysm," *J. Endovasc. Surg.* 59(November 1998):359–364.
288. J.D. Urschel, P.D. Myerowitz, "Catheter-induced pulmonary artery rupture in the setting of cardiopulmonary bypass," *Ann. Thorac. Surg.* 56(September 1993):585–589.
289. M.H. Mullerworth, P. Angelopoulos, M.A. Couyant, A.M. Horton, S.M. Robinson, O.U. Petring, P.J. Mitchell, J.J. Presneill, "Recognition and management of catheter-induced pulmonary artery rupture," *Ann. Thorac. Surg.* 66(October 1998):1242–1245.
290. E.D. Stancofski, A. Sardi, G.L. Conaway, "Successful outcome in Swan–Ganz catheter-induced rupture of pulmonary artery," *Am. Surg.* 64(November 1998):1062–1065.
291. S.P. Rivers, E.S. Lee, R.T. Lyon, S. Monrad, T. Hoffman, F.J. Veith, "Successful conservative management of iatrogenic femoral arterial trauma," *Ann. Vasc. Surg.* 6(January 1992):45–49.
292. S.C. Stoica, M. Fleet, A. Howd, "Subclavian artery injury following percutaneous insertion of dialysis catheter," *Rev. Med. Chir. Soc. Med. Nat. Iasi.* 102(July–December 1998):194–197.

293. V. Fourestie, B. Godeau, J.L. Lejonc, A. Schaeffer, "Left innominate vein stenosis as a late complication of central vein catheterization," *Chest* 88(October 1985):636–638.
294. M.J. Schoo, F.A. Scott, J.A. Boswick Jr., "High–pressure injection injuries of the hand," *J. Trauma* 20(March 1980):229–238.
295. Y. Sato, T. Kondo, T. Ohshima, "Traumatic tear of the basilar artery associated with vertebral column injuries," *Am. J. Forensic Med. Pathol.* 18(June 1997):129–134.
296. R.J. Siegel, M. Koponen, "Spontaneous coronary artery dissection causing sudden death. Mechanical arterial failure or primary vasculitis?" *Arch. Pathol. Lab. Med.* 118(February 1994):196–198; *Arch. Pathol. Lab. Med.* 118(September 1994):863–864 (comment).
297. F. Hammer, D. Becker, P. Goffette, P. Mathurin, "Crushed stents in benign left brachiocephalic vein stenoses," *J. Vasc. Surg.* 32(August 2000):392–396.
298. B.F. Rigney, "Case report: mechanical failure of a spinal transabdominal teflon stent in tuboplasty," *Fertil. Steril.* 26(February 1975):186–189.
299. C.T. Johnson, L.A. Osborn, "Indwelling pericardial drainage catheter break secondary to heart movement and catheter angulation," *Cathet. Cardiovasc. Diagn.* 42(September 1997):58–60.
300. B. Peskin, M. Soudack, A. Ben–Nun, "Hickman catheter rupture and embolization – a life–threatening complication," *Isr. Med. Assoc.* 1(December 1999):289.
301. S. Dakshinamurti, J. Ducas, J.N. Odum, "Retrieval of Silastic catheter fragment from heart in septic thromboembolism complicating aplastic anemia," *Can. J. Cardiol.* 12(September 1996):794–796.
302. G. Roggla, M. Linkesch, M. Roggla, A. Wagner, P. Haber, W. Linkesch, "A rare complication of a central venous catheter system (Port–a–Cath). A case report of a catheter embolization after catheter fracture during power training," *Int. J. Sports Med.* 14(August 1993):345–346.
303. W.Y. Hou, W.Z. Sun, Y.A. Chen, S.M. Wu, S.Y. Lin, "'Pinch–off sign' and spontaneous fracture of an implanted central venous catheter: report of a case," *J. Formos. Med. Assoc.* 93(March 1994):S65–S69. In

Chinese.

304. J.M. Debets, J.A. Wils, J.T. Schlangen, "A rare complication of implanted central-venous access devices: catheter fracture and embolization," *Support Care Cancer* 3(November 1995):432-434.

305. P. Vadlamani, B. Dawn, M.C. Perry, "Catheter fracture and embolization from totally implanted venous access ports - case reports," *Angiology* 49(December 1998):1013-1016.

306. E. Desruennes, "Mechanical complications at implantation sites," *Pathol. Biol. (Paris)* 47(March 1999):269-272. In French.

307. J.W. Mazel, F.J. Idenburg, O.M. van Delden, "Catheter fracture and embolization: a rare complication of a permanent implanted intravenous catheter system," *Ned. Tijdschr. Geneesk.* 144(8 July 2000):1360-1363. In Dutch.

308. J.M. Suarez-Penaranda, Guitian-Barreiro, L. Concheiro-Carro, "Longstanding intracardiac catheter embolism. An unusual autopsy finding," *Am. J. Forensic Med. Pathol.* 16(June 1995):124-126.

309. K.M. Alle, G.H. White, J.P. Harris, J. May, D. Baird, "Iatrogenic vascular trauma associated with intra-aortic balloon pumping: identification of risk factors," *Am. Surg.* 59(December 1993):813-817.

310. S. Sumita, Y. Ujike, A. Namiki, H. Watanabe, O. Satoh, "Rupture of pulmonary artery induced by balloon occlusion pulmonary angiography," *Intensive Care Med.* 21(January 1995):79-81.

311. R.H. Plack, G.M. Hutchins, J.A. Brinker, "Conduction system injury after aortic valve dilation in the dog: single versus double-balloon catheters," *Angiology* 41(November 1990):929-935.

312. J.S. Lee, "Epithelial cell extrusion during fluid transport in canine small intestine," *Am. J. Physiol.* 232(April 1977):E408-E414.

313. Anthony G. Gristina, Quentin N. Myrvik, Lawrence X. Webb, "Biomaterial surfaces: Tissue cells and bacteria, compatibility versus infection," in Richard Skalak, C. Fred Fox, eds., *Tissue Engineering*, Alan R. Liss, Inc., New York, 1988, pp. 99-107.

314. R.J. Hamill, J.M. Vann, R.A. Proctor, "Phagocytosis of *Staphylococcus aureus* by cultured bovine aortic endothelial cells: model for postadherence events in endovascular infections," *Infect. Immun.* 54(December 1986):833–836.
315. L.K. Birinyi, E.C. Douville, S.A. Lewis, H.S. Bjornson, R.F. Kempczinski, "Increased resistance to bacteremic graft infection after endothelial cell seeding," *J. Vasc. Surg.* 5(January 1987):193–197.
316. L.M. Switalski, C. Ryden, K. Rubin, A. Ljungh, M. Hook, T. Wadstrom, "Binding of fibronectin to *Staphylococcus* strains," *Infect. Immun.* 42(November 1983):628–633.
317. L.X. Webb, R.T. Myers, A.R. Cordell, C.D. Hobgood, J.W. Costerton, A.G. Gristina, "Inhibition of bacterial adhesion by antibacterial surface pretreatment of vascular prostheses," *J. Vasc. Surg.* 4(July 1986):16–21.
318. D.M. Nelson, A.C. Enders, B.F. King, "Galactosyltransferase activity of the microvillous surface of human placental syncytial trophoblast," *Gynecol. Invest.* 8(1977):267–281.
319. V.A. Krylenkov, K.A. Samoilova, S.V. Levin, "Destructive changes in the outer perimembrane layers (glycocalyx) of Zajdela ascites hepatoma cells under the action of UV radiation," *Tsitologiya* 21(May 1979):594–601. In Russian.
320. D. Vasmant, G. Feldmann, J.L. Fontaine, "Ultrastructural localization of concanavalin A surface receptors on brush-border enterocytes in normal children and during celiac disease," *Pediatr. Res.* 16(June 1982):441–445.
321. P. Sithigorngul, P. Burton, T. Nishihata, L. Caldwell, "Effects of sodium salicylate on epithelial cells of the rectal mucosa of the rat: a light and electron microscopic study," *Life Sci.* 33(12 September 1983):1025–1032.
322. J.S. Frank, "Ca depletion of the sarcolemma – ultrastructural changes," *Eur. Heart J.* 4(December 1983):23–27 (Suppl. H); J.S. Elz, W.G. Nayler, "Ultrastructural damage associated with the Ca²⁺ paradox. The protective effect of Mn²⁺," *Am. J. Pathol.* 117(October 1984):131–139.

323. J.R. Poley, "Loss of the glycocalyx of enterocytes in small intestine: a feature detected by scanning electron microscopy in children with gastrointestinal intolerance to dietary protein," *J. Pediatr. Gastroenterol. Nutr.* 7(May–June 1988):386–394.
324. M. Takumida, D. Bagger–Sjoberg, Y. Harada, D. Lim, J. Wersall, "Sensory hair fusion and glycocalyx changes following gentamicin exposure in the guinea pig vestibular organs," *Acta Otolaryngol.* 107(January–February 1989):39–47.
325. S. Mukerjee, R.K. Upreti, B.L. Tekwani, A.M. Kidwai, "Biochemical analysis of jejunal brush border membrane of golden hamster: pathogenic modulations due to ancylostomiasis," *Indian J. Biochem. Biophys.* 29(February 1992):82–86.
326. Y. Qiao, M. Yokoyama, K. Kameyama, G. Asano, "Effect of vitamin E on vascular integrity in cholesterol–fed guinea pigs," *Arterioscler. Thromb.* 13(December 1993):1885–1892.
327. D.V. Parke, "The cytochromes P450 and mechanisms of chemical carcinogenesis," *Environ. Health Perspect.* 102(October 1994):852–853.
328. R. Funfstuck, K.J. Halbhuber, B. Kuhn, R. Kuhn, H. Oehring, C. Scheven, W. Linss, G. Stein, "Dysmorphic erythrocytes in glomerulonephritis. 1. Electron microscopical and histochemical investigation," *Cell Mol. Biol. (Noisy–le–grand)* 40(December 1994):1113–1124.
329. H.K. Manner, C.A. Hart, B. Getty, D.F. Kelly, S.H. Sorensen, R.M. Batt, "Characterization of intestinal morphologic, biochemical, and ultrastructural features in gluten–sensitive Irish Setters during controlled oral gluten challenge exposure after weaning," *Am. J. Vet. Res.* 59(November 1998):1435–1440.
330. S. Walbaum, S. al Nahhas, C. Gabrion, M. Mesnil, A.F. Petavy, "Echinococcus multilocularis: in vitro interactions between protoscolices and Kupffer cells," *Parasitol. Res.* 80(1994):381–387.
331. R.J. Rothbaum, J.C. Partin, K. Saalfield, A.J. McAdams, "An ultrastructural study of enteropathogenic *Escherichia coli* infection in human infants," *Ultrastruct. Pathol.* 4(June 1983):291–304.
332. P. Horstedt, A. Danielsson, H. Nyhlin, R. Stenling, O. Suhr, "Adhesion of bacteria to the human small–intestinal mucosa. A scanning electron microscopic study," *Scand. J. Gastroenterol.* 24(September 1989):877–885.

333. S.M. el-Shoura, "*Helicobacter pylori*: I. Ultrastructural sequences of adherence, attachment, and penetration into the gastric mucosa," *Ultrastruct. Pathol.* 19(July–August 1995):323–333.
334. U. Fagundes–Neto, I.C. Scaletsky, "The gut at war: the consequences of enteropathogenic *Escherichia coli* infection as a factor of diarrhea and malnutrition," *Sao Paulo Med. J.* 118(6 January 2000):21–29.
335. U.S. Ryan, J.W. Ryan, "The ultrastructural basis of endothelial cell surface functions," *Biorheology* 21(1984):155–170.
336. P. Gorog, J.D. Pearson, "Sialic acid moieties on surface glycoproteins protect endothelial cells from proteolytic damage," *J. Pathol.* 146(July 1985):205–212.
337. E.D.P. de Robertis, E.M.F. de Robertis, *Cell and Molecular Biology*, Eighth Edition, Lea & Febiger, Philadelphia PA, 1987.
338. E. Czarnowska, E. Karwatowska–Prokopczuk, "Ultrastructural demonstration of endothelial glycocalyx disruption in the reperfused rat heart. Involvement of oxygen free radicals," *Basic Res. Cardiol.* 90(September–October 1995):357–364.
339. J.R. Lindner, S. Ismail, W.D. Spotnitz, D.M. Skyba, A.R. Jayaweera, S. Kaul, "Albumin microbubble persistence during myocardial contrast echocardiography is associated with microvascular endothelial glycocalyx damage," *Circulation* 98(17 November 1998):2187–2194.
340. W.M. Kemp, P.R. Brown, S.C. Merritt, R.E. Miller, "Tegument–associated antigen modulation by adult male *Schistosoma mansoni*," *J. Immunol.* 124(February 1980):806–811.
341. M. Marikovsky, R. Arnon, Z. Fishelson, "Proteases secreted by transforming schistosomula of *Schistosoma mansoni* promote resistance to killing by complement," *J. Immunol.* 141(1 July 1988):273–278.
342. Robert I. Lehrer, Tomas Ganz, "Chapter 87. Biochemistry and function of monocytes and macrophages," in *William's Hematology*, Fifth Edition, McGraw–Hill, New York, 1995, pp. 869–875.

343. Robert K. Murray, Daryl K. Granner, Peter A. Mayes, Victor W. Rodwell, Harper's Biochemistry, 23rd Edition, Appleton & Lange, Norwalk CT, 1993.
344. Mark S. Bretscher, Sean Munro, "Cholesterol and the Golgi apparatus," Science 261(3 September 1993):1280–1281.
345. Wayne M. Becker, David W. Deamer, The World of the Cell, Second Edition, Benjamin/Cummings Publishing Company, Redwood City CA, 1991.
346. Jonathan Black, Biological Performance of Materials: Fundamentals of Biocompatibility, Third Edition, Marcel Dekker, New York, 1999.
347. Jan Kilhamn, "The protective mucus and its mucins produced by enterocytes and goblet cells," Centrum for Gastroenterologisk Forskning, Goteborgs Universitet; <http://www.cgf.gu.se/fouschema.html>
348. M. Marikovsky, M. Parizade, R. Arnon, Z. Fishelson, "Complement regulation on the surface of cultured schistosomula and adult worms of *Schistosoma mansoni*," Eur. J. Immunol. 20(January 1990):221–227.
349. N. Saunders, R.A. Wilson, P.S. Coluson, "The outer bilayer of the adult schistosome tegument surface has a low turnover rate in vitro and in vivo," Mol. Biochem. Parasitol. 25(September 1987):123–131.
350. Bruce Alberts, Dennis Bray, Julian Lewis, Martin Raff, Keith Roberts, James D. Watson, The Molecular Biology of the Cell, Second Edition, Garland Publishing, Inc., New York, 1989.
351. Erle E. Peacock, Jr., Wound Repair, W.B. Saunders Company, Philadelphia, 1984.
352. B.J. Jones, C.R. Murphy, "A high resolution study of the glycocalyx of rat uterine epithelial cells during early pregnancy with the field emission gun scanning electron microscope," J. Anat. 185(October 1994):443–446.
353. Sidney F. Stein, Bruce Evatt, "Chapter 13–2. Thrombocytopenia," in J. Willis Hurst, Medicine for the Practicing Physician, Third Edition, Butterworth–Heinemann, Boston MA, 1992, pp. 769–771.

354. I.K. Gipson, M. Yankauckas, S.J. Spurr–Michaud, A.S. Tisdale, W. Rinehart, “Characteristics of a glycoprotein in the ocular surface glycocalyx,” *Invest. Ophthalmol. Vis. Sci.* 33(January 1992):218–227.
355. A.M. Glauert, D.A. Lammas, W.P. Duffus, “Ultrastructural observations on the interaction in vitro between bovine eosinophils and juvenile *Fasciola hepatica*,” *Parasitology* 91(December 1985):459–470.
356. A.S. Verkman, “Water permeability measurement in living cells and complex tissues,” *J. Membr. Biol.* 173(15 January 2000):73–87.
357. Michael Pinneo, “Diamond Growth: Today and Tomorrow,” in Markus Krummenacker, James Lewis, eds., *Prospects in Nanotechnology: Toward Molecular Manufacturing*, Proceedings of the First General Conference on Nanotechnology: Development, Applications, and Opportunities, 11–14 November 1992, John Wiley & Sons, New York, 1995, pp. 147–172.
358. Robert A. Freitas Jr., “Is Diamond Biocompatible With Living Cells?” *Foresight Update* No. 39, 30 December 1999, pp. 7–9; <http://www.imm.org/Reports/Rep012.html>
359. G. Ryu, D. Han, Y. Kim, B. Min, “Albumin immobilized polyurethane and its blood compatibility,” *ASAIO J.* 38(July–September 1992):M644–M648.
360. T. Iizuka, H. Fujimoto, T. Ono, “A new material (single crystal sapphire screw) for internal fixation of the mandibular ramus,” *J. Craniomaxillofac. Surg.* 15(February 1987):24–27.
361. N. Kossovsky, A. Gelman, H.J. Hnatyszyn, S. Rajguru, R.L. Garrell, S. Torbati, S.S. Freitas, G.M. Chow, “Surface–modified diamond nanoparticles as antigen delivery vehicles,” *Bioconjug. Chem.* 6(September–October 1995):507–511.
362. David Malakoff, “Aluminum is put on trial as a vaccine booster,” *Science* 288(26 May 2000):1323–1324.
363. Peter J. Eng, Thomas P. Trainor, Gordon E. Brown Jr., Glenn A. Waychunas, Matthew Newville, Stephen R. Sutton, Mark L. Rivers, “Structure of the Hydrated alpha–Al₂O₃ (0001) Surface,” *Science* 288(12 May 2000):1029–1033.

364. John W. Boretos, "Alumina as a Biomedical Material," in L.D. Hart, ed., *Alumina Chemicals Science and Technology Handbook*, The American Ceramic Society, Inc., Westerville, OH, 1990, pp. 337–340.

365. V.V. Rozas, F.K. Port, R.E. Easterling, "An outbreak of dialysis dementia due to aluminum in the dialysate," *J. Dial.* 2(1978):459–470; (no authors), "Editorial: Dialysis dementia: aluminium again?" *Lancet* 1(14 February 1976):349; S.D. Mahurkar, R. Salta, E.C. Smith, S.K. Dhar, L. Meyers Jr., G. Dunea, "Dialysis dementia," *Lancet* 1(23 June 1973):1412–1415.

366. F. Khalil–Manesh, C. Agness, H.C. Gonick, "Aluminum–binding protein in dialysis dementia," *Nephron* 52(1989):323–328 (Part I), 329–333 (Part II).

367. G. Dunea, "Dialysis dementia: an epidemic that came and went," *ASAIO J.* 47(May–June 2001):192–194.

368. K. Zaman, A. Zaman, J. Batcabe, "Hematological effects of aluminum on living organisms," *Comp. Biochem. Physiol. C* 106(October 1993):285–293.

369. Mary Dan Eades, *The Doctor's Complete Guide to Vitamins and Minerals*, Dell Publishing, New York, 1994.

370. R.G. Pina, C. Cervantes, "Microbial interactions with aluminum," *Biometals* 9(July 1996):311–316.

371. G.F. van Landeghem, M.E. de Broe, P.C. D'Haese, "Al and Si: Their speciation, distribution, and toxicity," *Clin. Biochem.* 31(July 1998):385–397.

372. W.J. Lukiw, H.J. LeBlanc, L.A. Carver, D.R. McLachlan, N.G. Bazan, "Run–on gene transcription in human neocortical nuclei. Inhibition by nanomolar aluminum and implications for neurodegenerative disease," *J. Mol. Neurosci.* 11(August 1998):67–78.

373. J.A. Hobkirk, "Tissue reactions to implanted vitreous carbon and high purity sintered alumina," *J. Oral Rehabil.* 4(October 1977):355–368.

374. C. Schlatter, A. Steinegger, U. Rickenbacher, C. Hans, A. Lengeyl, "Blood aluminum levels in workers in the aluminum industry," *Sozial Praventivmed.* 31(1986):125–129. In German.
375. J.L. Greger, *Food Technol.* 39(1985):73–; J.L. Greger, E.N. Bula, E.T. Gum, "Mineral metabolism of rats fed moderate levels of various aluminum compounds for short periods of time," *J. Nutr.* 115(December 1985):1708–1716; J.L. Greger, M.J. Baier, "Effect of dietary aluminum on mineral metabolism of adult males," *Am. J. Clin. Nutr.* 38(September 1983):411–419.
376. J.P. Muller, A. Steinegger, C. Schlatter, "Contribution of aluminum from packaging materials and cooking utensils to the daily aluminum uptake," *Z. Lebensm. Unters Forsch.* 197(October 1993):332–341.
377. M. Lewandowska–Szumiel, J. Komender, "Aluminium release as a new factor in the estimation of alumina bioceramic implants," *Clin. Mater.* 5(1990):167–175.
378. P.S. Christel, "Biocompatibility of surgical–grade dense polycrystalline alumina," *Clin. Orthop.* 282(September 1992):10–18.
379. A. Toni, C.G. Lewis, A. Sudanese, S. Stea, F. Calista, L. Savarino, A. Pizzoferrato, A. Giunti, "Bone demineralization induced by cementless alumina–coated femoral stems," *J. Arthroplasty* 9(August 1994):435–444.
380. Z.X. Wang, B.F. Chai, Y.Q. Ye, Q.Y. Fang, "Local changes in aluminium, calcium and phosphorus content of bone caused by alumina implant," *Chin. Med. J. (Engl.)* 105(September 1992):749–752.
381. P.W. May, C.A. Rego, C.G. Trevor, E.C. Williamson, M.N.R. Ashfold, K.N. Rosser, N.M. Everitt, "Deposition of diamond films on sapphire: Studies of interfacial properties and patterning techniques," *Diam. Rel. Mater.* 3(1994):1375.
382. M. Nagase, "Antigenicity of alumina ceramic and calcium phosphate ceramics – genetic control of the immune response," *Nippon Seikeigeka Gakkai Zasshi* 59(February 1985):183–191. In Japanese.
383. P. Pospiech, P. Rammelsberg, G. Goldhofer, W. Gernet, "All–ceramic resin–bonded bridges. A 3–dimensional finite–element analysis study," *Eur. J. Oral Sci.* 104(August 1996):390–395.

384. J.L. Charissoux, A. Najid, J.C. Moreau, D. Setton, M. Rigaud, "Development of in vitro biocompatibility assays for surgical material," *Clin. Orthop.* 326(May 1996):259–269.
385. C. Sella, J.C. Martin, J. Lecoeur, J.P. Bellier, M.F. Harmand, A. Naji, J.P. Davidas, A. Le Chanu, "Corrosion protection of metal implants by hard biocompatible ceramic coatings deposited by radiofrequency sputtering," *Clin. Mater.* 5(1990):297–307.
386. G. Szabo, L. Kovacs, K. Vargha, J. Barabas, Z. Nemeth, "A new advanced surface modification technique – titanium oxide ceramic surface implants: the background and long-term results," *J. Long Term Eff. Med. Implants* 9(1999):247–259.
387. N. Martin, N.M. Jedyakiewicz, "Clinical performance of CEREC ceramic inlays: a systematic review," *Dent. Mater.* 15(January 1999):54–61.
388. M.A. Bergman, "The clinical performance of ceramic inlays: a review," *Aust. Dent.* 44(September 1999):157–168.
389. H. Erpenstein, R. Borchard, T. Kerschbaum, "Long-term clinical results of galvano-ceramic and glass-ceramic individual crowns," *J. Prosthet. Dent.* 83(May 2000):530–534.
390. M. Thordrup, F. Isidor, P. Horsted-Bindslev, "A 3-year study of inlays milled from machinable ceramic blocks representing 2 different inlay systems," *Quintessence Int.* 30(December 1999):829–836.
391. R.J. Royer, J.L. Delongas, P. Netter, G. Faure, J.M. Mur, D. Burnel, A. Gaucher, "Inflammatory effect of aluminium phosphate on rat paws," *Pathol. Biol. (Paris)* 30(April 1982):211–215.
392. J.L. Delongas, P. Netter, P. Boz, G. Faure, R.J. Royer, A. Gaucher, "Experimental synovitis induced by aluminium phosphate in rabbits. Comparison of the changes produced in synovial tissue and in articular cartilage by aluminium phosphate, carrageenin, calcium hydrogen phosphate dihydrate, and natural diamond powder," *Biomed. Pharmacother.* 38(1984):44–48.
393. Mikael Hedenborg, Matti Klockars, "Quartz-dust-induced production of reactive oxygen metabolites by human granulocytes," *Lung* 167(1989):23–32.

394. Per Aspenberg, Asko Anttila, Yrjo T. Kontinen, Reijo Lappalainen, Stuart B. Goodman, Lars Nordsletten, Seppo Santavirta, "Benign response to particles of diamond and SiC: bone chamber studies of new joint replacement coating materials in rabbits," *Biomaterials* 17(April 1996):807–812.
395. R.L. Tse, P. Phelps, "Polymorphonuclear leukocyte motility in vitro. V. Release of chemotactic activity following phagocytosis of calcium pyrophosphate crystals, diamond dust, and urate crystals," *J. Lab. Clin. Med.* 76(September 1970):403–415.
396. F.K. Higson, O.T. Jones, "Oxygen radical production by horse and pig neutrophils induced by a range of crystals," *J. Rheumatol.* 11(December 1984):735–740.
397. L. Tang, C. Tsai, W.W. Gerberich, L. Kruckeberg, D.R. Kania, "Biocompatibility of chemical–vapor–deposited diamond," *Biomaterials* 16(1995):483–488.
398. L. Anne Thomson, Frances C. Law, Neil Rushton, J. Franks, "Biocompatibility of diamond–like carbon coating," *Biomaterials* 12(January 1991):37–40.
399. A. Swan, B. Dularay, P. Dieppe, "A comparison of the effects of urate, hydroxyapatite and diamond crystals on polymorphonuclear cells: relationship of mediator release to the surface area and adsorptive capacity of different particles," *J. Rheumatol.* 17(October 1990):1346–1352.
400. Karsten Bubka, Harald Gnewuch, Martin Hempstead, Jens Hammer, Malcolm L.H. Green, "Optical anisotropy of dispersed carbon nanotubes induced by an electric field," *Appl. Phys. Lett.* 71(1997):1906–1908.
401. A.G. Rinzler, R.E. Smalley, unpublished data; cited in Jie Liu et al., "Fullerene Pipes," *Science* 280(22 May 1998):1253–1256.
402. B. Fartash, K. Arvidson, I. Ericsson, "Histology of tissues surrounding single crystal sapphire endosseous dental implants: an experimental study in the beagle dog," *Clin. Oral Implants Res.* 1(December 1990):13–21.
403. G. Anneroth, A.R. Ericsson, L. Zetterqvist, "Tissue integration of Al₂O₃–ceramic dental implants (Frialit) – a case report," *Swed. Dent. J.* 14(1990):63–70.

404. K. Arvidson, B. Fartash, L.E. Moberg, R. Grafstrom, I. Ericsson, "In vitro and in vivo experimental studies on single crystal sapphire dental implants," *Clin. Oral Implants Res.* 2(April–June 1991):47–55.
405. B. Fartash, T. Tangerud, J. Silness, K. Arvidson, "Rehabilitation of mandibular edentulism by single crystal sapphire implants and overdentures: 3–12 year results in 86 patients. A dual center international study," *Clin. Oral Implants Res.* 7(September 1996):220–229.
406. P. Friedberg, R. Reck, "Aluminum oxide ceramics in reconstructive nose surgery. Histological studies in rabbits," *HNO* 32(March 1984):105–107. In German.
407. A. Piattelli, G. Podda, A. Scarano, "Histological evaluation of bone reactions to aluminium oxide dental implants in man: a case report," *Biomaterials* 17(April 1996):711–714.
408. H. Oonishi, L.L. Hench, J. Wilson, F. Sugihara, E. Tsuji, S. Kushitani, H. Iwaki, "Comparative bone growth behavior in granules of bioceramic materials of various sizes," *J. Biomed. Mater. Res.* 44(January 1999):31–43.
409. Y. Akagawa, M. Hashimoto, N. Kondo, A. Yamasaki, H. Tsuru, "Tissue reaction to implanted biomaterials," *J. Prosthet. Dent.* 53(May 1985):684–686.
410. K. Arvidson, B. Fartash, M. Hilliges, P.A. Kondell, "Histological characteristics of peri-implant mucosa around Branemark and single-crystal sapphire implants," *Clin. Oral Implants Res.* 7(March 1996):1–10.
411. M. Di Silvestre, S. Guizzardi, N. Bettini, G. Gargiulo, R. Savini, "Powdered alumina implants in the experimental animal: a histological study conducted in the rat," *Chir. degli Organi. di Mov.* 76(April–June 1991):167–172.
412. Peter Griss, Gunther Heimke, "Biocompatibility of High Density Alumina and its Applications in Orthopedic Surgery," in David F. Williams, ed., *Biocompatibility of Clinical Implant Materials, Volume I*, CRC Press, Boca Raton, FL, 1981, pp. 155–198.
413. Q. Ye, K. Ohsaki, K. Ii, D.J. Li, H. Matsuoka, S. Tenshin, T. Yamamoto, "A subcutaneous tissue reaction in the early stage to a synthetic auditory ossicle (Bioceram) in rats," *J. Med. Invest.* 44(February 1998):173–177.

414. Elizabeth J. Harfenist, Robert K. Murray, "Chapter 59. Plasma Proteins, Immunoglobulins, & Blood Coagulation," in Robert K. Murray, Daryl K. Granner, Peter A. Mayes, Victor W. Rodwell, eds., Harper's Biochemistry, 23rd Edition, Appleton & Lange, Norwalk CT, 1993, pp. 665–687.
415. Alexander Duncan, "Coagulation defects," in J. Willis Hurst, ed., Medicine for the Practicing Physician, Third Edition, Butterworth–Heinemann, Boston MA, 1992, pp. 786–788.
416. Torben Halkier, Paul Woolley (Translator), Mechanisms in Blood Coagulation Fibrinolysis and the Complement System, Cambridge University Press, New York, 1991.
417. Robert W. Colman, Jack Hirsch, Victor J. Marder, Edwin W. Salzman, eds., Hemostasis and Thrombosis: Basic Principles and Clinical Practice, Third Edition, Lippincott, Williams & Wilkins Publishers, 1994.
418. Arthur L. Bloom, Charles D. Forbes, Duncan P. Thomas, Edward G.D. Tuddenham, eds., Haemostasis and Thrombosis, Third Edition, Churchill Livingstone, New York, 1994.
419. Katherine A. High, Harold R. Roberts, eds., Molecular Basis of Thrombosis and Hemostasis, Marcel Dekker, Inc., New York, 1995.
420. Joseph Loscalzo, Andrew J. Schafer, eds., Thrombosis and Hemorrhage, Second Edition, Williams & Wilkins, Baltimore, MD, 1998.
421. Z.M. Ruggeri, "Structure and function of von Willebrand factor," Thromb. Haemost. 82(August 1999):576–584.
422. F. De Clerck, "The role of serotonin in thrombogenesis," Clin. Physiol. Biochem. 8(1990):40–49 (Suppl 3).
423. A. McNicol, J.M. Gerrard, "Post–receptor events associated with thrombin–induced platelet activation," Blood Coagul. Fibrinolysis 4(December 1993):975–991.

424. Huzoor–Akbar, N.G. Ardlie, “Platelet activation in haemostasis: role of thrombin and other clotting factors in platelet–collagen interaction,” *Haemostasis* 6(1977):59–71.
425. “Stents: The New Phytis Stent,” 3 August 1998; <http://phytis.com/stent1.htm>
426. Kai Gutensohn, “Flow Cytometric Analysis of Coronary Stent–Induced Alterations of Platelet Antigens in an In–Vitro Model,” 23 April 1998; <http://www.phytis.com/stent6.htm>
427. K. Yamazaki, P. Litwak, O. Tagusari, T. Mori, K. Kono, M. Kameneva, M. Watach, L. Gordon, M. Miyagishima, J. Tomioka, M. Umezu, E. Outa, J.F. Antaki, R.L. Kormos, H. Koyanagi, B.P. Griffith, “An implantable centrifugal blood pump with a recirculating purge system (Cool–Seal system),” *Artif. Organs* 22(June 1998):466–474.
428. K. Yamazaki, P. Litwak, R.L. Kormos, T. Mori, O. Tagusari, J.F. Antaki, M. Kameneva, M. Watach, L. Gordon, M. Umezu, J. Tomioka, H. Koyanagi, B.P. Griffith, “An implantable centrifugal blood pump for long term circulatory support,” *ASAIO J.* 43(September–October 1997):M686–M691.
429. I. Dion, C. Baquey, J.R. Monties, “Diamond: the biomaterial of the 21st century?” *Int. J. Artif. Organs* 16(September 1993):623–627.
430. J.R. Monties, P. Havlik, T. Mesana, J. Trinkl, J.L. Tourres, J.L. Demunck, “Development of the Marseilles pulsatile rotary blood pump for permanent implantable left ventricular assistance,” *Artif. Organs* 18(July 1994):506–511.
431. J.R. Monties, I. Dion, P. Havlik, F. Rouais, J. Trinkl, C. Baquey, “Cora rotary pump for implantable left ventricular assist device: biomaterial aspects,” *Artif. Organs* 21(July 1997):730–734.
432. Richard D. Schaub, Marina V. Kameneva, Harvey S. Borovetz, William R. Wagner, “Assessing acute platelet adhesion on opaque metallic and polymeric biomaterials with fiber optic microscopy,” *J. Biomed. Mater. Res.* 49(2000):460–468.
433. I. Dion, X. Roques, C. Baquey, E. Baudet, B. Basse Cathalinat, N. More, “Hemocompatibility of diamond–like carbon coating,” *Biomed. Mater. Eng.* 3(Spring 1993):51–55.

434. M.I. Jones, I.R. McColl, D.M. Grant, K.G. Parker, et al, "Haemocompatibility of DLC and TiC-TiN interlayers on titanium," *Diam. Rel. Mat.* 8(March 1999):457-462.
435. Y. Takami, T. Nakazawa, K. Makinouchi, J. Glueck, Y. Nose, "Biocompatibility of alumina ceramic and polyethylene as materials for pivot bearings of a centrifugal blood pump," *J. Biomed. Mater. Res.* 36(5 September 1997):381-386.
436. Y. Takami, S. Yamane, K. Makinouchi, G. Otsuka, J. Glueck, R. Benkowski, Y. Nose, "Protein adsorption onto ceramic surfaces," *J. Biomed. Mater. Res.* 40(April 1998):24-30.
437. Y. Takami, S. Yamane, K. Makinouchi, Y. Niimi, A. Sueoka, Y. Nose, "Evaluation of platelet adhesion and activation on materials for an implantable centrifugal blood pump," *Artif. Organs* 22(September 1998):753-758.
438. A.A. de-Queiroz, E.P. Vianna, L.A. Genova, O.Z. Higa, J.C. Bressiani, A.H. Bressiani, "The interaction of blood proteins with alpha-alumina," *Braz. J. Med. Biol. Res.* 27(November 1994):2569-2571.
439. I. Dion, M. Lahaye, R. Salmon, C. Baquey, J.R. Monties, P. Havlik, "Blood haemolysis by ceramics," *Biomaterials* 14(1993):107-110.
440. J. McLean, *Am. J. Physiol.* 41(1976):250.
441. G.P. Stewart, M.A. Wilkov, "Mechanism of failure of biocompatible-treated surfaces," *J. Biomed. Mater. Res.* 10(May 1976):413-428.
442. H. Mohri, T. Ishitoya, E.A. Hessel 2d, G. Schmer, D.H. Dillard, K.A. Merendino, "Use of athrombogenic tubing for perfusion rewarming following surface-induced deep hypothermia," *J. Thorac. Cardiovasc. Surg.* 77(February 1979):277-282.
443. Y. Noishiki, T. Miyata, "A simple method to heparinize biological materials," *J. Biomed. Mater. Res.* 20(1986):337-346.
444. A.S. Hoffman, "Modification of material surfaces to affect how they interact with blood," *Ann. N.Y. Acad. Sci.* 516(1987):96-101.

445. S.W. Kim, H. Jacobs, J.Y. Lin, C. Nojori, T. Okano, "Nonthrombogenic bioactive surfaces," *Ann. N.Y. Acad. Sci.* 516(1987):116–130.
446. S.C. Lin, H.A. Jacobs, S.W. Kim, "Heparin immobilization increased through chemical amplification," *J. Biomed. Mater. Res.* 25(June 1991):791–795.
447. S.W. Kim, H. Jacobs, "Design of nonthrombogenic polymer surfaces for blood–contacting medical devices," *Blood Purif.* 14(1996):357–372.
448. P.V. Narayanan, "Surface functionalization by RF plasma treatment of polymers for immobilization of bioactive molecules," *J. Biomater. Sci. Polym. Ed.* 6(1994):181–193.
449. M.S. Beena, T. Chandy, C.P. Sharma, "Heparin immobilized chitosan – polyethyleneglycol interpenetrating network: antithrombogenicity," *Art. Cells Blood Subst. Immobil. Biotech.* 23(1995):175–192.
450. H. Baumann, R. Keller, "Which glycosaminoglycans are suitable for antithrombogenic or athrombogenic coatings of biomaterials? Part II. Covalently immobilized endothelial cell surface heparan sulfate (ESHS) and heparin (HE) on synthetic polymers and results of animal experiments," *Semin. Thromb. Hemost.* 23(1997):215–223.
451. M. Erdtmann, R. Keller, H. Baumann, "Photochemical immobilization of heparin, dermatan sulphate, dextran sulphate and endothelial cell surface heparan sulphate onto cellulose membranes for the preparation of athrombogenic and antithrombogenic polymers," *Biomaterials* 15(October 1994):1043–1048.
452. "Angiogenesis: a brief introduction"; <http://www.med.unibs.it/~airc/angiogen.html>
453. W. Risau, I. Flamme, "Vasculogenesis," *Annu. Rev. Cell Dev. Biol.* 11(1995):73–91.
454. I.D. Goldberg, E.M. Rosen, eds., *Regulation of Angiogenesis*, Birkhauser, 1997.

455. N. Ferrara, "Vascular endothelial growth factor and the regulation of angiogenesis," *Recent Prog. Horm. Res.* 55(2000):15–35, 35–36 (discussion).
456. M. Presta, M. Rusnati, P. Dell'Era, E. Tanghetti, C. Urbinati, R. Giuliani, D. Leali, "Examining new models for the study of autocrine and paracrine mechanisms of angiogenesis through FGF2–transfected endothelial and tumour cells," *Adv. Exp. Med. Biol.* 476(2000):7–34.
457. Shaker A. Mousa, ed., *Angiogenesis Inhibitors and Stimulators: Potential Therapeutic Implications*, Landes Bioscience, Austin, TX, 2000.
458. E.C. Breen, E.C. Johnson, H. Wagner, H.M. Tseng, L.A. Sung, P.D. Wagner, "Angiogenic growth factor mRNA responses in muscle to a single bout of exercise," *J. Appl. Physiol.* 81(July 1996):355–361.
459. T. Gustafsson, A. Puntchart, L. Kaijser, E. Jansson, C.J. Sundberg, "Exercise–induced expression of angiogenesis–related transcription and growth factors in human skeletal muscle," *Am. J. Physiol.* 276(February 1999):H679–H685; <http://ajpheart.physiology.org/cgi/content/full/276/2/H679>
460. T. Gustafsson, W.E. Kraus, "Exercise–induced angiogenesis–related growth and transcription factors in skeletal muscle, and their modification in muscle pathology," *Front. Biosci.* 6(1 January 2001):D75–D89.
461. P.D. Wagner, F. Masanes, H. Wagner, E. Sala, O. Miro, J.M. Campistol, R.M. Marrades, J. Casademont, V. Torregrosa, J. Roca, "Muscle angiogenic growth factor gene responses to exercise in chronic renal failure," *Am. J. Physiol. Regul. Integr. Comp. Physiol.* 281(August 2001):R539–R546.
462. Gerardo Beni, Jing Wang, "Swarm intelligence in cellular robotic systems," in Paolo Dario, Giulio Sandini, Patrick Aebischer, eds., *Robots and Biological Systems: Towards a New Bionics*, Springer–Verlag, New York, 1993, pp. 701–712.
463. R. Alami, S. Fleury, M. Herrb, F. Ingrand, S. Qutub, "Operating a large fleet of mobile robots using the plan–merging paradigm," *Proc. 1997 IEEE International Conference on Robotics and Automation*, 20–25 April 1997, IEEE Robotics and Automation Society, pp. 2312–2317.
464. Naoki Mitsumoto, Toshio Fukuda, Fumihito Arai, Hidenori Ishihara, "Control of the distributed autonomous robotic system based on the biologically inspired immunological architecture," *Proc. 1997 IEEE International Conference on Robotics and Automation*, 20–25 April 1997, IEEE Robotics and Automation Society, pp. 3551–3556.

465. Ronald C. Arkin, Behavior-Based Robotics, MIT Press, 1998.
466. Joseph L. Jones, Anita M. Flynn, Bruce A. Seiger, Mobile Robots: Inspiration to Implementation, Second Edition, A.K. Peters Ltd., 1999.
467. E. Bonabeau, M. Dorigo, G. Theraulaz, Swarm Intelligence: From Natural to Artificial Systems, Oxford University Press, 1999.
468. Eric Bonabeau, Guy Theraulaz, "Swarm smarts," Scientific American 282(March 2000):72–79.
469. Tad Hogg, "Multiagent control of separable modular robots," Hewlett-Packard Technical Report, January 2002; preprint courtesy of Tad Hogg.
470. Per Bak, Chao Tang, Kurth Wiesenfeld, "Self-organized criticality," Phys. Rev. A 38(1 July 1988):364–374.
471. P. Bak, K. Sneppen, "Punctuated equilibrium and criticality in a simple model of evolution," Phys. Rev. Lett. 71(1993):4083–4086.
472. Z. Olami, H.J. Feder, C. Christensen, "Self-organized criticality in a cellular automaton modeling earthquakes," Phys. Rev. E 48(1993):3361–3372.
473. P. Bak, M. Paczuski, "Complexity, contingency, and criticality," Proc. Natl. Acad. Sci. (USA) 92(1995):6689–6696.
474. Per Bak, How Nature Works: The Science of Self-Organized Criticality, Oxford University Press, Oxford, 1997.
475. Howard W. French, Dennis Overbye, "Accident curbs Japan research into cosmos's ghostly particles," New York Times, 13 November 2001, <http://www.nytimes.com/2001/11/13/science/physical/13JAPA.html>; Edwin Cartlidge, "Accident grounds neutrino lab," IoP PhysicsWeb, 15 November 2001, <http://physicsweb.org/article/news/5/11/9>; Chiaki Yanagisawa, Tokufumi Kato, transl., "Report on the

Super-Kamiokande Accident (As of November 22, 2001),”
<http://www-sk.icrr.u-tokyo.ac.jp/cause-committee/1st/report-nov22e.pdf>

476. Tom Dworetzky, “A Walking Miracle,” Discover Magazine 23(January 2002):47;
http://www.discover.com/jan_02/medicine.html

477. F. Sterz, P. Safar, S. Tisherman, A. Radovsky, K. Kuboyama, K. Oku, “Mild hypothermic cardiopulmonary resuscitation improves outcome after prolonged cardiac arrest in dogs,” Crit. Care Med. 19(March 1991):379–389; Crit. Care Med 19(March 1991):315 (comments), Crit. Care Med. 20(March 1992):441–443 (comments).

478. A. Capone, P. Safar, A. Radovsky, Y.F. Wang, A. Peitzman, S.A. Tisherman, “Complete recovery after normothermic hemorrhagic shock and profound hypothermic circulatory arrest of 60 minutes in dogs,” J. Trauma 40(March 1996):388–395.

479. P. Safar, N.S. Abramson, M. Angelos, R. Cantadore, Y. Leonov, R. Levine, E. Pretto, H. Reich, F. Sterz, S.W. Stezoski et al, “Emergency cardiopulmonary bypass for resuscitation from prolonged cardiac arrest,” Am. J. Emerg. Med. 8(January 1990):55–67. See also: Safar Center for Resuscitation Research, “Hemorrhagic Shock and Suspended Animation Program: Cardiopulmonary Bypass (CPB)”;
<http://www.safar.pitt.edu/cpb.html>

480. J.N. Stinner, D.L. Newlon, N. Heisler, “Extracellular and intracellular carbon dioxide concentration as a function of temperature in the toad *Bufo marinus*,” J. Exp. Biol. 195(October 1994):345–360;
<http://jeb.biologists.org/cgi/reprint/195/1/345.pdf>

481. R. Araki, M. Tamura, I. Yamazaki, “The effect of intracellular oxygen concentration on lactate release, pyridine nucleotide reduction, and respiration rate in the rat cardiac tissue,” Circ. Res. 53(October 1983):448–455.

482. R.D. Kilgour, C.E. Riggs Jr., “Glycogenolysis and lactogenesis in the ischemic diabetic rat heart,” Diabetes Res. 4(January 1987):27–29.

483. C.W. Castor, M. Yaron, “Connective tissue activation: VIII. The effects of temperature studied in vitro,” Arch. Phys. Med. Rehabil. 57(January 1976):5–9; L.E. Taylor, P.L. Ferrante, D.S. Kronfeld, T.N. Meacham, “Acid–base variables during incremental exercise in sprint–trained horses fed a high–fat diet,” J. Anim. Sci. 73(July 1995):2009–2018.

484. G.A. Brooks, H. Dubouchaud, M. Brown, J.P. Sicurello, C.E. Butz, "Role of mitochondrial lactate dehydrogenase and lactate oxidation in the intracellular lactate shuttle," Proc. Natl. Acad. Sci. (USA) 96(2 February 1999):1129–1134; <http://www.pnas.org/cgi/content/full/96/3/1129>
485. G.A. Brooks, "Are arterial, muscle and working limb lactate exchange data obtained on men at altitude consistent with the hypothesis of an intracellular lactate shuttle?" Adv. Exp. Med. Biol. 474(1999):185–204.
486. J. Han, I. So, E.Y. Kim, Y.E. Earm, "ATP-sensitive potassium channels are modulated by intracellular lactate in rabbit ventricular myocytes," Pflugers Arch. 425(December 1993):546–548.
487. D.J. Combs, R.J. Dempsey, M. Maley, D. Donaldson, C. Smith, "Relationship between plasma glucose, brain lactate, and intracellular pH during cerebral ischemia in gerbils," Stroke 21(June 1990):936–942.
488. F. da Fonseca-Wollheim, K.G. Heinze, "The influence of pCO₂ on the rate of ammonia formation in blood," Eur. J. Clin. Chem. Clin. Biochem. 30(December 1992):867–869.
489. Bloch and Rittenberg, J. Biol. Chem. 159(1948):45.
490. B.P. McNicholl, "The golden hour and prehospital trauma care," Injury 25(May 1994):251–254.
491. E. Boersma, A.C. Maas, J.W. Deckers, M.L. Simoons, "Early thrombolytic treatment in acute myocardial infarction: reappraisal of the golden hour," Lancet 348(21 September 1996):771–775.
492. O. Blow, L. Magliore, J.A. Claridge, K. Butler, J.S. Young, "The golden hour and the silver day: detection and correction of occult hypoperfusion within 24 hours improves outcome from major trauma," J. Trauma 47(November 1999):964–969.
493. E.B. Lerner, R.M. Moscatti, "The golden hour: scientific fact or medical 'urban legend'?" Acad. Emerg. Med. 8(July 2001):758–760.
494. Y. Leonov, P. Safar, F. Sterz, S.W. Stezoski, "Extending the golden hour of hemorrhagic shock tolerance with oxygen plus hypothermia in awake rats. An exploratory study," Resuscitation 52(February 2002):193–202.

495. K.E. Wood, "Major pulmonary embolism: review of a pathophysiologic approach to the golden hour of hemodynamically significant pulmonary embolism," *Chest* 121(March 2002):877–905.
496. K. Matsuyama, Y. Chiba, A. Ihaya, T. Kimura, N. Tanigawa, R. Muraoka, "Effect of spinal cord preconditioning on paraplegia during cross-clamping of the thoracic aorta," *Ann. Thorac. Surg.* 63(May 1997):1315–1320.
497. P. Uceda, S. Basu, R.R. Robertazzi, M.A. Bottali, J. Edwards, I.J. Jacobowitz, A.J. Acinapura, J.N. Cunningham, "Effect of cerebrospinal fluid drainage and/or partial exsanguination on tolerance to prolonged aortic cross-clamping," *J. Card. Surg.* 9(November 1994):631–637.
498. A.Z. Apaydin, S. Buket, "Regional lidocaine infusion reduces postischemic spinal cord injury in rabbits," *Tex. Heart Inst. J.* 28(2001):172–176.
499. O. Tetik, T. Yagdi, F. Islamoglu, T. Calkavur, H. Posacioglu, Y. Atay, F. Ayik, L. Canpolat, M. Yuksel, "The effects of L-Carnitine on spinal cord ischemia/reperfusion injury in rabbits thorac," *Cardiovasc. Surg.* 50(February 2002):11–15.
500. W. Ko, J. Zelano, A.L. Fahey, K. Berman, O.W. Isom, K.H. Krieger, "Ischemic tolerance of the arrested heart during warm cardioplegia," *Eur. J. Cardiothorac. Surg.* 7(1993):295–299.
501. C. Hahn, F. Simonet, "Resistance and tolerance of the myocardium to ischemia," *J. Cardiovasc. Surg. (Torino)* 16(May–June 1975):265–267.
502. W. Schaper, J. Schaper, J. Palmowski, U. Thiedemann, F. Hehrlein, "Ischemia-tolerance following cardioplegic arrest in human patients and in experimental animals," *J. Cardiovasc. Surg. (Torino)* 16(May–June 1975):268–277.
503. R.W. Landymore, A.E. Marble, A. Trillo, G. Faulkner, M.A. MacAulay, C. Cameron, "Prevention of myocardial electrical activity during ischemic arrest with verapamil cardioplegia," *Ann. Thorac. Surg.* 43(May 1987):534–538.
504. W. Haider, H. Benzer, W. Schutz, E. Wolner, "Improvement of cardiac preservation by preoperative high insulin supply," *J. Thorac. Cardiovasc. Surg.* 88(August 1984):294–300.

505. R.A. Kloner, D. Yellon, "Does ischemic preconditioning occur in patients?" *J. Am. Coll. Cardiol.* 24(October 1994):1133–1142.
506. N. Maulik, R.M. Engelman, Z. Wei, X. Liu, J.A. Rousou, J.E. Flack, D.W. Deaton, D.K. Das, "Drug-induced heat-shock preconditioning improves postischemic ventricular recovery after cardiopulmonary bypass," *Circulation* 92(1 November 1995):II381–II388.
507. S. Vogt, D. Troitzsch, H. Abdul-Khaliq, W. Bottcher, P.E. Lange, R. Moosdorf, "Improved myocardial preservation with short hyperthermia prior to cold cardioplegic ischemia in immature rabbit hearts," *Eur. J. Cardiothorac. Surg.* 18(August 2000):233–240.
508. S. Nishio, M. Yunoki, Z.F. Chen, M.J. Anzivino, K.S. Lee, "Ischemic tolerance in the rat neocortex following hypothermic preconditioning," *J. Neurosurg.* 93(November 2000):845–851.
509. K.B. Storey, D.D. Mosser, D.N. Douglas, J.E. Grundy, J.M. Storey, "Biochemistry below 0 degrees C: nature's frozen vertebrates," *Braz. J. Med. Biol. Res.* 29(March 1996):283–307.
510. J. Suarez, R. Rubio, "Regulation of glycolytic flux by coronary flow in guinea pig heart. Role of vascular endothelial cell glycocalyx," *Am. J. Physiol.* 261(December 1991):H1994–H2000.
511. A.R. Prasad, S.A. Logan, R.M. Nerem, C.J. Schwartz, "Sprague flow-related responses of intracellular," *Circ. Res.* 72(April 1993):827–836.
512. M. Uematsu, Y. Ohara, J.P. Navas, J.P. Nishida, T.J. Murphy, R.W. Alexander, R.M. Nerem, D.G. Harrison, "Regulation of endothelial cell nitric oxide synthase mRNA expression by shear stress," *Am. J. Physiol.* 269(December 1995):C1371–C1378.
513. K. Lin, P.P. Hsu, B.P. Chen, S. Yuan, S. Usami, J.Y. Shyy, Y.S. Li, S. Chien, "Molecular mechanism of endothelial growth arrest by laminar shear stress," *Proc. Natl. Acad. Sci. (USA)* 97(15 August 2000):9385–9389; <http://www.pnas.org/cgi/content/full/97/17/9385>
514. C.G. Lee, M. Heijn, E. di Tomaso, G. Griffon-Etienne, M. Ancukiewicz, C. Koike, K.R. Park, N. Ferrara, R.K. Jain, H.D. Suit, Y. Boucher, "Anti-vascular endothelial growth factor treatment augments tumor radiation response under normoxic or hypoxic conditions," *Cancer Res.* 60(1 October

2000):5565–5570.

515. X. Bao, C. Lu, J.A. Frangos, “Mechanism of temporal gradients in shear–induced ERK1/2 activation and proliferation in endothelial cells,” *Am. J. Physiol. Heart Circ. Physiol.* 281(July 2001):H22–H29.

516. R.P. Alston, L. Murray, A.D. McLaren, “Changes in hemodynamic variables during hypothermic cardiopulmonary bypass. Effects of flow rate, flow character, and arterial pH,” *J. Thorac. Cardiovasc. Surg.* 100(July 1990):134–144.

517. H.A. Hennein, “Cardiopulmonary bypass / deep hypothermic circulatory arrest,” 22 November 1998; <http://pedscm.wustl.edu/All-Net/english/cardpage/operate/bypass/cpb-19.htm>

518. J.E. Bailes, M.L. Leavitt, E. Teeple Jr., J.C. Maroon, S.R. Shih, M. Marquardt, A.E. Rifai, L. Manack, “Ultraprofound hypothermia with complete blood substitution in a canine model,” *J. Neurosurg.* 74(May 1991):781–788.

519. M.J. Taylor, J.E. Bailes, A.M. Elrifai, S.R. Shih, E. Teeple, M.L. Leavitt, J.G. Baust, J.C. Maroon, “A new solution for life without blood. Asanguineous low–flow perfusion of a whole–body perfusate during 3 hours of cardiac arrest and profound hypothermia,” *Circulation* 91(15 January 1995):431–444; <http://circ.ahajournals.org/cgi/content/full/91/2/431>

520. M.J. Taylor, J.E. Bailes, A.M. Elrifai, T.S. Shih, E. Teeple, M.L. Leavitt, J.C. Baust, J.C. Maroon, “Asanguineous whole body perfusion with a new intracellular acellular solution and ultraprofound hypothermia provides cellular protection during 3.5 hours of cardiac arrest in a canine model,” *ASAIO J.* 40(July–September 1994):M351–M358.

521. T. Miura, P. Laussen, H.G. Lidov, A. DuPlessis, T. Shin'oka, R.A. Jonas, “Intermittent whole–body perfusion with ‘somatoplegia’ versus blood perfusate to extend duration of circulatory arrest,” *Circulation* 94(1 November 1996):II56–II62.

522. M. Ikonovic, K.M. Kelly, T.M. Hentosz, S.R. Shih, D.M. Armstrong, M.J. Taylor, “Ultraprofound cerebral hypothermia and blood substitution with an acellular synthetic solution maintains neuronal viability in rat hippocampus,” *Cryo. Letters* 22(January–February 2001):19–26.

523. N.M. Dearden, “Ischaemic brain,” *Lancet* 2(3 August 1985):255–259.

524. L. Hertz, "Features of astrocytic function apparently involved in the response of central nervous tissue to ischemia-hypoxia," *J. Cereb. Blood Flow Metab.* 1(1981):143-153.
525. N.H. Diemer, F.F. Johansen, H. Benveniste, T. Bruhn, M. Berg, E. Valente, M.B. Jorgensen, "Ischemia as an excitotoxic lesion: protection against hippocampal nerve cell loss by denervation," *Acta Neurochir. Suppl.* 57(1993):94-101.
526. S.J. Weiss, "Tissue destruction by neutrophils," *N. Engl. J. Med.* 320(9 February 1989):365-376.
527. G. Klebanoff, D. Hollander, A.B. Cosimi, W. Stanford, W.T. Kemmerer, "Asanguineous hypothermic total body perfusion (TBW) in the treatment of stage IV hepatic coma," *J. Surg. Res.* 12(January 1972):1-7.
528. Safar Center for Resuscitation Research, "Hemorrhagic Shock and Suspended Animation Program: Suspended Animation"; <http://www.safar.pitt.edu/suspended.html>
529. P. Safar, S.A. Tisherman, W. Behringer, A. Capone, S. Prueckner, A. Radovsky, W.S. Stezoski, R.J. Woods, "Suspended animation for delayed resuscitation from prolonged cardiac arrest that is unresuscitable by standard cardiopulmonary-cerebral resuscitation," *Crit. Care Med.* 28(November 2000):N214-N218.
530. M. Ando, Y. Okita, O. Tagusari, S. Kitamura, N. Nakanishi, S. Kyotani, "Surgical treatment for chronic thromboembolic pulmonary hypertension under profound hypothermia and circulatory arrest in 24 patients," *J. Card. Surg.* 14(September-October 1999):377-385.
531. N. Shiiya, Y. Suto, S. Sasaki, K. Yasuda, "Profound hypothermia and low flow cardiopulmonary bypass in resectioning a massive facial arteriovenous malformation," *Jpn. J. Thorac. Cardiovasc. Surg.* 48(March 2000):186-189.
532. C.B. Kan, C.H. Huang, S.T. Lai, "Surgical management of traumatic thoracic aortic rupture from falling," *Chung Hua I Hsueh Tsa Chih (Taipei)* 63(October 2000):779-783.
533. K. Haneda, R. Thomas, M.P. Sands, D.G. Breazeale, D.H. Dillard, "Whole body protection during three hours of total circulatory arrest: an experimental study," *Cryobiology* 23(December 1986):483-494.

534. M.L. Leavitt, J.E. Bailes, T.S. Shih, A.M. Elrifai, E. Teeple, K. Ciongoli, C. Devenyi, B. Bazmi, J.C. Maroon, "Complete blood substitution during profound hypothermic cardiac arrest in dogs," *Biomater. Artif. Cells Immobilization Biotechnol.* 20(1992):1063–1067.

535. Alien Technology™, "Overview," 2001; <http://www.alientechnology.com/technology/overview.html>

536. The FLUTEC™ Perfluorocarbon Liquids, "Table 1: Solubilities of nitrogen in a various solvents"; <http://www.fluoros.co.uk/flutec/technote/gasexpl.htm>

537. Acetone as rinse fluid for laboratory glassware:

<http://www.wpi.edu/Academics/Depts/Chemistry/Courses/CH1010/Stream1/labtechnique.html>;

<http://www.umsl.edu/~orglab/documents/introduction.htm>;

<http://www.cerritos.edu/lwaldman/Chem211labsafe.htm>;

<http://energy.cr.usgs.gov/other/oglab/method.htm>;

http://faculty.smu.edu/pwisian/index_files/Chem3359/General%20Information.htm;

<http://www.science.mcmaster.ca/biochem/faculty/andrew/lab/projects/methodsandprograms/labman/johnson.htm>;

<http://departments.oxy.edu/tops/Esters/estersreference.htm>;

<http://www.setonresourcecenter.com/29CFR/19101029.htm>

538. http://www.gwu.edu/~vertes/course_http/chem23experiments.html

539. H. Crato, G. Walther, A. Herrmann, "The occurrence of acetone in blood samples forwarded for alcohol content analysis," *Beitr. Gerichtl. Med.* 36(1978):275–279. In German.

540. R. Iffland, M.P. Balling, G. Borsch, C. Herold, W. Kaschade, T Loffler, U. Schmidtman, J. Stettner, "Evaluation of an increased blood level of GGT, CDT, methanol, acetone and isopropanol in alcohol intoxicated automobile drivers. Alcoholism indicators instead of medical–psychological examination," *Blutalkohol* 31(1994):273–314. In German.

541. R. Iffland, G. Berghaus, "Experiences with Volatile Alcoholism Indicators (Methanol, Acetone, Isopropanol) in WI Car Drivers"; <http://www.druglibrary.org/schaffer/Misc/driving/s3p4.htm>

542. Wisconsin State Laboratory of Hygiene, "The Reference Manual"; <http://www.slh.wisc.edu/cgi-bin/manual/makeman.pl?pagecode=409>

543. M.P. Kalapos, "Possible physiological roles of acetone metabolism in humans," *Med. Hypotheses* 53(September 1999):236–242.
544. C.L. Winek, *Drug and Chemical Blood-Level Data 1985*, Allied Fischer Scientific, Pittsburgh PA, 1985.
545. R.E. Gosselin, R.P. Smith, H.C. Hodge, *Clinical Toxicology of Commercial Products*, 5th edition, Williams and Wilkins, Baltimore, MD, 1984, p. III-168.
546. Kirk-Othmer *Encyclopedia of Chemical Technology*, 3rd edition, John Wiley and Sons, New York, Vol. 1, 1978, p.186.
547. G. Ferretti, G. Antonutto, C. Denis, H. Hoppeler, A.E. Minetti, M.V. Narici, D. Desplanches, "The interplay of central and peripheral factors in limiting maximal O₂ consumption in man after prolonged bed rest," *J. Physiol.* 501(15 June 1997):677–686.
548. Benjamin D. Levine, Julie H. Zuckerman, James A. Pawelczyk, "Cardiac atrophy after bed–rest deconditioning: a nonneural mechanism for orthostatic intolerance," *Circulation* 96(15 July 1997):517–525; <http://circ.ahajournals.org/cgi/content/full/96/2/517>
549. M.A. Perhonen, F. Franco, L.D. Lane, J.C. Buckey, C.G. Blomqvist, J.E. Zerwekh, R.M. Peshock, P.T. Weatherall, B.D. Levine, "Cardiac atrophy after bed rest and spaceflight," *J. Appl. Physiol.* 91(August 2001):645–653.
550. Robert A. Freitas Jr., "Some Limits to Global Ecophagy by Biovorous Nanoreplicators, with Public Policy Recommendations," ZyveX preprint, April 2000; <http://www.foresight.org/NanoRev/Ecophagy.html>
551. C. Messow, "Morphological changes in the heart of cats following cardiopuncture," *Dtsch. Tierarztl. Wochenschr.* 74(15 March 1967):164–166. In German.
552. H.J. Weis, E.U. Baas, "Cardiopuncture in the rat for repeated sampling of blood and injection," *Z. Gesamte. Exp. Med.* 156(1971):314–316. In German.

553. E.R. Jacobson, "Immobilization, blood sampling, necropsy techniques and diseases of crocodilians: a review," *J. Zoo Animal Med.* 15(1984):38–45.
554. J.V. Scorza, M. Oviedo, H. Lobo, J.C. Marquez, "Leishmania braziliensis spp. in the nasal mucosa of guinea pigs inoculated in the tarsi," *Mem. Inst. Oswaldo Cruz* 87(January–March 1992):81–86.
555. Mark Lloyd, Patrick J. Morris, "*Phlebotomy techniques in crocodilians,*" *Assoc. Reptilian Amphibian Vet.* 9(Fall 1999):12–13; <http://www.arav.org/Journals/JA014225.htm>
556. C.M. Lin, J.C. Hsu, "Anterior mediastinal tumour identified by intraoperative transesophageal echocardiography," *Can. J. Anaesth.* 48(January 2001):78–80.
557. N. Karam, P. Patel, C. deFilippi, "Diagnosis and management of chronic pericardial effusions," *Am. J. Med. Sci.* 322(August 2001):79–87.
558. G. Brown, L. Baxi, A. Monteagudo, T. Tharakan, A. Saad, S. Sharma, "Fetal faciocervical teratoma with anemia and thrombocytopenia. A case report," *J. Reprod. Med.* 40(January 1995):80–82.
559. A.I. Antsaklis, N.E. Papantoniou, S.A. Mesogitis, P.T. Koutra, A.M. Vintzileos, D.I. Aravantinos, "Cardiocentesis: an alternative method of fetal blood sampling for the prenatal diagnosis of hemoglobinopathies," *Obstet. Gynecol.* 79(April 1992):630–633.
560. A.F. Tarantal, S.E. Gargosky, "Characterization of the insulin-like growth factor (IGF) axis in the serum of maternal and fetal macaques (*Macaca mulatta* and *Macaca fascicularis*)," *Growth Regul.* 5(December 1995):190–198.
561. A. Chinnaiya, A. Venkat, C. Dawn, W.Y. Chee, K.B. Choo, L.A. Gole, C.T. Meng, "Intrahepatic vein fetal blood sampling: current role in prenatal diagnosis," *J. Obstet. Gynaecol. Res.* 24(August 1998):239–246.
562. G. Wang, R. Williamson, G. Mueller, P. Thomas, B.L. Davidson, P.B. McCray Jr., "Ultrasound-guided gene transfer to hepatocytes in utero," *Fetal Diagn. Ther.* 13(July–August 1998):197–205.
563. O. Bakos, U. Ewald, P.G. Lindgren, "Fetal cardiocentesis in care of severe Kell immunization," *Fetal Diagn. Ther.* 13(November–December 1998):372–374.

564. R.D. Estes, *The Behavior Guide to African Mammals*, University of California Press, Berkeley, CA, 1991, pp. 4–5.
565. R.A. Nelson, “Protein and fat metabolism in hibernating bears,” *Fed. Proc.* 39(October 1980):2955–2958; “Urea metabolism in the hibernating black bear,” *Kidney Int. Suppl.* 8(June 1978):S177–S179.
566. P.A. Wright, M.E. Obbard, B.J. Battersby, A.K. Felskie, P.J. LeBlanc, J.S. Ballantyne, “Lactation during hibernation in wild black bears: effects on plasma amino acids and nitrogen metabolites,” *Physiol. Biochem. Zool.* 72(September–October 1999):597–604.
567. D. Fernandez–Mosquera, M. Vila–Taboada, A. Grandal–d’Anglade, “A stable isotopes data ($\delta^{13}\text{C}$, $\delta^{15}\text{N}$) from the cave bear (*Ursus spelaeus*): a new approach to its palaeoenvironment and dormancy,” *Proc. R. Soc. Lond. B Biol. Sci.* 268(7 June 2001):1159–1164.
568. B.L. Schmidt, D.H. Perrott, D. Mahan, G. Kearns, “The removal of plates and screws after Le Fort I osteotomy,” *J. Oral Maxillofac. Surg.* 56(February 1998):184–188.
569. S.T. O’Sullivan, G. Limantzakis, S.F. Kay, “The role of low–profile titanium miniplates in emergency and elective hand surgery,” *J. Hand Surg. (Br)* 24(June 1999):347–349.
570. F. Montorsi, G. Guazzoni, E. Bergamaschi, P. Rigatti, “Patient–partner satisfaction with semirigid penile prostheses for Peyronie’s disease: a 5–year followup study,” *J. Urol.* 150(December 1993):1819–1821.
571. P. Knoringer, “Long–term results of plastic skull repairs with acrylic resins,” *Zentralbl. Neurochir.* 40(1979):197–202. In German.
572. P.J. Murphy, S. Patel, P.B. Morgan, J. Marshall, “The minimum stimulus energy required to produce a cooling sensation in the human cornea,” *Ophthalmic Physiol. Opt.* 21(September 2001):407–410.
573. G. Havenith, E.J. van de Linde, R. Heus, “Pain, thermal sensation and cooling rates of hands while touching cold materials,” *Eur. J. Appl. Physiol. Occup. Physiol.* 65(1992):43–51.

574. M. Terraneo, M. Peyrard, G. Casati, "Controlling the energy flow in nonlinear lattices: a model for a thermal rectifier," Phys. Rev. Lett. 88(4 March 2002):94302; <http://link.aps.org/abstract/PRL/v88/e094302>
575. M. Schwerzmann, C. Seiler, "Recreational scuba diving, patent foramen ovale and their associated risks," Swiss Med. Wkly. 131(30 June 2001):365–374.
576. K.L. Huang, P.S. Chien, Y. Kishi, Y.C. Lin, "Application of conservation principle in estimating body volume in rats," J. Appl. Physiol. 76(January 1994):391–396.
577. M.M. Cohen, "Combining techniques to enhance protection against high sustained accelerative forces," Aviation Space Environ. Med. 54(1983):338–342.
578. United States Naval Flight Surgeon's Manual, Third Edition, 1991; Chapter 2: "Acceleration and Vibration," Virtual Naval Hospital, Naval Aerospace Medical Institute, revised March 2000; <http://www.vnh.org/FManual/02/SectionTop.html>
579. "Centrifuge: History"; <http://www.brooks.af.mil/HSW/PA/Centrifuge.html>
580. AMAL–NADC, Human Tolerance to High Acceleration Stress; letter report concerning (2 May 1958); Bondurant et al., Human Tolerance to Some of the Accelerations Anticipated in Space Flight; Aviation Week, 12 May 1958; interview, Dr. C. Clark, AMAL–NADC, by Dr. Bushnell, 6 June 1958. Cited in: History of Research in Space Biology and Biodynamics, PART V – Other Research Related to G–Forces Anticipated in Space Flight; <http://www.hq.nasa.gov/office/pao/History/afspbio/part5–4.htm>
581. "Project 91, Performance Data," 5 July 1957, chart in library of Aeromedical Field Laboratory; ltr., Lt. Col. John P. Stapp, Chief, Aeromedical Field Laboratory, to Maj. Rufus R. Hessberg, Jr., Chief, Biophysics Branch, Aeromedical Laboratory, WADC, subj.: [Windblast Tests], 2 January 1957; interviews, Capt. John D. Mosely, Chief, Biodynamics Branch, Aeromedical Field Laboratory, by Dr. David Bushnell, AFMDC Historian, 13 November 1957 and 7 February 1958; interview, Col. John P. Stapp, Chief, Aeromedical Field Laboratory, by Dr. Bushnell, 11 February 1958; "Chimpanzees Pass Space Speed Test," New York Times, 31 January 1958. Cited in: History of Research in Space Biology and Biodynamics, PART V – Later Deceleration Studies on the High–Speed Track; <http://www.hq.nasa.gov/office/pao/History/afspbio/part5–3.htm>
582. P.R. May, J.M. Fuster, J. Haber, A. Hirschman, "Woodpecker drilling behavior. An endorsement of the rotational theory of impact brain injury," Arch. Neurol. 36(June 1979):370–373; R.D. Snyder, "Woodpecker drilling behavior," Arch. Neurol. 36(December 1979):860.

583. P.R. May, J.M. Fuster, P. Newman, A. Hirschman, "Woodpeckers and head injury," Lancet 1(28 February 1976):454–455, 1(19 June 1976):1347–1348; D. Gordon, "Letter: Woodpeckers, gannets, and head injury," Lancet 1(10 April 1976):801–802.

584. Carey Sublette, "Nuclear Weapons Frequently Asked Questions. Section 5.0 Effects of Nuclear Explosions," version 2.14, 15 May 1997;
<http://www.fas.org/nuke/hew/Nwfaq/Nfaq5.html#nfaq5.6>

585. Air Force Pamphlet 161–3, NATO Handbook on the Medical Aspects of NBC Defensive Operations AMed P–6; cited in: Mark J. Tedesco, "U.S. Flight Surgeon's Guide, Chapter 23. Medical Disaster Preparedness and Nuclear, Biological, and Chemical (NBC) Operations";
http://wwwsam.brooks.af.mil/af/files/fsguide/HTML/Chapter_23.html

586. Charles Darwin, The Origin of Species by Means of Natural Selection, 1859; definitive 6th London edition: <http://www.literature.org/authors/darwin-charles/the-origin-of-species-6th-edition/>

587. Edward O. Wilson, Sociobiology: The New Synthesis, Harvard University Press, Cambridge, MA, 1975.

[Home](#)

DR. RUPNATHJIK (DR. RUPAK NATH)